E-ISSN: 2147-1959

MIRT

Molecular Imaging and Radionuclide Therapy

February 2021 Volume 30 Issue 1 www.tsnm.org

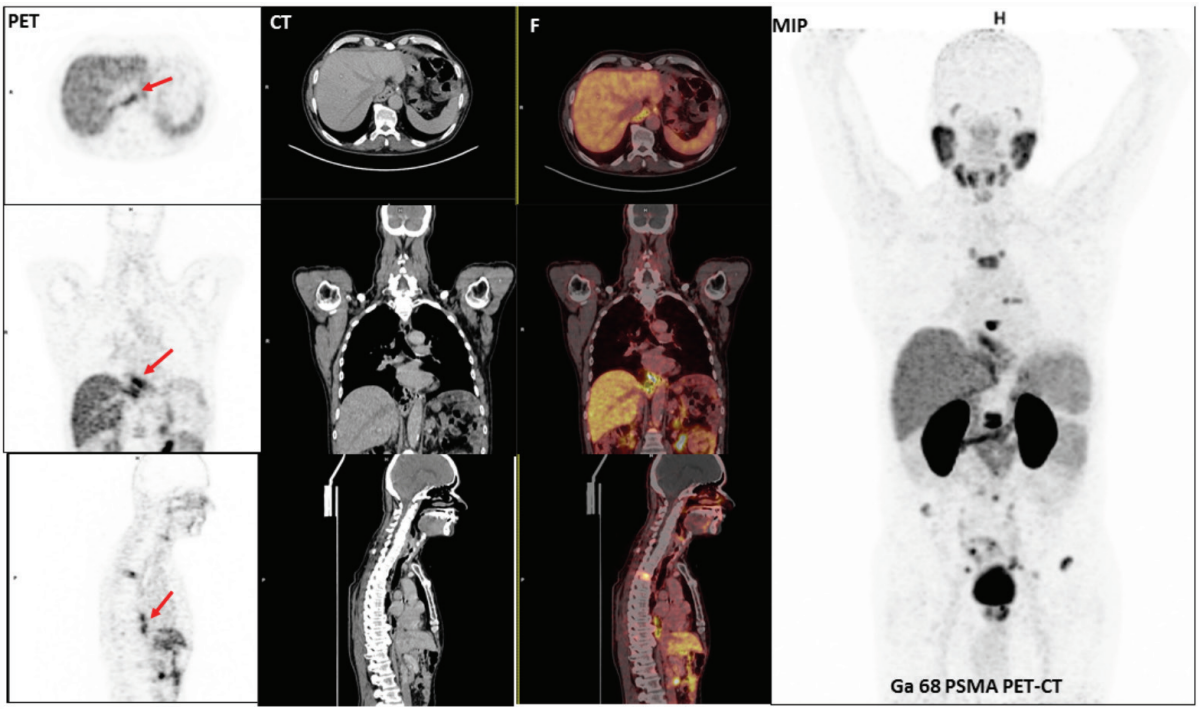

"Official Journal of the Turkish Society of Nuclear Medicine"

galenos yayınevi

TURKISH SOCIETY OF NUCLEAR MEDICINE 1975

MIRT

Molecular Imaging and Radionuclide Therapy

Scientific Advisory Board

MIRT

Molecular Imaging and Radionuclide Therapy

Turkish Society of Nuclear Medicine
Cinnah Caddesi Pilot Sokak No: 10/12 Çankaya 06650 Ankara, Turkey **Phone:** +90 312 441 00 45 **Fax:** +90 312 441 12 95 **Web:** www.tsnm.org **E-mail:** dernekmerkezi@tsnm.org
"Formerly Turkish Journal of Nuclear Medicine"

Reviewing the articles' conformity to the publishing standards of the Journal, typesetting, reviewing and editing the manuscripts and abstracts in English, creating links to source data, and publishing process are realized by Galenos.

Galenos Publishing House
Owner and Publisher
Derya Mor
Erkan Mor

Publication Coordinator
Burak Sever

Web Coordinators
Fuat Hocalar
Turgay Akpınar

Graphics Department
Ayda Alaca
Çiğdem Birinci
Gülşah Özgül

Finance Coordinator
Sevinç Çakmak

Project Coordinators
Aysel Balta
Duygu Yıldırm
Gamze Aksoy
Gülay Akın
Hatice Sever
Melike Eren
Meltem Acar
Özlem Çelik
Pınar Akpınar
Rabia Palazoğlu

Research&Development
Mert Can Köse
Özlem Akgüney Küççük

Digital Marketing Specialist
Seher Altundemir

Publisher Contact
Address: Molla Gürani Mah. Kaçamak Sk. No: 21/1
34093 İstanbul, Turkey
Phone: +90 (212) 621 99 25 **Fax:** +90 (212) 621 99 27
E-mail: info@galenos.com.tr/yayin@galenos.com.tr
Web: www.galenos.com.tr
Publisher Certificate Number: 14521

Online Publication Date: February 2021
ISSN: 2146-1414 **E-ISSN:** 2147-1959
International scientific journal published quarterly.

MIRT

Molecular Imaging and Radionuclide Therapy

ABOUT US

Molecular Imaging and Radionuclide Therapy (formerly Turkish Journal of Nuclear Medicine) is the official publication of Turkish Society of Nuclear Medicine.

Focus and Scope

Molecular Imaging and Radionuclide Therapy (Mol Imaging Radionucl Ther, MIRT) is a double-blind peer-review journal published in English language. It publishes original research articles, invited reviews, editorials, short communications, letters, consensus statements, guidelines and case reports with a literature review on the topic, in the field of molecular imaging, multimodality imaging, nuclear medicine, radionuclide therapy, radiopharmacy, medical physics, dosimetry and radiobiology. MIRT is published three times a year (February, June, October). Audience: Nuclear medicine physicians, medical physicists, radiopharmaceutical scientists, radiobiologists.

The editorial policies are based on the "Recommendations for the Conduct, Reporting, Editing, and Publication of Scholarly Work in Medical Journals (ICMJE Recommendations)" by the International Committee of Medical Journal Editors (2016, archived at http://www.icmje.org/) rules.

Molecular Imaging and Radionuclide Therapy is indexed in **Pubmed, Pubmed Central (PMC), Emerging Sources Citation Index (ESCI), TUBITAK-ULAKBIM, Scopus, Gale/Cengage Learning, EBSCO databases, ProQuest Health & Medical Complete, CINAHL, DOAJ, Index Copernicus, J-Gate, IdealOnline, ROOT INDEXING, Türkiye Atıf Dizini-Turkiye Citation Index, Turk Medline, EuroPub, Hinari, GOALI, ARDI, OARE** and **AGORA**.

Open Access Policy

This journal provides immediate open access to its content on the principle that making research freely available to the public supports a greater global exchange of knowledge.

Open Access Policy is based on rules of Budapest Open Access Initiative (BOAI) (http://www.budapestopenaccessinitiative.org/). By "open access" to [peer-reviewed research literature], we mean its free availability on the public internet, permitting any users to read, download, copy, distribute, print, search, or link to the full texts of these articles, crawl them for indexing, pass them as data to software, or use them for any other lawful purpose, without financial, legal, or technical barriers other than those inseparable from gaining access to the internet itself. The only constraint on reproduction and distribution, and the only role for copyright in this domain, should be to give authors control over the integrity of their work and the right to be properly acknowledged and cited.

Subscription Information

Manuscripts can only be submitted electronically through the Journal Agent website (http://www.journalagent.com/mirt/?plng=eng) after creating an account. This system allows online submission and review.

All published volumes in full text can be reached free of charge through the website http://mirt.tsnmjournals.org

Copyright Statement

Turkish Society of Nuclear Medicine holds the international copyright of all the content published in the journal.

Republication and reproduction of images or tables in any published material should be done with proper citation of source providing authors names; article title; journal title; year (volume) and page of publication; copyright year of the article.

The author(s) hereby affirms that the manuscript submitted is original, that all statement asserted as facts are based on author(s) careful investigation and research for accuracy, that the manuscript does not, in whole or part, infringe any copyright, that it has not been published in total or in part and is not being submitted or considered for publication in total or in part elsewhere.

Completed Copyright Statement form should be submitted to the online article system.

By signing this form,

1. Each author acknowledge that he/she participated in the work in a substantive way and is prepared to take public responsibility for the work.

2. Each author further affirms that he or she has read and understands the "Ethical Guidelines for Publication of Research".

3. The author(s), in consideration of the acceptance of the manuscript for publication, does hereby assign and transfer to the Molecular Imaging and Radionuclide Therapy all of the rights and interest in and the copyright of the work in its current form and in any form subsequently revised for publication and/or electronic dissemination.

Instructions for Authors

Instructions for authors are published in the journal and on the website http://mirt.tsnmjournals.org

Material Disclaimer

Scientific and legal responsibilities pertaining to the papers belong to the authors. Contents of the manuscripts and accuracy of references are also the author's responsibility. The Turkish Society of Nuclear Medicine, the Editor, the Editorial Board or the publisher do not accept any responsibility for opinions expressed in articles.

Financial expenses of the journal are covered by Turkish Society of Nuclear Medicine.

Correspondence Address

Editor in Chief Prof. Dr. Zehra Özcan, Ege University, Medical School, Department of Nuclear Medicine, İzmir, Turkey

E-mail: zehra.ozcan@yahoo.com

Web page: http://mirt.tsnmjournals.org/

Publisher Corresponding Address

Galenos Yayınevi Tic. Ltd. Şti.
Address: Molla Gürani Mah. Kaçamak Sk. No: 21/1 34093 Fındıkzade, İstanbul, Turkey
Phone: +90 212 621 99 25
Fax: +90 212 621 99 27
E-mail: info@galenos.com.tr

MIRT

Molecular Imaging and Radionuclide Therapy

INSTRUCTIONS TO AUTHORS

Molecular Imaging and Radionuclide Therapy (Mol Imaging Radionucl Ther, MIRT) publishes original research articles, short communications, invited reviews, editorials, case reports with a literature review on the topic, interesting images, consensus statements, guidelines, letters in the field of molecular imaging, multimodality imaging, nuclear medicine, radionuclide therapy, radiopharmacy, medical physics, dosimetry and radiobiology. MIRT is published by the Turkish Society of Nuclear Medicine three times a year (February, June, October).

Molecular Imaging and Radionuclide Therapy does not charge any article submission or processing fees.

GENERAL INFORMATION

MIRT commits to rigorous peer review, and stipulates freedom from commercial influence, and promotion of the highest ethical and scientific standards in published articles. Neither the Editor(s) nor the publisher guarantees, warrants or endorses any product or service advertised in this publication. All articles are subject to review by the editors and peer reviewers. If the article is accepted for publication, it may be subjected to editorial revisions to aid clarity and understanding without changing the data presented.

Manuscripts must be written in English and must meet the requirements of the journal. The journal is in compliance with the uniform requirements for manuscripts submitted to biomedical journals published by the International Committee of Medical Journal Editors (NEJM 1997; 336:309-315, updated 2016). Manuscripts that do not meet these requirements will be returned to the author for necessary revision before the review. Authors of manuscripts requiring modifications have a maximum of two months to resubmit the revised text. Manuscripts returned after this deadline will be treated as new submissions.

It is the authors' responsibility to prepare a manuscript that meets ethical criteria. The Journal adheres to the principles set forth in the Helsinki Declaration October 2013 (https://www.wma.net/policies-post/wma-declaration-of-helsinki-ethical-principles-for-medical-research-involving-human-subjects/) and holds that all reported research involving "Human beings" conducted in accordance with such principles.

Reports describing data obtained from research conducted in human participants must contain a statement in the MATERIALS AND METHODS section indicating approval by the ethical review board (including the approval number) and affirmation that INFORMED CONSENT was obtained from each participant.

All manuscripts reporting experiments using animals must include a statement in the MATERIALS AND METHODS section giving assurance that all animals have received humane care in compliance with the Guide for the Care and Use of Laboratory Animals (www.nap.edu) and indicating approval by the ethical review board.

If the study should have ethical approval, authors asked to provide ethical approval in order to proceed the review process. If they provide approval, review of the manuscript will continue.

In case report(s) and interesting image(s) a statement regarding the informed consent of the patients should be included in the manuscript and the identity of the patient(s) should be hidden.

Subjects must be identified only by number or letter, not by initials or names. Photographs of patients' faces should be included only if scientifically relevant. Authors must obtain written consent from the patient for use of such photographs. In cases of image media usage that potentially expose patients' identity requires obtaining permission for publication from the patients or their parents/guardians.

If the proposed publication concerns any commercial product, the author must include in the cover letter a statement indicating that the author(s) has (have) no financial or other interest with the product or explaining the nature of any relations (including consultancies) between the author(s) and editor the manufacturer or distributor of the product.

All submissions will be screened by Crossref Smilarity Check powered by "iThenticate". Manuscripts with an overall similarity index of greater than 25%, or duplication rate at or higher than 5% with a single source will be returned back to authors.

MANUSCRIPT CATEGORIES

1. Original Articles

2. Short Communications are short descriptions of focused studies with important, but very straightforward results.

3. Reviews address important topics in the field. Authors considering the submission of uninvited reviews should contact the editor in advance to determine if the topic that they propose is of current potential interest to the Journal. Reviews will be considered for publication only if they are written by authors who have at least three published manuscripts in the international peer reviewed journals and these studies should be cited in the review. Otherwise only invited reviews will be considered for peer review from qualified experts in the area.

4. Editorials are usually written by invitation of the editor by the editors on current topics or by the reviewers involved in the evaluation of a submitted manuscript and published concurrently with that manuscript.

5. Case Report and Literature Reviews are descriptions of a case or small number of cases revealing a previously undocumented disease process, a unique unreported manifestation or treatment of a known disease process, unique unreported complications of treatment regimens or novel and important insights into a condition's pathogenesis, presentation, and/or management. The journal's policy is to accept case reports only if it is accompanied by a review of the literature on the related topic. They should include an adequate number of images and figures.

6. Interesting Image

One of the regular parts of Molecular Imaging and Radionuclide Therapy is a section devoted to interesting images. Interesting image(s) should describe case(s) which are unique and include interesting findings adding insights into the interpretation of patient images, a condition's pathogenesis, presentation, and/or management.

7. Consensus Statements or Guidelines may be submitted by professional societies. All such submissions will be subjected to peer review, must be modifiable in response to criticisms, and will be published only if they meet the Journal's usual editorial standards.

8. Letters to the Editor may be submitted in response to work that has been published in the Journal. Letters should be short commentaries related to specific points of agreement or disagreement with the published work.

Note on Prior Publication

Articles are accepted for publication on the condition that they are original, are not under consideration by another journal, or have not been previously published. Direct quotations, tables, or illustrations that have appeared in

MIRT

Molecular Imaging and Radionuclide Therapy

copyrighted material must be accompanied by written permission for their use from the copyright owner and authors. Materials previously published in whole or in part shall not be considered for publication. At the time of submission, authors must report that the manuscript has not been published elsewhere. Abstracts or posters displayed at scientific meetings need not be reported.

MANUSCRIPT SUBMISSION PROCEDURES

MIRT only accepts electronic manuscript submission at the web site http://www.journalagent.com/mirt/. After logging on to the website Click the 'online manuscript submission' icon. All corresponding authors should be provided with a password and a username after entering the information required. If you already have an account from a previous submission, enter your username and password to submit a new or revised manuscript. If you have forgotten your username and/or password, please send an e-mail to the editorial office for assistance. After logging on to the article submission system please read carefully the directions of the system to give all needed information and attach the manuscript, tables and figures and additional documents.

All Submissions Must Include:

1. Completed Copyright Assignment & Disclosure of Potential Conflict of Interest Form; This form should be downloaded from the website (provided in the author section), filled in thoroughly and uploaded to the website during the submission.
2. All manuscripts describing data obtained from research conducted in human participants must be accompanied with an approval document by the ethical review board.
3. All manuscripts reporting experiments using animals must include approval document by the animal ethical review board.
4. All submissions must include the authorship contribution form which is signed by all authors.

Authors must complete all online submission forms. If you are unable to successfully upload the files please contact the editorial office by e-mail.

MANUSCRIPT PREPARATION

General Format

The Journal requires that all submissions be submitted according to these guidelines:

- Text should be double spaced with 2.5 cm margins on both sides using 12-point type in Times Roman font.
- All tables and figures must be placed after the text and must be labeled.
- Each section (abstract, text, references, tables, figures) should start on a separate page.
- Manuscripts should be prepared as a word document (*.doc) or rich text format (*.rtf).
- Please make the tables using the table function in Word.
- Abbreviations should be defined in parenthesis where the word is first mentioned and used consistently thereafter.
- Results should be expressed in metric units. Statistical analysis should be done accurately and with precision. Please consult a statistician if necessary.
- Authors' names and institutions should not be included in the manuscript text and should be written only in the title page.

Title Page

The title page should be a separate form from the main text and should include the following:

- Full title (in English and in Turkish). Turkish title will be provided by the editorial office for the authors who are not Turkish speakers.
- Authors' names and institutions.
- Short title of not more than 40 characters for page headings.
- At least three and maximum eight keywords. (in English and in Turkish). Do not use abbreviations in the keywords. Turkish keywords will be provided by the editorial office for the authors who are not Turkish speakers. If you are not a native Turkish speaker, please reenter your English keywords to the area provided for the Turkish keywords. English keywords should be provided from http://www.nlm.nih.gov/mesh (Medical Subject Headings) while Turkish keywords should be provided from http://www.bilimterimleri.com.
- Word count (excluding abstract, figure legends and references).
- Corresponding author's e-mail and address, telephone and fax numbers.
- Name and address of person to whom reprint requests should be addressed.

Original Articles

Authors are required to state in their manuscripts that ethical approval from an appropriate committee and informed consents of the patients were obtained.

Original Articles should be submitted with a structured abstract of no more than 250 words. All information reported in the abstract must appear in the manuscript. The abstract should not include references. Please use complete sentences for all sections of the abstract. Structured abstract should include background, objective, methods, results and conclusions. Turkish abstract will be provided by the editorial office for the authors who are not Turkish speakers. If you are not a native Turkish speaker, please reenter your English abstract to the area provided for the Turkish abstract.

- Introduction
- Materials and Methods
- Results
- Discussion
- Study Limitations
- Conclusion

May be given for contributors who are not listed as authors, or for grant support of the research.

References should be cited in numerical order (in parentheses) in the text and listed in the same numerical order at the end of the manuscript on a separate page or pages. The author is responsible for the accuracy of references. Examples of the reference style are given below. Further examples will be found in the articles describing the Uniform Requirements for Manuscripts Submitted to Biomedical Journals (Ann Intern Med.1988; 208:258-265, Br Med J. 1988; 296:401-405). The titles of journals should be abbreviated according to the style used in the Index Medicus. Journal Articles and Abstracts: Surnames and initials of author's name, title of the article, journal name, date, volume number, and pages. All authors should be listed regardless of number. The citation of unpublished papers, observations or personal communications is not permitted. Citing an abstract is not recommended. Books: Surnames and initials of author's names, chapter title, editor's name, book title, edition, city, publisher, date and pages.

MIRT
Molecular Imaging and Radionuclide Therapy

INSTRUCTIONS TO AUTHORS

Sample References

Journal Article: Sayit E, Söylev M, Capa G, Durak I, Ada E, Yilmaz M. The role of technetium-99m-HMPAO-labeled WBC scintigraphy in the diagnosis of orbital cellulitis. Ann Nucl Med 2001;15:41-44.

Erselcan T, Hasbek Z, Tandogan I, Gumus C, Akkurt I. Modification of Diet in Renal Disease equation in the risk stratification of contrast induced acute kidney injury in hospital inpatients. Nefrologia 2009 doi: 10.3265/Nefrologia.2009.29.5.5449.en.full.

Article in a journal published ahead of print: Ludbrook J. Musculovenous pumps in the human lower limb. Am Heart J 2009;00:1-6. (accessed 20 February 2009).

Lang TF, Duryea J. Peripheral Bone Mineral Assessment of the Axial Skeleton: Technical Aspects. In: Orwoll ES, Bliziotes M (eds). Osteoporosis: Pathophsiology and Clinical Management. New Jersey, Humana Pres Inc, 2003;83-104.

Books: Greenspan A. Orthopaedic Radiology a Pratical Approach. 3th ed. Philadelphia, Lippincott Williams Wilkins 2000, 295-330.

Website: Smith JR. 'Choosing Your Reference Style', Online Referencing 2(3), http://orj.sagepub.com (2003, accessed October 2008).

- Tables

Tables must be constructed as simply as possible. Each table must have a concise heading and should be submitted on a separate page. Tables must not simply duplicate the text or figures. Number all tables in the order of their citation in the text. Include a title for each table (a brief phrase, preferably no longer than 10 to 15 words). Include all tables in a single file following the manuscript.

– Figure Legends

Figure legends should be submitted on a separate page and should be clear and informative.

– Figures

Number all figures (graphs, charts, photographs, and illustrations) in the order of their citation in the text. At submission, the following file formats are acceptable: AI, EMF, EPS, JPG, PDF, PPT, PSD, TIF. Figures may be embedded at the end of the manuscript text file or loaded as separate files for submission. All images MUST be at or above intended display size, with the following image resolutions: Line Art 800 dpi, Combination (Line Art + Halftone) 600 dpi, Halftone 300 dpi. Image files also must be cropped as close to the actual image as possible.

Short Communications:

Short communications should be submitted with a structured abstract of no more than 200 words. These manuscripts should be no longer than 2000 words, and include no more than two figures and tables and 20 references. Other rules which the authors are required to prepare and submit their manuscripts are the same as described above for the original articles.

Invited Review Articles:

- Title page (see above)
- Abstract: Maximum 250 words; without structural divisions; in English and in Turkish . Turkish abstract will be provided by the editorial office for the authors who are not Turkish speakers. If you are not a native Turkish speaker, please reenter your English abstract to the area provided for the Turkish abstract.
- Text
- Conclusion
- Acknowledgements (if any)
- References

Editorial:

- Title page (see above)
- Abstract: Maximum 250 words; without structural divisions; in English and in Turkish. Turkish abstract will be provided by the editorial office for the authors who are not Turkish speakers. If you are not a native Turkish speaker, please re enter your English abstract to the area provided for the Turkish abstract.
- Text
- References

Case Report and Literature Review

- Title page (see above)
- Abstract: Approximately 100-150 words; without structural divisions; in English and in Turkish. Turkish abstract will be provided by the editorial office for the authors who are not Turkish speakers. If you are not a native Turkish speaker, please re-enter your English abstract to the area provided for the Turkish abstract.
- Introduction
- Case report
- Literature Review and Discussion
- References

Interesting Image:

No manuscript text is required. Interesting Image submissions must include the following:

Title Page: (see Original article section)

Abstract: Approximately 100-150 words; without structural divisions; in English and in Turkish. Turkish abstract will be provided by the editorial office for the authors who are not Turkish speakers. If you are not a native Turkish speaker, please re-enter your English abstract to the area provided for the Turkish abstract.

Image(s): The number of images is left to the discretion of the author. (See Original article section)

Figure Legend: Reference citations should appear in the legends, not in the abstract. Since there is no manuscript text, the legends for illustrations should be prepared in considerable detail but should be no more than 500 words total. The case should be presented and discussed in the Figure legend section.

References: Maximum eight references (see original article section).

Letters to the Editor:

- Title page (see above)
- Short comment to a published work, no longer than 500 words, no figures or tables.
- References no more than five.

Consensus Statements or Guidelines: These manuscripts should typically be no longer than 4000 words and include no more than six figures and tables and 120 references.

Proofs and Reprints

Proofs and a reprint orders are sent to the corresponding author. The author should designate by footnote on the title page of the manuscript the name and

MIRT
Molecular Imaging and Radionuclide Therapy

address of the person to whom reprint requests should be directed. The manuscript when published will become the property of the journal.

Archiving

The editorial office will retain all manuscripts and related documentation (correspondence, reviews, etc.) for 12 months following the date of publication or rejection.

Submission Preparation Checklist

As part of the submission process, authors are required to check off their submission's compliance with all of the following items, and submissions may be returned to authors that do not adhere to these guidelines.

1. The submission has not been previously published, nor is it before another journal for consideration (or an explanation has been provided in Comments to the Editor).
2. The submission file is in Microsoft Word, RTF, or WordPerfect document file format. The text is double-spaced; uses a 12-point font; employs italics, rather than underlining (except with URL addresses); and the location for all illustrations, figures, and tables should be marked within the text at the appropriate points.
3. Where available, URLs for the references will be provided.
4. All authors should be listed in the references, regardless of the number.
5. The text adheres to the stylistic and bibliographic requirements outlined in the Author Guidelines, which is found in About the Journal.
6. English keywords should be provided from http://www.nlm.nih.gov/mesh(Medical Subject Headings), while Turkish keywords should be provided fromhttp://www.bilimterimleri.com
7. The title page should be a separate document from the main text and should be uploaded separately.
8. The "Affirmation of Originality and Assignment of Copyright/The Disclosure Form for Potential Conflicts of Interest Form" and Authorship Contribution Form should be downloaded from the website, filled thoroughly and uploaded during the submission of the manuscript.

TO AUTHORS

Copyright Notice

The author(s) hereby affirms that the manuscript submitted is original, that all statement asserted as facts are based on author(s) careful investigation and research for accuracy, that the manuscript does not, in whole or part, infringe any copyright, that it has not been published in total or in part and is not being submitted or considered for publication in total or in part elsewhere. Completed Copyright Assignment & Affirmation of Originality Form will be uploaded during submission. By signing this form;

1. Each author acknowledges that he/she participated in the work in a substantive way and is prepared to take public responsibility for the work.
2. Each author further affirms that he or she has read and understands the "Ethical Guidelines for Publication of Research".
3. The author(s), in consideration of the acceptance of the manuscript for publication, does hereby assign and transfer to the Molecular Imaging and Radionuclide Therapy all of the rights and interest in and the copyright of the work in its current form and in any form subsequently revised for publication and/or electronic dissemination.

Privacy Statement

The names and email addresses entered in this journal site will be used exclusively for the stated purposes of this journal and will not be made available for any other purpose or to any other party.

Peer Review Process

1. The manuscript is assigned to an editor, who reviews the manuscript and makes an initial decision based on manuscript quality and editorial priorities.
2. For those manuscripts sent for external peer review, the editor assigns at least two reviewers to the manuscript.
3. The reviewers review the manuscript.
4. The editor makes a final decision based on editorial priorities, manuscript quality, and reviewer recommendations.
5. The decision letter is sent to the author.

Contact Address

All correspondence should be directed to the Editorial Office:
Cinnah Caddesi Pilot Sokak No:10/12 06650 Çankaya / Ankara, Turkey
Phone: +90 312 441 00 45
Fax: +90 312 441 12 97
E-mail: info@tsnmjournals.org

MIRT
Molecular Imaging and Radionuclide Therapy

CONTENTS

Original Articles

Interesting Images

MIRT
Molecular Imaging and Radionuclide Therapy

CONTENTS

Original Article
Mol Imaging Radionucl Ther 2021;30:1-7 DOI:10.4274/mirt.galenos.2020.63634

The Role of ^{18}F-FDG PET/CT in Evaluating the Efficacy of Radiofrequency Ablation in Metastatic and Primary Liver Tumors: Preliminary Results

Metastatik ve Primer Karaciğer Tümörlerinde Radyofrekans Ablasyonun Etkinliğinin Değerlendirilmesinde ^{18}F-FDG PET/BT'nin Rolü: Ön Sonuçlar

Gabriela Mateva[1], Stoyan Handzhiev[2], Irena Kostadinova[1]

[1]*Acibadem City Clinic Mladost, Clinic of Nuclear Medicine, Sofia, Bulgaria*
[2]*Acibadem City Clinic Mladost, Clinic of Gastroenterology, Sofia, Bulgaria*

Abstract

Objectives: The aim of the study was to investigate the role of ^{18}fluorine-fluorodeoxyglucose (^{18}F-FDG) positron emission tomography/computed tomography (PET/CT) for evaluating the efficacy of radiofrequency ablation (RFA) in primary and metastatic liver tumors compared with contrast-enhanced ultrasound examination (CEUS) and to find its place in overall staging and the follow-up diagnostic algorithm.

Methods: PET/CT examinations were performed 2 months after RFA for 20 patients with a total of 34 liver lesions. CEUS was performed within 10 days after PET/CT, and the results were compared. Seven patients were staged with PET/CT and the others with a contrast-enhanced CT.

Results: A total of 48 ^{18}F-FDG PET/CT examinations were performed. We observed complete response in 8 patients (40%), 2 patients (10%) had stable disease, one (5%) had partial response, and 9 patients (45%) had progression (including 2 cases with extrahepatic involvement). Compared with CEUS, there was a mismatch in 3 cases. Five patients underwent additional RFA for 7 lesions.

Conclusion: According to our preliminary data, PET/CT may be a valuable method, with comparable or eventually even better sensitivity than CEUS, for early evaluation of the efficacy of RFA for the treatment of metastatic and primary liver lesions and planning of future treatment. PET/CT might be recommended as a staging method before undergoing RFA of liver lesions for determining the local extent of the disease in the liver in combination with CEUS with an advantage in visualization of extrahepatic involvement. However, more patients need to be investigated in order to demonstrate and confirm the obtained results with certainty.

Keywords: Radiofrequency ablation, PET/CT, CEUS, metastatic liver lesions, primary liver tumors

Öz

Amaç: Bu çalışmanın amacı, primer ve metastatik karaciğer tümörlerinde radyofrekans ablasyonunun (RFA) etkinliğini değerlendirmede ^{18}flor-florodeoksiglukoz (^{18}F-FDG) pozitron emisyon tomografisi/bilgisayarlı tomografinin (PET/BT) rolünü kontrastlı ultrason tetkikine (CEUS) kıyasla araştırmak ve genel evreleme ve takip tanı algoritmasındaki yerini bulmaktır.

Yöntem: Toplam 34 karaciğer lezyonu olan 20 hastaya RFA'dan 2 ay sonra PET/BT tetkikleri yapıldı. PET/BT'den sonraki 10 gün içinde CEUS yapıldı ve sonuçlar karşılaştırıldı. Yedi hasta PET/BT ile diğerleri ise kontrastlı BT ile evrelendirildi.

Bulgular: Toplam 48 adet ^{18}F-FDG PET/BT incelemesi yapıldı. Sekiz hastada (%40) tam yanıt, 2 hastada (%10) stabil hastalık, 1 hastada (%5) kısmi yanıt ve 9 hastada (%45) progresyon (ekstrahepatik tutulumlu 2 olgu dahil) gözlemlendi. CEUS ile karşılaştırıldığında, 3 olguda uyumsuzluk bulundu. Beş hastaya, toplam 7 lezyon için ek RFA uygulandı.

Address for Correspondence: Gabriela Mateva MD, Acibadem City Clinic Mladost, Clinic of Nuclear Medicine, Sofia, Bulgaria
Phone: +359894680648 **E-mail:** gabriela.mateva@abv.bg ORCID ID: orcid.org/0000-0001-8834-995X
Received: 26.05.2020 **Accepted:** 23.10.2020

Sonuç: Ön verilerimize göre PET/BT, metastatik ve primer karaciğer lezyonlarının tedavisinde RFA'nın etkinliğinin erken değerlendirilmesi ve gelecekteki tedavinin planlanması için CEUS ile karşılaştırılabilir veya sonuç olarak daha iyi hassasiyete sahip değerli bir yöntem olabilir. PET/BT, ekstrahepatik tutulumun görselleştirilmesinde avantajlı olması ile birlikte, CEUS ile birlikte karaciğerdeki hastalığın lokal boyutunu belirlemede karaciğer lezyonları için RFA öncesinde bir evreleme yöntemi olarak önerilebilir. Bununla birlikte, elde edilen sonuçları kesin olarak göstermek ve doğrulamak için daha fazla hastanın araştırılması gerekir.

Anahtar kelimeler: Radyofrekans ablasyon, PET/BT, CEUS, metastatik karaciğer lezyonları, primer karaciğer tümörleri

Introduction

Radiofrequency ablation (RFA) of liver lesions is a minimally invasive treatment option for patients with primary and metastatic hepatic tumors. RFA of liver lesions is performed under visual control, most often using ultrasound-rarely computed tomography (CT)-and there is also a report of the procedure being performed under positron emission tomography (PET)/CT control (1).

The main indications for thermal ablation include unresectable liver lesions; combination with hepatectomy as an additional treatment; patients with significant medical comorbidities or poor performance status; and small (<3 cm), solitary lesions, which would otherwise necessitate a major liver resection (2).

PET/CT is not a standard method for patient follow-up after RFA, but a literature review and our experience suggest that it is applicable, highly sensitive and specific, and might even have advantages over other imaging methods (contrast-enhanced ultrasound and CT) in certain clinical situations.

The aim of the study is to investigate the role of ^{18}fluorine-fluorodeoxyglucose (^{18}F-FDG) PET/CT for evaluating the efficacy of RFA in primary and metastatic liver tumors and to compare the results with those of contrast-enhanced ultrasound examination (CEUS) in overall staging and the follow-up diagnostic algorithm.

Materials and Methods

Our initial experience was an examination of 20 patients, 9 men and 11 women, with a mean age of 63 years, during the period 2017-2019, with a total of 34 liver lesions, with the following primary tumors: Six with colon cancer, 5 with breast cancer, 3 with pancreatic cancer, 2 with hepatocellular carcinoma (HCC), 2 with stomach cancer, one cancer of the ampulla of Vater, and 1 with carcinoma of the epipharynx. PET/CT examinations were performed 2 months after RFA. We used a standard scanning protocol: Intravenous injection of ^{18}F-FDG 2-2.2 MBq per kilogram and whole-body scanning (calvaria to mid-thigh), after 60 minutes of rest, 2 minutes per bed position combined with dynamic CT scanning with a 2.5 mm slice thickness. For interpretation of the results and evaluation of efficacy of RFA, we used qualitative/visual and quantitative criteria: Maximum standard uptake value (SUV_{max}) values and changes in lesion size (3).

The RFA generator was used to apply a power of 40 kW for 5,10, 15, or 20 min, depending on the size of the lesion, with 1 and 2 working antennas with a working electrode length of 15-20-25 mm in monopolar or bipolar mode. Ultrasound navigation was performed with contrast-enhancing mode software, with a mechanical index of -0.18, and bolus application of 2.5 mL contrast agent. The lesion size was measured, and the contrast enhancement was observed.

In all cases, a CEUS was performed within 10 days before or after PET/CT, and the results were compared.

For 7 of the patients, a staging PET/CT was performed, and the others already had a recent contrast-enhanced CT, which was used for staging.

The exclusion criteria were extrahepatic involvement and cases where the number, size, or location of the hepatic lesions precluded total ablation.

The study protocol was approved by the Ethics Committee of Acibadem City Clinic (date: 12.10.2018, approval no: 11-07-80). Before undergoing the studies and RFA, all patients signed informed consent forms, agreeing that the obtained data be used for scientific purposes.

Statistical analysis was not performed since the number of included subjects was not suitable for drawing reliable conclusions.

Results

A total of 48 ^{18}F-FDG PET/CT examinations were performed. The patients were restaged for local status after RFA of liver lesions and for distant metastases with 41 follow-up PET/CT studies.

We observed complete response in 8 patients (40%), 2 patients (10%) had stable disease, 1 (5%) had partial response, and 9 patients (45%) had progression (including 2 cases with extrahepatic involvement).

Compared to CEUS, there was a mismatch in three cases. In 2 patients where PET/CT showed increased metabolic

activity of lesions, respectively, interpreted as progression, in CEUS the same lesions were considered as necrosis and good therapeutic effect. In 1 case, PET/CT showed 2 metabolically active lesions, while CEUS could identify only one pathological liver lesion.

As a result of the follow-up, including PET/CT, five patients underwent additional RFA for 7 lesions.

In 5 patients that were clinically intended for treatment with RFA, the ^{18}F-FDG PET/CT staging revealed additional extrahepatic lesions; therefore, the treatment plan was changed to a systematic instead of local approach, and the procedure was abandoned. These patients were excluded from the observation group.

Discussion

The use of RFA for liver metastases has been reported to be effective and safe by many authors (4). It does not have as good results in terms of disease-free and long-term survival as surgical treatment (5), but for patients who are not eligible for surgery, it is a valuable non-invasive treatment option. Studies on the long-term survival of non-surgically treated patients with hepatic colorectal metastases who underwent RFA reported a 1-year survival rate of 86%-99%, a 3-year survival rate of 46%-68%, and a 5-year survival rate of 24%-44% (4). The expected effect of RFA is based on thermal destruction of the tumor by variable radiofrequency waves, delivered locally, most often percutaneously, by a special electrode, heating the tissues/aiming to reach 60 °C, which leads to coagulation necrosis (Figure 1).

In the patient group we investigated, RFA ablation was performed under direct ultrasound control with contrast enhancement, and the established clinical protocol for follow up and the evaluation of treatment response was also with CEUS. Contrast enhancement significantly

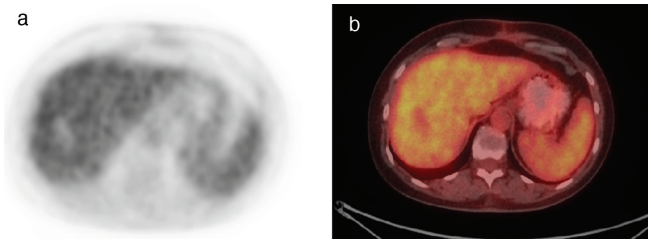

Figure 1. An ^{18}F-FDG-PET/CT of a patient with complete response to the treatment of a liver metastasis of breast cancer 2 months post RFA. The photophenic zone in the 4b liver segment on the metabolic images corresponds with coagulation necrosis. a) PET post-treatment image, axial slice on the level of the 4b segment of the liver, b) fused axial slice on the level of the 4b segment of the liver, post-treatment image

^{18}F-FDG: ^{18}Fluorine-fluorodeoxyglucose, PET/CT: Positron emission tomography/computed tomography, RFA: Radiofrequency ablation

increases the certainty and efficiency of the method. According to the guidelines of the European and World Association for the Application of Ultrasound Methods in Biology and Medicine from 2012, CEUS is indicated for monitoring the effect of RFA, performed on liver tumors, based on comparable results with CT and magnetic resonance imaging (MRI) (6), with sensitivity and specificity reaching 80%-90%, according to the literature data (7). It is inexpensive, accessible, not connected with any additional radiation burden for the patient, and it is possible to perform follow-up studies in a very short period before or after PET/CT and, if needed, serial additional studies. The final result is greater certainty for the therapeutic effect of RFA (Figure 2).

To get the most out of the obtained PET/CT information and to perform a reliable interpretation, it is important to select the patients correctly. Most often, patients with tumors that are not expected to utilize ^{18}F-FDG (such as differentiated HCC, mucinous colon carcinomas, clear cell renal cell carcinoma, etc.) should not be examined. All patients undergoing RFA of liver lesions, which are intended to be followed up with PET/CT, should have a baseline study before the procedure so that the metabolic changes in the lesion in addition to the morphological data can be tracked, and a more precise and complex treatment response decision can be made (Figure 3, 4).

As stated earlier, five patients were ruled out of the treated and investigated group (approximately 40% of the patients referred for staging) because the PET/CT showed a greater extent of the disease such as additional metastases in lymph nodes, lung, and bones or more extensive liver involvement than initially expected, and the management plan was changed.

To avoid false-positive results, e.g., inflamed tissue around the region of ablation, the timing of the PET/CT examination after the ablation is very important; it should either be before the beginning of the reparative processes or after they have resolved. The protocol we have adopted is to scan patients around 2 months after treatment. However, according to some data, PET/CT could be a very useful methodology for evaluating ablation immediately after the procedure-up to 48 hours, with high (up to 100%) (8) sensitivity for a residual tumor, much better than all other imaging methods. This is due to the loss of the ability of the ablation-treated cells to accumulate glucose and they are imaged as a photopenic zone. The concomitant peripheral hyperemia, in all other imaging studies, visible as peripheral enhancement, is very difficult to distinguish from a residual tumor. The nuclear medicine examination does not show increased glucose metabolism in such a

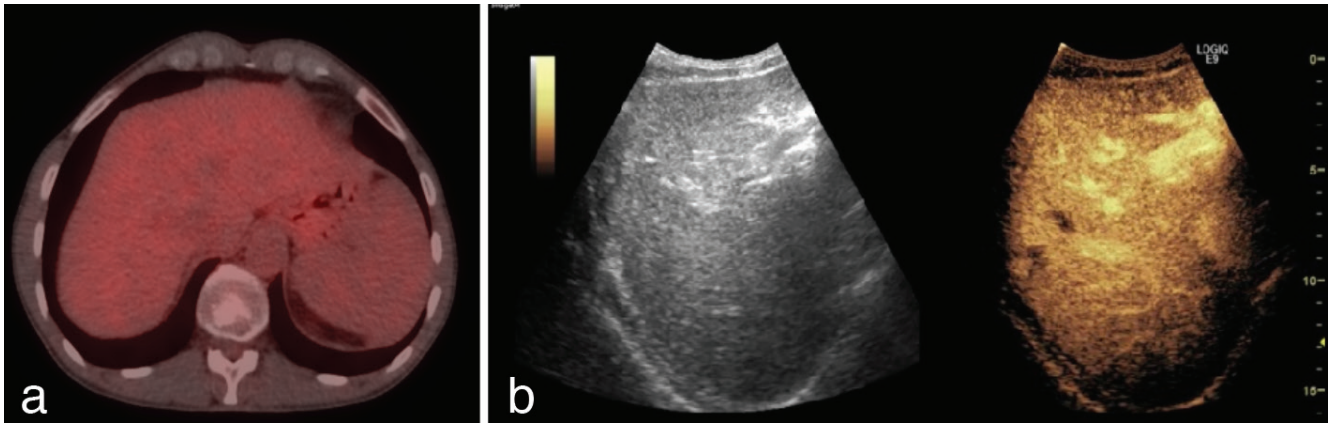

Figure 2. A patient with liver metastasis from colorectal cancer with complete response 2 months after RFA. The PET/CT images show no metabolic or morphological abnormalities in the area of the ablated lesion. CEUS shows full necrosis of the lesion in the 7th liver segment. a) Axial fused post-treatment image on the level of 7th liver segment, b) CEUS post-treatment image

RFA: Radiofrequency ablation, PET/CT: Positron emission tomography/computed tomography, CEUS: Contrast-enhanced ultrasound examination

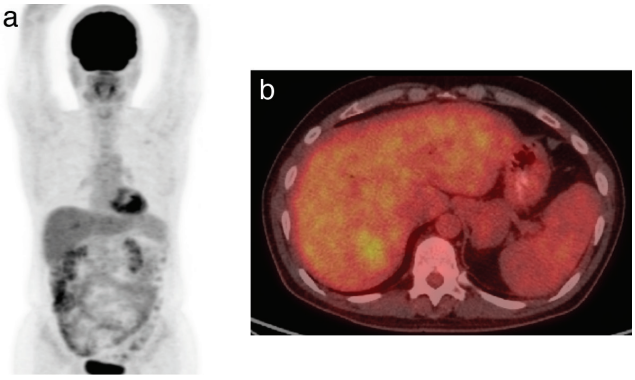

Figure 3. A baseline PET/CT examination of a patient with a solitary liver metastasis from pancreatic carcinoma in the 7th liver segment with SUV_{max} 3.6, which was treated with RFA a week after this study. a) MIP projection, pre-treatment image, b) axial fused pre-treatment image on the level of the 7th liver segment

PET/CT: Positron emission tomography/computed tomography, RFA: Radiofrequency ablation, SUV_{max}: Maximum standard uptake value, MIP: Maximum intensity projection

short period; accordingly, the presence of an area with increased metabolic activity up to the 48th hour on ^{18}F-FDG PET/CT is most likely due to a residual tumor and could be further re-ablated (9,10).

According to other authors, PET/CT examinations must be performed 2 months after RFA (9,11), as this is the shortest period that allows for evaluation of the treatment effect with a low likelihood of false-positive lesions due to active necrotic and inflammatory changes after treatment. We have accepted this protocol as it is more convenient than other approaches and safer for patients in terms of the radiation burden.

A study by Chen et al. (12) suggested that ^{18}F-FDG is superior to MRI and/or CT, with overall accuracies of 87.9%, 75.0%, and 64.3%, respectively, and is more cost-effective in post-RFA hepatic tumor assessment. The average scan numbers for PET, MRI, and CT to achieve a final accurate diagnosis were 1.121, 1.316, and 1.250, respectively. As stated earlier, CEUS is reported to have similar sensitivity and specificity of CT and MRT for assessment of liver metastases (7), thus it could be expected that PET/CT would also be superior to CEUS. However, there are no reliable data comparing directly the performance of both methods for this indication.

It is expected that in many patients, the disease will progress over time, despite treatment, so long-term follow-up is required and should include not only local treatment evaluation of the liver with US but also whole-body PET/CT scans, which have the potential to give more accurate information on the disease (Figure 5, 6).

According to our experience, patient monitoring and follow-up strategies need to be carried out by a multidisciplinary team consisting of a gastroenterologist, nuclear medicine specialist, oncologist, surgeon, and radiologist in order to determine further management. It is important that RFA, although intended to be a substitute, does not exclude the possibility of any subsequent surgical treatment if it is clinically appropriate.

If needed, RFA must be combined with systemic therapy (chemotherapy, hormones, immuno-, targeting, etc.), with an expected improvement in survival. There are active studies that specifically investigate certain therapies in combination with RFA of liver lesions, such as EORTC-1560-GITCG, which evaluates the effects of immunotherapy with

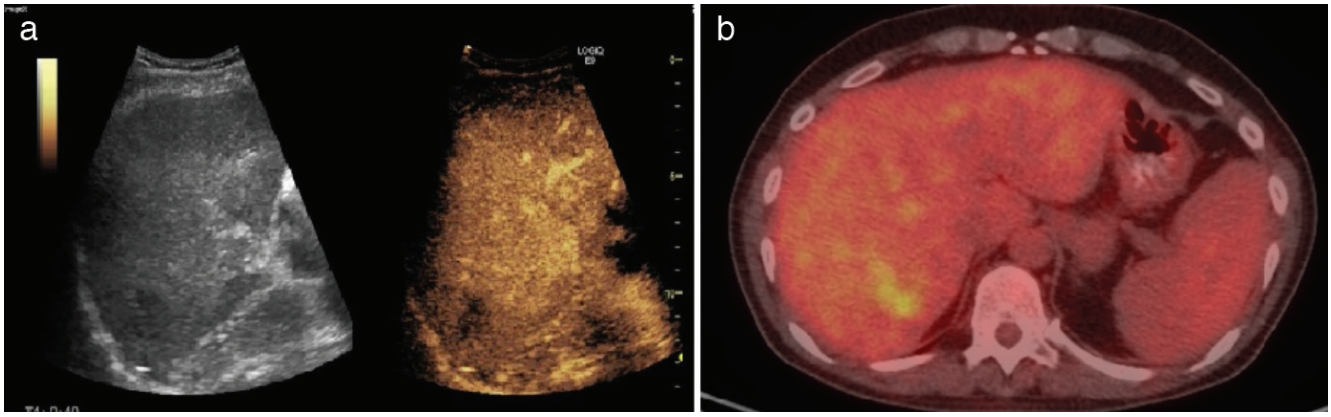

Figure 4. Results from the restaging PET/CT and CEUS of the same patient performed 2 months after the RFA were discrepant. The CEUS showed complete necrosis, interpreted as complete response, while on PET/CT there was a persistent metabolically active lesion with partial reduction of the size and activity (SUV_{max} 3), interpreted as partial response. a) CEUS, post-treatment image showing complete necrosis, b) fused axial image on the level of the 7th liver segment, post-treatment, showing a persistent metabolically active lesion with partial reduction of the size and activity

PET/CT: Positron emission tomography/computed tomography, CEUS: Contrast-enhanced ultrasound examination, RFA: Radiofrequency ablation, SUV_{max}: Maximum standard uptake value

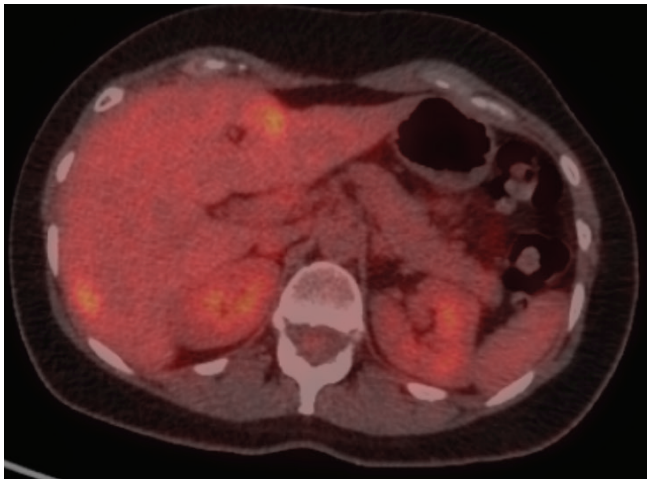

Figure 5. A baseline PET/CT of a patient with 2 liver metastases from breast cancer, who was treated with RFA. Pre-treatment axial fused slice on the level of liver segments 2 and 7, showing metabolically active liver lesions respectively with SUV_{max} 5.2 and SUV_{max} 4.3

PET/CT: Positron emission tomography/computed tomography, RFA: Radiofrequency ablation, SUV_{max}: Maximum standard uptake value

durvalumab and tremelimumab in combination with RFA or stereotactic radiosurgery. However, all of them are at an early stage, and further results are expected.

A few studies are available (13) on the role of SUV values as a prognostic biomarker prior to the ablation of liver lesions. At this stage, it has been found that low baseline SUV values for colorectal cancer correlate with prolonged liver failure-free survival.

Study Limitations

The main limitation of the study is the low number of included patients, which is not sufficient to make general conclusions and recommendations. However, the literature review showed that this is a common limitation of all of the research performed on this topic, so any additional data could make a contribution.

The lack of baseline PET/CT in many of the cases was challenging in terms of treatment response evaluation. However, in clinical settings, such as the one in which this study was conducted, there are some practical limitations (cost, time effectiveness, radiation burden, etc.), and having a PET/CT performed before each RFA was not achievable. When possible, a PET/CT should be conducted within a month before the ablation to select the patients that are likely to benefit from the treatment and to have a basis for comparison with the following PET/CT studies.

The possibility of false-negative results must also be considered for reliable and objective evaluation, most often in small (less than 5-10 mm). A more convincing result can be achieved by late scanning or additional software image processing. In both cases the aim is to improve the ratio of suspected lesions to background activity. The most common false-positive results that we should keep in mind are active reparative changes and liver abscesses (14).

Conclusion

According to our preliminary data, PET/CT may be a valuable method, with comparable or eventually even better sensitivity than CEUS, for early evaluation of the

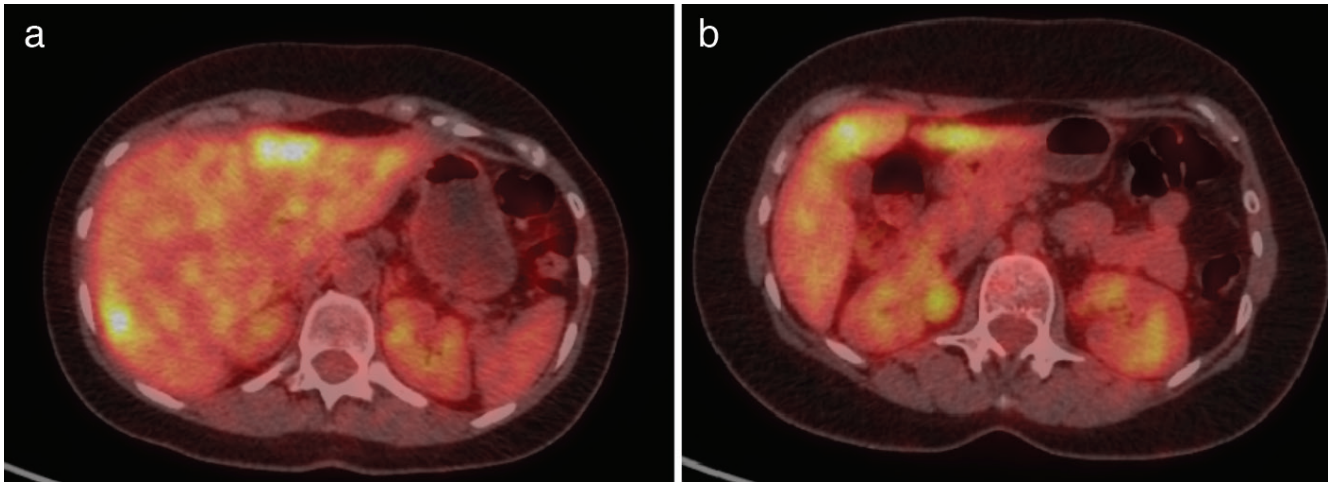

Figure 6. A restaging PET/CT of the same patient, showing progression 2 months after RFA with new liver lesion and increased size and activity of the ablated lesions. a) Fused axial post treatment image on the level of liver segments 2 and 7, showing metabolically active liver lesions respectively with SUV_{max} 5.5 and SUV_{max} 5.8. b) Fused axial post treatment image on the level of liver segment 4b, showing a new metastatic lesion with SUV_{max} 4.7

PET/CT: Positron emission tomography/computed tomography, RFA: Radiofrequency ablation, SUV_{max}: Maximum standard uptake value

efficacy of RFA for the treatment of metastatic and primary liver lesions and planning of future treatment.

PET/CT might be recommended as a staging method before undergoing RFA of liver lesions to determine the local extent of the disease in the liver in combination with CEUS with an advantage in visualization of extrahepatic involvement.

However, more patients must investigated in order to demonstrate and confirm the obtained results with certainty.

Ethics

Ethics Committee Approval: The study protocol was approved by the Ethics Committee of Acibadem City Clinic (date: 12.10.2018, approval no: 11-07-80).

Informed Consent: All patients signed informed consent forms, agreeing that the obtained data be used for scientific purposes.

Peer-review: Externally and internally peer-reviewed.

Authorship Contributions

Surgical and Medical Practices: G.M., S.H., I.K., Concept: G.M., S.H., I.K., Design: G.M., S.H., I.K., Data Collection or Processing: G.M., Analysis or Interpretation: G.M., Literature Search: G.M., Writing: G.M.

Conflict of Interest: No conflict of interest was declared by the authors.

Financial Disclosure: The authors declared that this study has received no financial support.

References

1. Cornelis F, Sotirchos V, Violari E, Sofocleous CT, Schoder H, Durack JC, Siegelbaum RH, Maybody M, Humm J, Solomon SB. 18F-FDG PET/CT Is an Immediate Imaging Biomarker of Treatment Success After Liver Metastasis Ablation. J Nucl Med 2016;57:1052-1057.
2. Takahashi H, Berber E. Role of thermal ablation in the management of colorectal liver metastasis. Hepatobiliary Surg Nutr 2020;9:49-58.
3. O JH, Lodge MA, Wahl RL. Practical PERCIST: A Simplified Guide to PET Response Criteria in Solid Tumors 1.0. Radiology 2016;280:576-584.
4. Lencioni R, Crocetti L. Radiofrequency ablation of liver cancer. Tech Vasc Interv Radiol 2007;10:38-46.
5. Abdalla EK, Vauthey JN, Ellis LM, Ellis V, Pollock R, Broglio KR, Hess K, Curley SA. Recurrence and outcomes following hepatic resection, radiofrequency ablation, and combined resection/ablation for colorectal liver metastases. Ann Surg 2004;239:825-827.
6. Claudon M, Dietrich CF, Choi BI, Cosgrove DO, Kudo M, Nolsøe CP, Piscaglia F, Wilson SR, Barr RG, Chammas MC, Chaubal NG, Chen MH, Clevert DA, Correas JM, Ding H, Forsberg F, Fowlkes JB, Gibson RN, Goldberg BB, Lassau N, Leen EL, Mattrey RF, Moriyasu F, Solbiati L, Weskott HP, Xu HX. Guidelines and good clinical practice recommendations for contrast enhanced ultrasound (CEUS) in the liver–update 2012: a WFUMB-EFSUMB initiative in cooperation with representatives of AFSUMB, AIUM, ASUM, FLAUS and ICUS. Ultraschall Med 2013;34:11-29.
7. Larsen LP. Role of contrast enhanced ultrasonography in the assessment of hepatic metastases: A review. World J Hepatol 2010;2:8-15.
8. Anderson GS, Brinkmann F, Soulen MC, Alavi A, Zhuang H. FDG positron emission tomography in the surveillance of hepatic tumors treated with radiofrequency ablation. Clin Nucl Med 2003;28:192-197.
9. McLoney ED, Isaacson AJ, Keating P. The Role of PET Imaging Before, During, and After Percutaneous Hepatic and Pulmonary Tumor Ablation. Semin Intervent Radiol 2014;31:187-192.
10. Antoch G, Vogt FM, Veit P, Freudenberg LS, Blechschmid N, Dirsch O, Bockisch A, Forsting M, Debatin JF, Kuehl H. Assessment of liver tissue after radiofrequency ablation: findings with different imaging procedures. J Nucl Med 2005;46:520-525.

11. Travaini LL, Trifirò G, Ravasi L, Monfardini L, Della Vigna P, Bonomo G, Chiappa A, Mallia A, Ferrari M, Orsi F, Paganelli G. Role of [18F] FDG-PET/CT after radiofrequency ablation of liver metastases: preliminary results. Eur J Nucl Med Mol Imaging 2008;35:1316-1322.
12. Chen W, Zhuang H, Cheng G, Torigian DA, Alavi A. Comparison of FDG-PET, MRI and CT for post radiofrequency ablation evaluation of hepatic tumors. Ann Nucl Med 2013;27:58-64.
13. Samim M, Prevoo W, de Wit-van der Veen BJ, Kuhlmann KF, Ruers T, van Hillegersberg R, van den Bosch MAAJ, Verkooijen HM, Lam MGEH, Stokkel MPM. 18F-FDG PET as novel imaging biomarker for disease progression after ablation therapy in colorectal liver metastases. Eur J Nucl Med Mol Imaging 2017;44:1165-1175.
14. Poulou LS, Ziakas PD, Ziogas DC, Doxani C, Xyla V, Vakrinos G, Voulgarelis M, Thanos L. FDG-PET for detecting local tumor recurrence of ablated liver metastases: a diagnostic meta-analysis. Biomarkers 012;17:532-538.

Original Article
Mol Imaging Radionucl Ther 2021;30:8-17 DOI:10.4274/mirt.galenos.2020.24392

The Diagnostic Contribution of SPECT/CT Imaging in the Assessment of Gastrointestinal Bleeding: Especially for Previously Operated Patients

Gastrointestinal Kanama Yeri Değerlendirilmesinde SPECT/BT'nin Tanısal Yeteneği ve Katkısı: Özellikle Ameliyat Öyküsü Bulunan Hastalarda

Selin Soyluoğlu, Ülkü Korkmaz, Büşra Özdemir, Gülay Durmuş Altun

Trakya University Faculty of Medicine, Department of Nuclear Medicine, Edirne, Turkey

Abstract

Objectives: Gastrointestinal bleeding (GIB) is a life-threatening problem that requires a multidisciplinary approach for successful treatment. This study aims to emphasize the clinical contribution of single photon emission computed tomography/computed tomography (SPECT/CT) for the diagnosis of acute bleeding.

Methods: All 14 patients referred to the nuclear medicine department in 3 years with suspicion of acute GIB were evaluated retrospectively. Clinical records were analyzed to assess the scintigraphic findings, emphasizing the correlative contribution of the CT portion on SPECT/CT studies.

Results: Five patients were negative on dynamic and static planar images. SPECT/CT was performed in 9 patients who had positive findings on planar imaging. SPECT/CT could identify the same bleeding site originating from the anastomosis in four patients with a history of abdominal surgery. SPECT/CT confirmed bleeding from the cecum in a patient with cervical cancer. SPECT/CT showed the bleeding focus in the bladder neck of a patient with bladder cancer and the bleeding from peritoneal metastases of a patient with gastric cancer. In 1 patient, the right upper quadrant activity accumulation, which may cause false positives, was found to be the gallbladder on SPECT/CT. Delayed images showed the true bleeding focus in the cecum. In 1 patient, suspicious activity accumulation in the midline of the abdomen was found to be due to a previously unknown aortic aneurysm on SPECT/CT.

Conclusion: SPECT/CT imaging is a feasible technique to facilitate image interpretation in patients with GIB. SPECT/CT imaging can guide the surgeon through more accurate localization. Therefore, for proper patient management, SPECT/CT should be applied to detect the bleeding focus, if present, especially in patients who had undergone a previous operation.

Keywords: Gastrointestinal hemorrhage, red blood cell scintigraphy, single photon emission computed tomography/computed tomography

Öz

Amaç: Gastrointestinal kanama (GİK), başarılı bir tedavi için multidisipliner yaklaşım gerektiren hayati önemde bir sorundur. Çalışmamızda akut kanama tanısında tek foton emisyonlu bilgisayarlı tomografi/bilgisayarlı tomografinin (SPECT/BT) klinik katkısını vurgulamayı amaçladık.

Yöntem: Üç yıllık bir dönemde akut GİK şüphesi ile nükleer tıp bölümüne başvuran 14 hastanın tümü retrospektif olarak incelendi. Sintigrafik bulguları, SPECT/BT çalışmalarında BT kısmının korelatif katkısına vurgu yaparak değerlendirebilmek için klinik kayıtlar analiz edildi.

Bulgular: Beş hastanın dinamik ve statik görüntüleme bulguları negatifti. Planar görüntülerde pozitif bulguları olan 9 hastaya SPECT/BT yapıldı. SPECT/BT, abdominal cerrahi öyküsü olan dört hastada anastomozdan kaynaklanan kanama yerini tam olarak gösterdi. Serviks kanseri tanılı bir hastada çekumdan kanama gösterildi. SPECT/BT, mesane kanseri olan bir hastanın primer tümörünün arka duvarından kaynaklanan kanama

Address for Correspondence: Selin Soyluoğlu MD, Trakya University Faculty of Medicine, Department of Nuclear Medicine, Edirne, Turkey
Phone: +90 555 749 11 83 **E-mail:** dr.selina@gmail.com ORCID ID: orcid.org/0000-0003-4473-7138
Received: 21.06.2020 **Accepted:** 09.08.2020

odağını ve mide kanseri olan diğer bir hastanın periton metastazına uyan alanda aktivite birikimini saptadı. Bir hastada sağ üst kadranda yanlış pozitifliğe neden olabilecek aktivite birikimi SPECT/BT'de safra kesesi olarak bulundu ve devam edilen geç görüntülerde çekumda gerçek kanama odağı saptanabildi. Bir hastada, karın orta hatta izlenen şüpheli aktivite birikiminin SPECT/BT'de, daha önceden bilinmeyen aort anevrizmasına bağlı olduğu bulundu.

Sonuç: SPECT/BT görüntüleme, GİK'li hastalarda görüntü yorumlanmasını kolaylaştırmak için kullanılabilecek bir tekniktir. SPECT/BT, tam lokalizasyonun belirlenebilmesi sayesinde cerraha rehberlik edebilir. Bu nedenle, özellikle geçirilmiş operasyon öyküsü bulunan hastalarda kanama odağını tespit etmek için SPECT/BT uygulanmalıdır.

Anahtar kelimeler: Gastrointestinal kanama, işaretli eritrosit sintigrafisi, tek foton emisyonlu bilgisayarlı tomografi/bilgisayarlı tomografi

Introduction

Gastrointestinal bleeding (GIB) is a serious clinical problem with 10% mortality despite advanced diagnostic and treatment methods. Eighty percent of lower GIB stop spontaneously, but 25% of them start to bleed again, and about 10%-15% require emergency surgery. It is essential to find the bleeding site before any intervention. If the location of lower GIB cannot be determined, surgical treatment options, such as left hemicolectomy, blind segmental colectomy, radical subtotal colectomy, or multiple colostomies, may be required to control bleeding. However, despite all these efforts, the source of upper or lower GIB may be due to unpredictable causes (1,2,3,4,5).

Diagnosis is based on history, physical examination, laboratory, endoscopy, selective angiography, and technetium-99m (Tc-99m) labeled red blood cell (RBC) scintigraphy. Compared with angiography, the advantages of the scintigraphic method are non-invasive and can show bleeding at lower rates, such as 0.05-0.1 mL/min compared with 0.5 mL/min for angiography. While endoscopy and angiography often fail to show intermittent bleeding, it is possible to perform imaging of the entire abdomen until the next day with a single radioactive drug dose administered for the scintigraphic method, allowing intermittent and slower bleeding rates to show. Therefore, some authors recommend evaluating patients by scintigraphic methods before endoscopy or angiography (6,7).

GIB scintigraphy can be performed with Tc-99m RBC or Tc-99m sulfur colloid. However, Tc-99m sulfur colloid has a lower sensitivity due to background activity in the reticuloendothelial system and shorter intravascular half-life. Tc-99m RBC allows continuous imaging over many hours with a convenient intravascular half-life.

Tc-99m RBC GIB scintigraphy is routinely started with 30 minutes of dynamic imaging. Continuous monitoring should be performed as far as possible to identify the source of bleeding. If no GIB is detected, a minimum of 60 minutes of initial imaging is recommended.

The correct localization of the bleeding site can be made by identifying the extravasated blood's initial location and monitoring the blood's movement from that region in the gut lumen. More images may be required to differentiate small bowel bleeding from large intestinal bleeding. The guideline recommends adding single photon emission computed tomography (SPECT) or SPECT/computed tomography (CT) to the imaging to localize the site precisely (8).

SPECT/CT hybrid devices are imaging systems that allow both SPECT and CT imaging to be performed using the same patient bed in the same system. In this way, both pathophysiological information from SPECT imaging and morphological information from CT can be obtained simultaneously. Anatomic localization of the lesions can be performed more accurately and efficiently. SPECT/CT imaging more useful than SPECT and CT imaging alone by improving localization of abnormal and physiologic findings, providing additional information for interpretation, and ensuring definitive diagnostic certainty (9).

This study aims to determine the contribution of SPECT/CT to the clinic by comparing the results of SPECT/CT fusion images taken in addition to standard planar images in patients referred to our department for Tc-99m RBC scintigraphy for the differential diagnosis of acute GIB.

Materials and Methods

Patients referred to the nuclear medicine department to identify a bleeding site between January 2017 and January 2020 were evaluated retrospectively. Fourteen patients who underwent Tc-99m RBC scintigraphies between these dates were included in the study.

The modified *in vivo* method was used to label RBCs. A lyophilized pyrophosphate (PYP) kit was prepared by diluting 6 cc saline. The kit was incubated for 10 minutes at room temperature, and patients were injected with 2-3 ccs of PYP intravenously. After 20 minutes, each patient had 15 ccs of blood drawn into a heparin-washed syringe. After adding 20 mCi Tc-99m, the injector was incubated for 20 minutes at room temperature with little shaking. At the end of the incubation period, all injector contents were injected into the patients.

After radioactivity administration, nuclear angiography images were acquired immediately at 1 second per frame for 1 minute, then with dynamic images at 60 seconds per frame for 60 minutes (matrix size, 128x128 pixels). At the end of dynamic imaging, additional static images were taken in posterior and lateral projections. If images were out of focus or there were no suspicious findings in the first evaluation, late static images were taken hourly at 2-6 hours (matrix size, 256x256 pixels). Static imaging was continued until 24 hours in cases evaluated as negative. In the early dynamic and subsequent static images, extra Tc-99m RBC accumulation sites other than the physiological areas and vascular structures were interpreted as positive and continued to delay imaging for accurate localization. SPECT/CT was performed when an abnormal RBC accumulation site was suspected based on the planar imaging findings. All SPECT/CT images were acquired using a hybrid system (GE Healthcare, Optima NM/CT 640). SPECT data were acquired for the region of interest (matrix size, 128x128 pixels, 6° angle steps, 20 s/frame). The acquisition parameters for CT were: 130 keV, pitch 1.0, rotation time 0.6 s, and slice thickness 2.5 mm.

Planar and SPECT/CT images were evaluated by two experienced nuclear medicine specialists. All final judgments were made by consensus.

All case images, reports, and follow-up files were evaluated individually to determine the relative performance of planar and SPECT/CT imaging. The additional contribution of SPECT/CT to detect the presence/absence of bleeding and identify the correct localization during scintigraphic evaluation. Patients were followed up to verify the planar and SPECT/CT results.

This retrospective study was performed in accordance with the ethical concepts of the Declaration of Helsinki, October 2013, and approved by the institutional ethical review board (approval number: 22 April 2019-TUTF-BAEK 2019/185). Informed consent was obtained from participants.

Descriptive statistics were used to describe the demographic characteristics of the patients. No other statistical method was needed.

Results

A total of fourteen patients, six females and eight males, aged between one and 75 (mean, 54.4±6.4) years, were included in the study.

Five patients were negative on dynamic and static planar images. Since in our department, SPECT/CT is not routinely applied to patients whose planar images are negative, in accordance with the guideline (8), SPECT/CT was not required in these patients. One patient had a colonoscopy diagnosed with chronic colitis. Three patients had endoscopy; their diagnoses were hemorrhagic antral gastritis, erythematous antral gastritis, and chronic gastritis. No further diagnostic study was required because they did not have any evidence of further bleeding, and their clinical findings improved. These patients were considered true negatives.

Nine patients had a suspicious appearance of bleeding on planar images; SPECT/CT was performed on all of them. The clinical and scintigraphic characteristics of all patients are summarized in Table 1.

Three patients had a high probability of bleeding at early planar images. One patient had a history of gastroenteropancreatic-neuroendocrine tumor (GEP-NET), and the other 2 had gastric cancer. They all had a Roux-en-Y surgical procedure. SPECT/CT imaging was performed to enhance the anatomy altered after surgery and the relationship between bleeding and the operation site. In SPECT/CT fusion images, it was evident that the bleeding focus matched the anastomosis area at the operation site. The patient with GEP-NET and one of the gastric cancer patients underwent a second operation to stop bleeding. Surgical intervention was not required for the other patient because of the patient's low bleeding rate and stable vital findings that did not progress. Follow-up was continued with oncological treatment.

In 1 of the 2 patients whose early images were negative for hemorrhage, in the second-hour study, there was a suspected area in the right lower quadrant. The patient had been treated for cervical cancer with chemotherapy and pelvic radiotherapy. SPECT/CT imaging was performed to identify the location of the bleeding. On SPECT/CT, the hemorrhage was reported to be consistent with the cecum. The anticoagulant drug that the patient was using was discontinued, and an elective colonoscopy was planned. However, as the bleeding findings regressed, it was not needed. The other patient's first day images showed no signs of bleeding. At the 24th hour, the planar image revealed a focal accumulation area in the abdomen's upper quadrant. SPECT/CT images of the patient who had a history of operation due to colon cancer revealed that bleeding focus was at the operating site (Figure 1). No further operation was required due to the intermittent feature and low flow rate of bleeding. Oncological treatment was continued.

The moderate activity accumulation area observed in the early images of a patient at the midline of the abdomen's upper quadrant showed an atypical diffuse distribution on

late images. The patient was diagnosed with metastatic gastric cancer and had no operation. SPECT/CT imaging was performed to localize the extravasated activity. Based on the findings of CT images, it was concluded that the activity in the upper abdomen was related to the hypervascular primary tumor area, and the mild diffuse accumulation in the abdomen that was seen on late images was due to bleeding from peritoneal metastases. Paracentesis was

Table 1. Clinical and scintigraphic characteristics of patients

Previous diagnosis	Previous surgery	Planar finding	SPECT/CT findings	Treatment
GEP-NET	Roux-en-Y surgery	SPE	Bleeding from anastomosis line	Re-surgery
Gastric cancer	Roux-en-Y surgery	SPE	Bleeding from anastomosis line	Re-surgery
Gastric cancer	Roux-en-Y surgery	SPE	Bleeding from anastomosis line	MT
Cervix cancer	No	SPL	Cecum	ADI
Colon cancer	Tumor resection	SPL	Bleeding from anastomosis line	MT
Gastric cancer	No	SPE	Hypervascular primary tumor area and bleeding from peritoneal metastases	MT and PPC
Bladder cancer	No	SPE	Bleeding focus in bladder neck	OT
None	No	SPE	Cecum (early false positivity in the gallbladder)	ADI
None	No	SPE	Incidentally detected abdominal aortic aneurysm	None, ICF
CCC	No	Negative	Has not been applied	None, ICF
None	No	Negative	Has not been applied	None, ICF
EHG	No	Negative	Has not been applied	None, ICF
EEG	No	Negative	Has not been applied	None, ICF
EHG	No	Negative	Has not been applied	None, ICF

SPECT/CT: Single photon emission computed tomography/computed tomography, GEP: Gastroenteropancreatic, NET: Neuroendocrine tumor, CCC: Colonoscopy chronic colitis, EHG: Endoscopy hemorrhagic antral gastritis, EEG: Endoscopy erythematous antral gastritis, SPE: Suspicion in early images, SPL: Suspicion in late images, MT: Medical treatment, ADI: Anticoagulant drug interrupted, PPC: Permanent peritoneal catheter, OT: Oncological treatment, ICF: Improvement in clinical findings

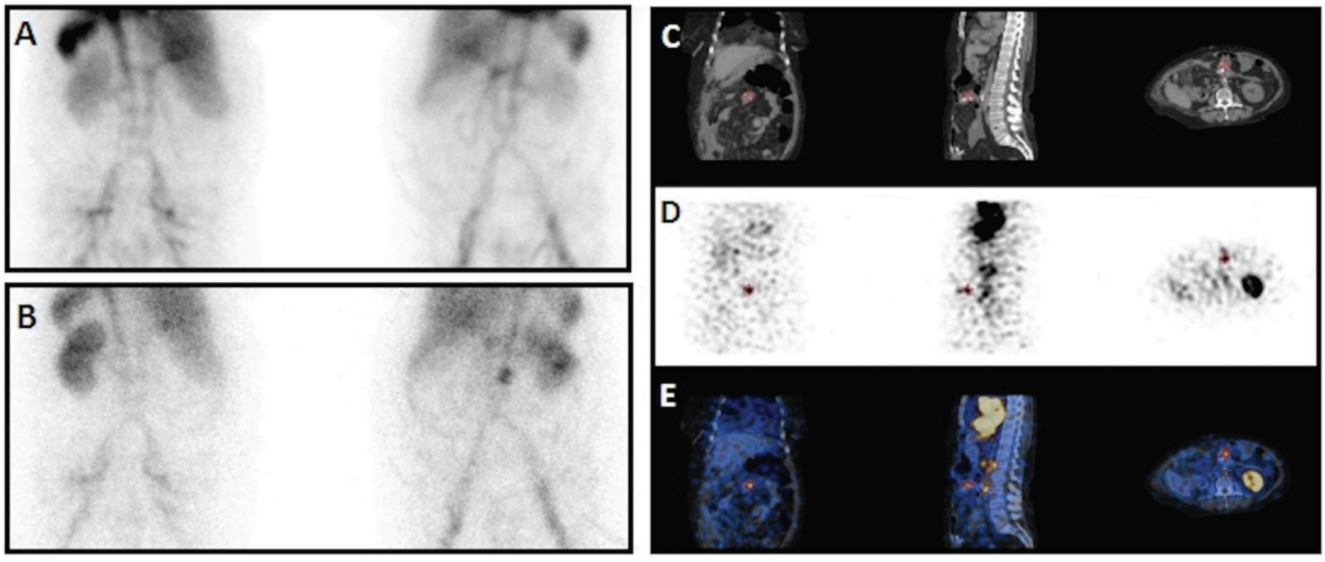

Figure 1. A 73-year-old female with a history of colon cancer, had no signs of bleeding on the 1st day of scintigraphic imaging [(A) posterior and anterior planar images]. At the 24th hour, a focal activity accumulation in the upper quadrant of the abdomen was revealed [(B) posterior and anterior planar images]. SPECT/CT images showed that bleeding focus was at the operating site of colon cancer [(C) CT, (D) SPECT, (E) fused SPECT/CT images in coronal, sagittal, and axial planes, respectively]

SPECT/CT: Single photon emission computed tomography/computed tomography

performed, and the peritoneal fluid was hemorrhagic. A permanent peritoneal catheter was inserted.

In a patient who had intermittent hematuria and progressive anemia, labeled RBC scintigraphy was performed to exclude any other bleeding foci. While there was no area to suggest bleeding in the abdomen, SPECT/CT showed that the bleeding focus was in the bladder neck. The patient had a diagnosis of ureteral cancer and bladder cancer and a history of transurethral resection of the bladder repeatedly. It was confirmed that hematuria was solely responsible for the patient's anemia.

In 1 case, early abdomen images showed increased activity in the right upper quadrant of the abdomen. Early SPECT/CT imaging revealed that this activity was due to increased physiological uptake in the gallbladder. Therefore, when imaging was continued to find the focus of the bleeding, in the third hour, several areas of increased activity appeared in the right lower quadrant. In the fifth hour, widespread accumulation of activity was observed in the caecum, ascending colon, transverse colon, and descending colon. A second SPECT/CT scan was performed. On SPECT/CT, the bleeding was confirmed to originate from the ileocecal region. Colonoscopy confirmed submucosal hemorrhages in this region. The anticoagulant drug that the patient was using for a while was discontinued. The bleeding stopped spontaneously. No operation was needed (Figure 2).

Early images of another patient showed increased uptake in the midline of the abdomen adjacent to the aorta. In the late images, increased uptake in this area continued, whereas nothing suggested active bleeding in any other region. SPECT/CT imaging was performed to interpret this area with increased uptake more accurately. In the CT component of SPECT/CT, it was clearly understood that this area was consistent with the previously unknown aortic aneurysm (Figure 3). A bleeding site could not be shown. No further intervention was done as the general condition of the patient improved.

All cases with SPECT/CT images had successful image fusion. Therefore, anatomic localization could be made easily. For cases in which the localization of bleeding could be predicted on planar images, SPECT/CT confirmed the exact location.

Discussion

GIB scintigraphy is a noninvasive method that can detect bleeding with high sensitivity, localize the bleeding area, and contribute to the predictive ability by showing the approximate bleeding volume (8). However, for some

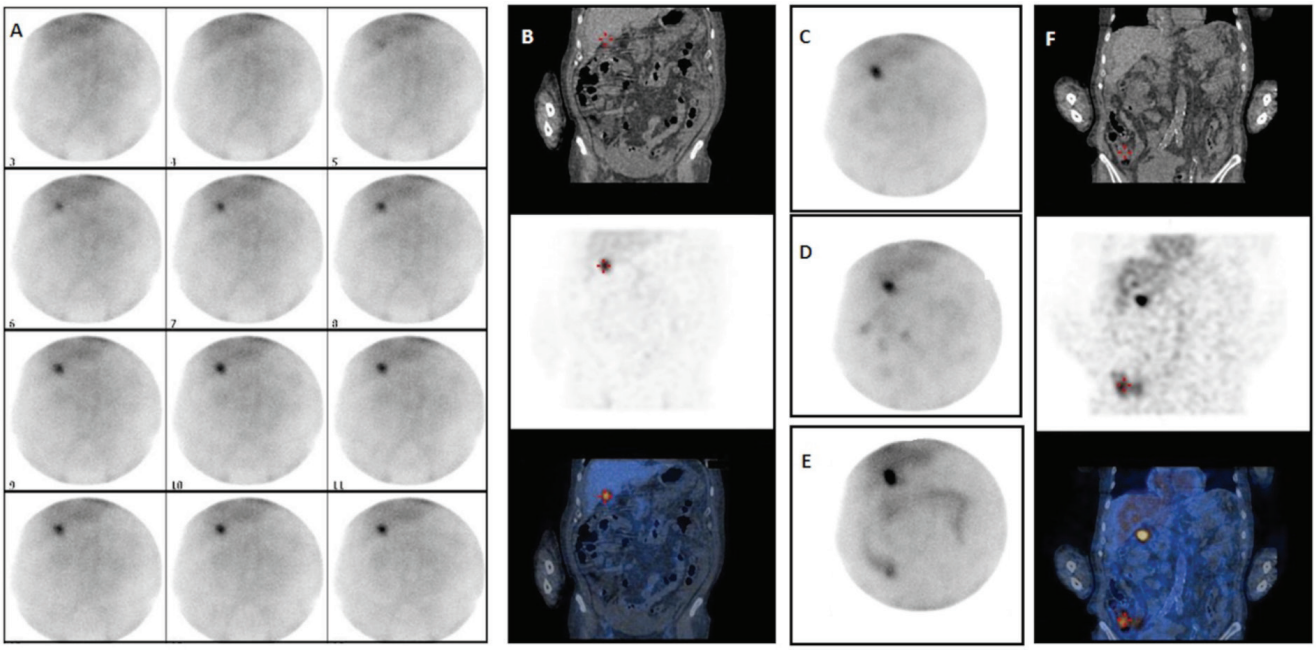

Figure 2. A 72-year-old male with intense activity in the upper right quadrant of the abdomen since the beginning of dynamic images (A). An early SPECT/CT imaging [(B) CT, SPECT, and fused SPECT/CT coronal planes] revealed that this area corresponded to the gallbladder. Therefore, imaging was continued to find the focus of the bleeding. While no additional finding was observed in the first-hour planar images (C), several areas of increased activity appeared in the third (D) and fifth hour (E) planar images. On a second late SPECT/CT, the bleeding was confirmed to originate from the ileocecal valve region [(F) CT, SPECT, and fused SPECT/CT coronal planes]

SPECT/CT: Single photon emission computed tomography/computed tomography

cases, it can be challenging to localize the particular hemorrhage site. Other conventional imaging modalities of the patient may be helpful, but the time interval between them would make it difficult to establish the relationship between bleeding and anatomy. Especially for bleeding that may require surgical procedures, it is more important to determine the exact location of the bleeding. Seven of our patients had previously been treated for various types of cancers. Four of them had a history of abdominal surgery. Knowing the surgically altered anatomy, understanding the characteristics of hypervascular primary tumors and their metastases, and determining the relationship between these areas and activity accumulation areas detected on planar images, can be achieved easily and non-invasively by SPECT/CT. In a study by Schillaci et al. (10), SPECT/CT was able to localize the focus of bleeding in 10 positive cases but non-localizing on planar images. In addition, SPECT/CT changed the results in seven of 19 patients. With the anatomical contribution of CT, SPECT/CT can provide higher overall accuracy than single nuclear imaging.

Four patients in our study had a history of abdominal surgery, and the bleeding site originated at the anastomosis. Three of them were in the jejunojejunal anastomosis region after the Roux-en-Y operation, and the other was in the stapled anastomosis region after colorectal surgery. GIB after GI operations and stapled anastomosis is a rare complication (11,12). SPECT/CT can be essential in operated patients to enhance the understanding of the anatomy altered after surgery and the relationship between bleeding and the operation site (13).

Although nuclear medicine bleeding scintigraphy is mostly used to establish the location of GIB, it is also possible to detect bleeding areas outside of the GI tract. We had 2 examinations, in which the bleeding sites were located outside of the GI tube. One involved the hemorrhage of peritoneal metastases of gastric cancer, and the other involved the bleeding focus in the bladder neck. In cases of suspicious bleeding in patients with a history of trauma or a predisposition to bleeding, Tc-99m RBC imaging may have a role in determining the presence and location of active bleeding in non-GI areas. The reason for this is that Tc-99m RBC imaging has the advantage of imaging for up to 24-hr postinjection and the ability to screen the entire body with a single drug dose. Gonzalez et al. (14) presented three cases of examples as labeled RBC scintigraphy showed the active hemorrhage areas outside of the GI system. Scintigraphy of a patient who had fallen down a flight of stairs two weeks ago and had severe anemia showing increased activity consistent with active bleeding in the chest wall. In another patient with a history of several falls, scintigraphy showed a large, cold defect consistent with a hematoma in his mid-thigh and multiple foci of increased uptake consistent with active bleeding areas around it. Otomi et al. (15) reported 2 patients with bleeding located outside of the GI system, in a study of 20 patients, one massive subcutaneous lumbar hematoma,

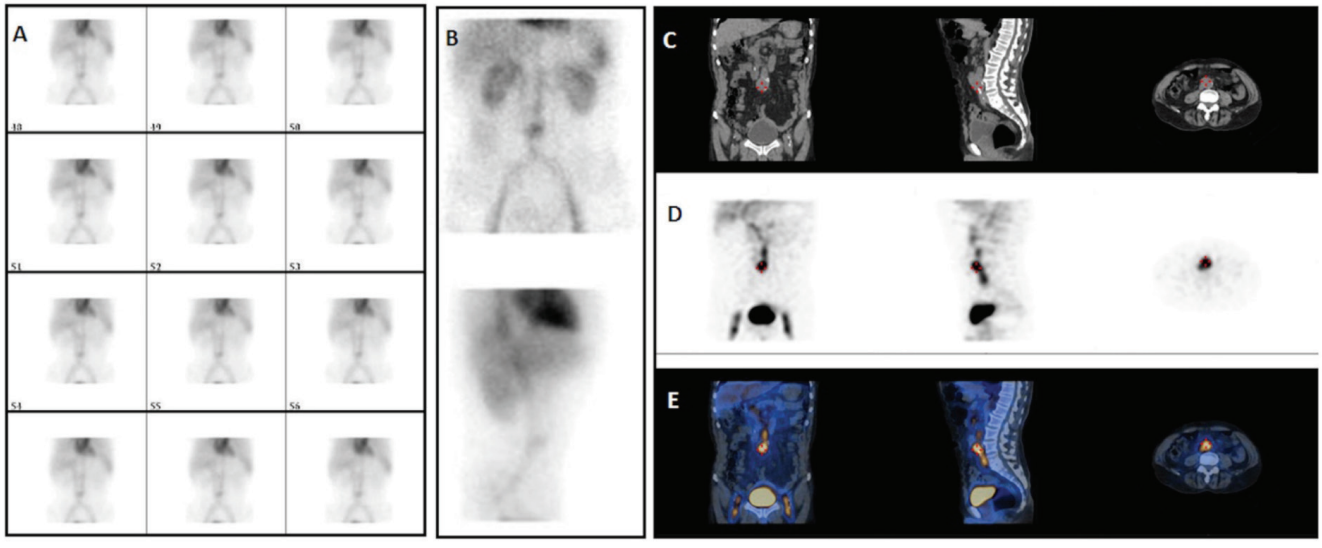

Figure 3. Increased uptake in the midline of the abdomen adjacent to the aorta was noted since the beginning of dynamic images of a 63-year-old male (A). In the late planar images, increased uptake in this area continued, whereas no other area suggested active bleeding in another region [(B) anterior and lateral planar images]. SPECT/CT imaging was performed to interpret this area more accurately with increased uptake. The CT component of SPECT/CT was consistent with the previously unknown aortic aneurysm [(C) CT, (D) SPECT, (E) fused SPECT/CT images in coronal, sagittal, and axial planes]

SPECT/CT: Single photon emission computed tomography/computed tomography

and one intraperitoneal rupture of a left gastric artery aneurysm. There are several studies in which the bleeding areas have been successfully identified in different parts of the body, such as the extremities, joints, lung, mesenteric region, breast, thyroid, and occult pericardial hemorrhage immediately after open-heart surgery (14,16,17,18). SPECT/CT will also be very beneficial when evaluating such cases.

One particular patient group for whom scintigraphy is even more critical for its non-invasive screening capability of active bleeding foci in the whole body are those with hemophilia, other coagulation disorders, and receiving anticoagulant therapy. In these patients, where invasive techniques are undesirable, any bleeding area's location and activity become crucial regarding an emergency intervention (19). Park et al. (20) reported that the incidence of GIB was 12.6% (28 of 222 patients) in adult patients with severe aplastic anemia, and in 34.4% (11 patients) of them, the bleeding site was unknown. Even differential diagnosis of chronic arthropathy and acutely bleeding joints can be performed safely in hemophilic arthropathy, which will develop in 50% of patients with hemophilia (21). We had no patients with hemophilia but had 2 patients who were receiving anticoagulant therapy. SPECT/CT could detect the intermittent- and low-volume bleeding sites non-invasively. After positive scintigraphy results, anticoagulant drugs that the patients were using for a while were interrupted.

According to the Society of Nuclear Medicine and Molecular Imaging guideline, it is recommended to start imaging with dynamic nuclear angiography images at a rate of 1-3 seconds per frame for 1 minute (8). Then, dynamic imaging should be continued with a maximum rate of 60 seconds per frame. Imaging should be continued, if possible, for at least one hour until the bleeding source is detected. Due to this, nuclear angiography and subsequent early dynamic images, vascular anatomy, anomalies, and malformations can be easily exposed, and false-positive results can be prevented. For example, in 1 of our patients, increased uptake in the abdomen's midline adjacent to the aorta was observed since the angiography phase. No other area was found to suggest active bleeding. SPECT/CT imaging was performed to interpret this area of increased uptake in the midline more accurately. In the CT component of SPECT/CT, it was clearly understood that this field was consistent with the previously unknown aortic aneurysm. An abdominal aortic aneurysm is the most common aortic pathology. It is mostly asymptomatic and found incidentally.

Aneurysm rupture is a medical emergency, and surgical intervention is recommended for all symptomatic aneurysms and asymptomatic aneurysms greater than 5.5 cm in diameter. It is fatal in roughly 80% of cases if not treated immediately (22). With Tc-99m RBC scintigraphy, an aortic aneurysm could be diagnosed incidentally. SPECT/CT may contribute by confirming this finding, determining its clinical significance, and whether it requires immediate intervention. In a case presented by Duarte et al. (23), a patient had a Tc-99m RBC scintigraphy to identify GIB, not a GIB site, but a persistent radioactive accumulation seen as a part of the aorta. Because bleeding stopped without intervention, their patient refused the further examination. However, he had a ruptured aortic aneurysm after 17 months. When such previously unknown abnormalities are detected, the addition of SPECT/CT to the standard imaging protocol might be a life-saving contribution to the patient's clinic and follow-up.

Although not included in our clinical series, many other vascular abnormalities other than aortic aneurysm may be incidentally detected on GIB scintigraphy studies, such as hemangiomas, great vessel tortuosity, varices, arteriovenous malformations, and aortaenteric fistulas (24,25,26,27). Clinicians should be aware that these vascular anomalies may cause false-positive results for GIB. Chen and Brown (28) reported a patient with ileal varices that led to a false-positive interpretation of GIB scintigraphy. Ileal varices in the right lower quadrant filling from the superior mesenteric and ileocolic veins of a patient with previously unknown cirrhosis simulate a GIB pattern. They emphasized that it would have been better if a SPECT/CT was done to determine the activity's exact location.

When evaluating Tc-99m RBC scintigraphy, activity accumulation in an area outside the normal distribution in the abdominal and pelvic regions is considered positive. However, if the patient's structural anomalies and other diseases are unknown, false-positive results may occur when the bleeding is interpreted. One of our patients had increased activity in the right upper quadrant of the abdomen on early static images, which was suspicious of bleeding in this region. However, this increased activity did not show any movement, and the intensity of the activity did not change much over time. SPECT/CT revealed that this increased activity belonged to the increased physiological gallbladder uptake. Therefore, when imaging continues to find the true focus of bleeding on late images, additional increased activity areas of the right abdomen were observed from the third hour onwards. In a late second SPECT/CT, activity was concentrated in the ileocecal region, and it was concluded that the bleeding originated here. During Tc-99m RBC scintigraphy, gallbladder visualization is not a common finding but has been reported in the literature. The mechanism of increased uptake in the gallbladder is

not well known, but the most common features are renal insufficiency, anemia, and multiple blood transfusions. Our patient had a history of chronic renal failure. As far as we can tell from the literature, there is no typical gallbladder uptake pattern.

In Wang et al.'s (29) case report, no suspicious focus was detected in the first and fifth hours of static images of a 50-year-old patient with chronic renal failure and resultant severe anemia. On the twenty-second hour images, they found suspicious and increased activity at the liver's inferior border on static images. The subsequently acquired SPECT/CT images located the activity in the gallbladder (29). In Kumar et al.'s (30) case, an abnormal focal uptake in the right hypochondrium was detected on second-hour static images of a 16-year-old boy known for chronic glomerulonephritis and had a history of renal transplantation. Subsequently, SPECT/CT imaging located the uptake in the gallbladder. In our patient, increased uptake in the right upper quadrant compatible with gallbladder fossa was noticed from the beginning of early dynamic images. The literature contains reports demonstrating visualization of the gallbladder at different hours and different intensities during Tc-99m RBC scintigraphy (31,32,33). SPECT/CT can verify that this increased uptake belongs to the gallbladder. Therefore, it helps to avoid false positivity and guides to continue imaging to find the true focus of bleeding.

SPECT/CT can also facilitate the differentiation of other conditions identified as pitfalls in GIB reporting. Physiological genital activities, such as physiological penile activity and endometrial proliferation in the ovulatory cycle, can be mistaken for the bleeding site (34,35). Kidney activity may be confused, especially in unknown abnormalities, such as ectopic and horseshoe kidneys (36,37). Even if it is known, SPECT/CT will make it much easier to make a differentiation. Splenic pathologies, such as the accessory spleen, splenius, and splenic infarct, may also mimic GIB (38,39,40).

Studies showed that SPECT/CT scan could better determine the bleeding site when it cannot be well localized, or indeterminate on planar images, or differentiate physiological causes from pathological activity. In a study, SPECT/CT could indicate a localization in all 10 patients whose location could not be determined by planar imaging. SPECT/CT showed the accurate bleeding focus verified by other modalities and surgery in 12 of 13 patients. In 10 patients where planar imaging localized the bleeding focus, SPECT/CT confirmed seven foci while correcting three localizations (10). In addition to its contribution to detecting and confirming the localization of bleeding, SPECT/CT can more accurately predict the length of the bleeding area and help decide which endoscopic approach to use for evaluation (41).

Study Limitations

There were some limitations to our study. First, the study was a retrospective, single-institution study with a limited sample size. Similar studies were published before by Schillaci et al. (10) and Otomi et al. (15), as we referenced. This study's proposed novelty was that SPECT/CT afforded the added benefit of localizing the bleeding, especially in patients with a history of previous operation or cancer, as they made up most of our patient group. We also aimed to demonstrate that there may be a wide variety of causes for false positives that can be quickly resolved with SPECT/CT. This limited number of patients made a significant contribution with SPECT/CT. However, the results of a more extensive series of studies will provide more reliable information about the true value of this contribution.

Conclusion

Tc-99m RBC scintigraphy is an easily applicable diagnostic test that can show the focus of bleeding, more sensitively than any other technique, even at low bleeding rates or intermittent bleeding.

In addition, if SPECT/CT imaging is added, it can provide information about the etiology of the bleeding site and identify additional anomalies that can cause false positives. Furthermore, SPECT/CT can quickly analyze altered anatomy and the relationship between bleeding site-primary tumor in cancer patients and bleeding site-operation site in previously operated patients. SPECT/CT imaging can guide the surgeon for more accurate localization. Therefore, for proper patient management, SPECT/CT should be applied to detect the bleeding focus, if present.

Ethics

Ethics Committee Approval: This retrospective study was performed in accordance with the ethical concepts of the Declaration of Helsinki, October 2013, and approved by the institutional ethical review board (approval number: 22 April 2019-TUTF-BAEK 2019/185).

Informed Consent: Informed consent was obtained from participants.

Peer-review: Externally and internally peer-reviewed.

Authorship Contributions

Surgical and Medical Practices: S.S., Ü.K., B.Ö., G.D.A., Concept: S.S., G.D.A., Design: S.S., G.D.A., Data Collection or Processing: S.S., Ü.K., B.Ö., Analysis or Interpretation: S.S., G.D.A., Literature Search: S.S., Ü.K., B.Ö., Writing: S.S.

Conflict of Interest: No conflict of interest was declared by the authors.

Financial Disclosure: The authors declared that this study has received no financial support.

References

1. Rollandi LP, Kasper J, Schaller T. Seltene Ursache einer gastrointestinalen Blutung [Rare cause of gastrointestinal bleeding]. Dtsch Med Wochenschr 2019;144:1505-1508.
2. Yilmaz S, Dursun M, Canoruç F, Bayan K, Büyükbayram H. Upper gastrointestinal bleeding caused by small-cell lung cancer: a case report. Dig Dis Sci 2006;51:788-790.
3. Hoekstra E, van den Berg MW, Veenendaal RA, Stuyt R. The natural progression of a fistulizing gallstone resulting in massive gastrointestinal hemorrhage and Bouveret syndrome, a rare case. Clin J Gastroenterol 2020;13:393-396.
4. Henderson L, Nour S, Dagash H. Heterotopic Pancreas: A Rare Cause of Gastrointestinal Bleeding in Children. Dig Dis Sci 2018;63:1363-1365.
5. Borum ML. Cavernous colorectal hemangioma: a rare cause of lower gastrointestinal bleeding and a review of the literatüre. Dig Dis Sci 1997;42:2468-2470.
6. Al Qahtani AR, Satin R, Stern J, Gordon PH. Investigative modalities for massive lower gastrointestinal bleeding. World J Surg 2002;26:620-625.
7. Winzelberg GG, McKusick KA, Froelich JW, Callahan RJ, Strauss HW. Detection of gastrointestinal bleeding with 99mTc-labeled red blood cells. Semin Nucl Med 1982;12:139-146.
8. Dam HQ, Brandon DC, Grantham VV, Hilson AJ, Howarth DM, Maurer AH, Stabin MG, Tulchinsky M, Ziessman HA, Zuckier LS. The SNMMI procedure standard/EANM practice guideline for gastrointestinal bleeding scintigraphy. 2.0. J Nucl Med Technol 2014;42:308-317.
9. Jacene HA, Goetze S, Patel H, Wahl RL, Ziessman HA. Advantages of Hybrid SPECT/CT vs SPECT Alone. The Open Medical Imaging Journal 2008;2:67-79.
10. Schillaci O, Spanu A, Tagliabue L, Filippi L, Danieli R, Palumbo B, Del Sole A, Madeddu G. SPECT/CT with a hybrid imaging system in the study of lower gastrointestinal bleeding with technetium-99m red blood cells. Q J Nucl Med Mol Imaging 2009;53:281-289.
11. Acquafresca PA, Palermo M, Rogula T, Duza GE, Serra E. Early surgical complications after gastric by-pass: a literature review. Arq Bras Cir Dig 2015;28:74-80.
12. Martínez-Serrano MA, Parés D, Pera M, Pascual M, Courtier R, Egea MJ, Grande L. Management of lower gastrointestinal bleeding after colorectal resection and stapled anastomosis. Tech Coloproctol 2009;13:49-53.
13. Kotani K, Kawabe J, Higashiyama S, Yoshida A, Kawamura E, Kawahata H, Yamanaga T, Katayama Y, Shiomi S. Diagnostic ability of (99m)Tc-HSA-DTPA scintigraphy in combination with SPECT/CT for gastrointestinal bleeding. Abdom Imaging 2014;39:677-684.
14. Gonzalez CE, Fig LM, Cano M, Gross MD, Shapiro B. Technetium-99m-red blood cell scintigraphy in the localization of nonenteric hemorrhage. J Nucl Med 1994;35:1333-1337.
15. Otomi Y, Otsuka H, Terazawa K, Yamanaka M, Obama Y, Arase M, Otomo M, Irahara S, Kubo M, Uyama N, Abe T, Harada M. The diagnostic ability of SPECT/CT fusion imaging for gastrointestinal bleeding: a retrospective study. BMC Gastroenterol 2018;18:183.
16. Gips S, Israel O. Scintigraphic detection of bleeding after transfemoral arteriography, using technetium-99m labeled RBCs. Clin Nucl Med 1986;11:669.
17. Kim EE, McConnell BG, Brown JS, McConnell RW, Close LG. Radionuclide demonstration of acute hemorrhage into follicular adenoma of the thyroid. Clin Nucl Med 1983;8:23-25.
18. Bateman TM, Czer LS, Gray RJ, Kass RM, Raymond MJ, Garcia EV, Chaux A, Matloff JM, Berman DS. Detection of occult pericardial hemorrhage early after open-heart surgery using technetium-99m red blood cell radionuclide ventriculography. Am Heart J 1984;108:1198-1206.
19. Orzel JA, Rudd TG, Oreskovich M. Evaluation of traumatic mesenteric hemorrhage in a hemophiliac with Tc-99m labeled red blood cell scintigraphy. J Trauma 1986;26:1056-1057.
20. Park YB, Lee JW, Cho BS, Min WS, Cheung DY, Kim JI, Cho SH, Park SH, Kim JK, Han SW. Incidence and etiology of overt gastrointestinal bleeding in adult patients with aplastic anemia. Dig Dis Sci 2010;55:73-81.
21. Green D, Spies SM, Rana NA, Milgram JW, Mintzer R. Hemophilic bleeding evaluated by blood pool scanning. Thromb Haemost 1981;45:208-210.
22. Verhoeven EL, Kapma MR, Groen H, Tielliu IF, Zeebregts CJ, Bekkema F, van den Dungen JJ. Mortality of ruptured abdominal aortic aneurysm treated with open or endovascular repair. J Vasc Surg 2008;48:1396-1400.
23. Duarte PS, Zhuang H, Aldighieri F, Ghesani N, Alavi A. Incidental detection of an abdominal aortic aneurysm during evaluation of gastrointestinal bleeding with Tc-99m-tagged erythrocytes. Clin Nucl Med 2002;27:824.
24. Lubin E, Zelikovski A, Trumper J, Weininger J, Rechnic J, Urca I. Saphenous vein varicosities–the use of Tc-99m-RBC blood-pool imaging for evaluation and followup. J Nucl Med 1978;19:1090-1091.
25. Brill DR. Colonic varices demonstrated by technetium-99m red cell scintigraphy. Clin Nucl Med 1987;12:176-179.
26. Hoseinzadeh S, Shafiei B, Salehian M, Neshandar Asli I, Ghodoosi I. Huge Varicose Inferior Mesenteric Vein: an Unanticipated (99m) Tc-labeled Red Blood Cell Scintigraphy Finding. Nucl Med Mol Imaging 2010;44:217-222.
27. Yen CK, Pollycove M, Parker H, Nalls G. Rupture of a spontaneous aortoduodenal fistula visualized with Tc-RBC scintigraphy. J Nucl Med 1983;24:332-333.
28. Chen PN, Brown RK. False positive GI bleed on Tc-99m RBC scintigraphy due to ileal varices. J Radiol Case Rep 2012;6:23-28.
29. Wang L, Jing H, Chen L, Wang Z, Li F. Gallbladder Activity on 99mTc-Labeled Red Cell Scintigraphy Confirmed by SPECT/CT Imaging. Clin Nucl Med 2016;41:734-736.
30. Kumar N, Singh RKR, Dutta D, Ravina M, Kheruka SC, Gambhir S. Gallbladder Visualization on Tc-99m-labeled Red Cell Scintigraphy: A Rare Finding with an Emphasis on Role of Single-photon Emission Computed Tomography/Computed Tomography. Indian J Nucl Med 2017;32:233-234.
31. Brill DR. Gallbladder visualization during technetium-99m-labeled red cell scintigraphy for gastrointestinal bleeding. J Nucl Med 1985;26:1408-1411.
32. Sato S, Kuwajima A, Watanabe S, Nagamoto M, Taki S, Murakami S, Hamada M. Delayed visualization of gallbladder with in vivo labeled Tc-99m-red blood cell scintigraphy for gastrointestinal bleeding. Radiat Med 1988;6:159-161.
33. Abello R, Haynie TP, Kim EE. Pitfalls of a 99mTc-RBC bleeding study due to gallbladder and ileal-loop visualization. Gastrointest Radiol 1991;16:32-34.
34. Wahl RL, Lee ME. Increased genital uptake of 99mTc red blood cells: a potential cause of false-positive studies for gastrointestinal bleeding. Eur J Nucl Med 1984;9:245-246.
35. Erdoğan A, Kara PÖ, Günay EC. A Potential False Positive Finding on 99mTc Red Blood Cell Gastrointestinal Bleeding Scintigraphy. Causa Pedia 2014;3:713.
36. Infante JR, González FM, Vallejo JA, Torres M, Pacheco C, Latre JM. False-positive results of a gastrointestinal bleeding study caused by an ectopic kidney. Clin Nucl Med 2000;25:645-646.

37. Anez LF, Gupta SM. Serendipitous detection of a horseshoe kidney during blood pool imaging for gastrointestinal bleeding. Clin Nucl Med 1992;17:132-133.
38. Heyman S, Sunaryo FP, Ziegler MM. Gastrointestinal bleeding: an accessory spleen causing a false-positive Tc-99m-sulfur colloid study. Clin Nucl Med 1982;7:38-40.
39. Mavi A, Degirmenci B, Bekis R, Durak H. Intra-abdominal splenosis mimicking massive gastrointestinal bleeding. Clin Nucl Med 2003;28:226-227.
40. Aktas GE, Demir SS, Genchellac H, Sarikaya A. Splenic infarction as a pitfall on labeled red blood cell imaging. Indian J Nucl Med 2016;31:72-73.
41. Bentley BS, Tulchinsky M. SPECT/CT helps in localization and guiding management of small bowel gastrointestinal hemorrhage. Clin Nucl Med 2014;39:94-96.

Original Article
Mol Imaging Radionucl Ther 2021;30:18-27 DOI:10.4274/mirt.galenos.2020.64436

^{18}Fluorine-fluorodeoxyglucose PET/CT Imaging in Childhood Malignancies

Çocukluk Çağı Malignitelerinde ^{18}Flor-florodeoksiglukoz PET/BT Görüntüleme

Nilüfer Bıçakçı[1], Murat Elli[2]

[1]*University of Health Sciences Turkey, Samsun Training and Research Hospital, Clinic of Nuclear Medicine, Samsun, Turkey*
[2]*İstanbul Medipol University Faculty of Medicine, Department of Pediatric Oncology, İstanbul, Turkey*

Abstract

Objectives: The aim of the study was to evaluate the utility of ^{18}fluorine-fluorodeoxyglucose (^{18}F-FDG) positron emission tomography/computed tomography (PET/CT) in the diagnosis, staging, restaging, and treatment response of childhood malignancies.

Methods: This study included 52 patients (32 boys, 20 girls) who were referred to our clinic between November 2008 and December 2018 with the diagnosis of malignancy. The patients were evaluated retrospectively. Median age of the patients was 13 years (range 2-17). ^{18}F-FDG was given to the patients intravenously, and time of flight with PET/16 slice CT was performed 1 hour thereafter. The lowest dose was 2 mCi (74 MBq) and the highest dose was 10 mCi (370 MBq). Fasting blood sugars of all patients were found below 200 mg/dL (11.1 mmol/L).

Results: ^{18}F-FDG PET/CT was performed to evaluate the response to treatment in 38 of 52 children, staging in 11 patients (staging and evaluation of the response to treatment in nine of them), restaging in 2 patients, restaging, and evaluation of the response to treatment in 1 patient. ^{18}F-FDG PET/CT examination was reported as normal in 13 patients (5 girls, 8 boys). The pathological ^{18}F-FDG uptake was detected in 39 patients (14 girls, 25 boys), which indicated metastasis and/or recurrence of the primary disease. Total number of deaths was 30 (13 girls, 17 boys).

Conclusion: ^{18}F-FDG PET/CT has a significant role for staging, restaging, treatment response, and detection of metastatic disease but it is limited for the early diagnosis of childhood cancers.

Keywords: ^{18}F-FDG PET/CT, childhood malignancy, staging, restaging, response

Öz

Amaç: Çalışmamızın amacı, çocukluk çağı malignitelerinin tanı, evreleme, yeniden evreleme ve tedaviye cevabın değerlendirilmesinde ^{18}flor-florodeoksiglukoz (^{18}F-FDG) pozitron emisyon tomografisi/bilgisayarlı tomografinin (PET/BT) yararını göstermektir.

Yöntem: Kasım 2008 ve Aralık 2018 tarihleri arasında, malignensi tanılı 52 hastanın (32 erkek, 20 kız) dosyaları ve görüntüleri geriye dönük olarak incelendi. Ortalama yaş 13 (2-17) idi. ^{18}F-FDG'nin intravenöz enjeksiyonundan 1 saat sonra, time of flight/16 kesit BT yapıldı. Çalışmamızda en düşük doz 2 mCi (74 MBq), en yüksek doz 10 mCi (370 MBq). Tüm hastaların açlık kan şekerleri 200 mg/dL'nin (11,1 mmol/L) altındaydı.

Bulgular: ^{18}F-FDG PET/BT, 52 hastanın 38'ine tedaviye yanıt değerlendirilmesi, 11 hastaya evreleme (9 hasta evreleme ve aynı zamanda tedaviye yanıt değerlendirilmesi), 2 hastaya yeniden evreleme, 1 hastaya yeniden evreleme ve tedaviye yanıt değerlendirilmesi amacıyla yapıldı. ^{18}F-FDG PET/BT çalışması 13 hastada (5 kız, 8 erkek) normaldi. Otuz dokuz hastada (14 kız, 25 erkek) çalışma, metastaz ve/veya primer hastalığın nüksü ile uyumlu bulundu. Toplam ölüm sayısı 30 (13 kız, 17 erkek) idi.

Sonuç: ^{18}F-FDG PET/BT çocukluk çağı malignensilerinin tanı, evreleme, yeniden evreleme ve tedaviye yanıt değerlendirilmesi açısından çok faydalıdır ancak erken tanıda yararı sınırlıdır.

Anahtar kelimeler: ^{18}F-FDG PET/BT, çocukluk çağı maligniteleri, evreleme, yeniden evreleme, tedaviye yanıt

Address for Correspondence: Nilüfer Bıçakçı MD, University of Health Sciences Turkey, Samsun Training and Research Hospital, Clinic of Nuclear Medicine, Samsun, Turkey
Phone: +90 362 311 15 00 **E-mail:** niluferbicakci@gmail.com ORCID ID: orcid.org/0000-0003-4124-1225
Received: 08.08.2020 **Accepted:** 13.10.2020

Introduction

^{18}Fluorine-fluorodeoxyglucose (^{18}F-FDG) positron emission tomography/computed tomography (PET/CT) plays an important role for diagnosis, staging, restaging, response to treatment, and evaluation of prognosis in childhood malignancies (1,2). PET-only examinations have been replaced by hybrid systems in the recent decades, where PET and CT are used together in oncology (3). In this imaging system, PET and CT are used together for functional data and morphological information, respectively (4). ^{18}F-FDG PET/CT is also known to have high sensitivity and specificity (86% and 80%, respectively) in childhood malignancies (5,6,7).

The type of childhood malignancies varies according to the age groups. The most common childhood malignancy is leukemia with a rate of 30%; other malignancies are brain tumors (20%), lymphomas (14%), neuroblastoma (7%), soft tissue sarcomas (7%), Wilms' tumor (6%), bone tumors (5%), germ cell tumors (3%), melanoma (3%), hepatic tumors (1%), etc. Lymphoma and germ cell tumors are more common in children between the ages of 14 and 19 years (8,9,10,11,12,13,14). The childhood tumors in which ^{18}F-FDG PET/CT is used frequently include lymphomas, brain tumors, soft tissue sarcomas, neuroblastoma, Wilms' tumor, germ cell tumors, and neurofibromatosis 1 (15). The most commonly used radionuclides in nuclear medicine for the cancer imaging are gallium-67 (^{67}Ga) citrate, thallium-201 chloride, technetium-99m sestamibi, and ^{18}F-FDG. ^{18}F-FDG causes lower radiation exposure due to relatively short half-life (110 minutes), and it is also a widely available radionuclide agent (2). ^{18}F-FDG mimics glucose in cell uptake process and thus acts as a marker of glucose usage. ^{18}F-FDG is not a tumor-specific agent and can be kept in cells in case of many physiological and pathological conditions. Dual-time-point imaging can help to increase the specificity of ^{18}F-FDG imaging (3).

We evaluated the role of ^{18}F-FDG PET/CT in diagnosis, staging, restaging, treatment response, and detection of metastatic disease of childhood malignancies in this study.

Materials and Methods

Fifty-two children (32 boys, 20 girls) with tissue-confirmed malignancies underwent ^{18}F-FDG PET/CT examination between November 2008 and December 2018. The median age of the patients was 13 years (range 2-17 years). The study was approved by the University of Health Sciences Turkey, Samsun Training and Research Hospital of Local Ethics Committee (protocol number: GOKA/2020/10/6).

All imaging studies were performed under at least 4 hours of total fasting. The dose of ^{18}F-FDG was calculated as 0.15 mCi/kg (5.55 MBq/kg) between 2008 and 2010. After 2010, it was calculated according to the radiopharmaceutical doses published in the 2016 North American Consensus Guidelines, which has been updated as the whole-body ^{18}F-FDG with 3.7-5.2 MBq/kg (0.1-0.4 mCi/kg), and the minimum dose was recommended as 37 MBq (1 mCi). In our study, the lowest dose was 2 mCi (74 MBq), and the highest dose was 10 mCi (370 MBq). Fasting blood sugar level of all patients was found to be less than 200 mg/dL (11.1 mmol/L). CT parameters were obtained with ultra-low dose (80 kVp, 5 mAs, and 1.5:1 pitch). After 45-60 minutes from application of ^{18}F-FDG, CT images were obtained for attenuation correction without intravenous contrast, and then PET images were gathered. ^{18}F-FDG examination was performed with time of flight PET/16 section CT (Philips Gemini TF), and the PET detector crystal material was LYSO.

Sedation was used in 6 patients who were under 8 years of age during the ^{18}F-FDG PET/CT examination. We used the oral chloral hydrate as 50-70 mg/kg for young children less than 15 kg of body weight, according to application guide of the American Academy of Pediatrics (16,17). This dosage is appropriate in most nuclear medicine applications. In our study it was sufficient for the younger age group.

Brown adipose tissue produces heat in case of exposure to cold and causes focal increased ^{18}F-FDG uptake and may mimic muscle or malignancy (18,19,20). However, diazepam was not used in any of our patients as the waiting room temperatures were ensured to be high enough to prevent cold exposure in our clinic.

^{18}F-FDG PET/CT indications and findings of the patients were analyzed retrospectively. Patient characteristics are listed in Table 1.

No statistical analysis was performed.

Results

^{18}F-FDG PET/CT was applied to 52 children for evaluation of response to treatment in 38, staging in 11 (2 staging and nine staging and evaluating response to treatment), restaging in 2, evaluation of response to treatment with restaging in 1 patient.

Twenty-three patients had the diagnosis of lymphoma [14 non-Hodgkin's lymphoma (NHL), 9 HL], and ^{18}F-FDG PET/CT was performed for staging and response to treatment in 10, for response to treatment in 11, and for restaging in 2 patients. ^{18}F-FDG PET/CT detected more nodal lesions than CT in 10 staged patients. Detection of multiple lesions

Table 1. Patient characteristics

Age	Gender	Diagnosis	Site of primary tumor	PET indication
16	M	Ewing's sarcoma	Right fibula	Therapy response assessment
12	M	Neuroblastoma	Left adrenal gland	Therapy response assessment
16	M	Rhabdomyosarcoma (Li-Fraumeni syndrome)	Right inguinal mass	Therapy response assessment
8	M	Nasopharyngeal cancer	Right posterior wall of the nasopharynx	Therapy response assessment
9	M	Rhabdomyosarcoma	Retroperitoneal mass	Therapy response assessment
11	M	NHL	Abdominal lymphadenopathy	Therapy response assessment
16	F	Ewing's sarcoma	Right femur	Therapy response assessment
7	F	Neuroblastoma	Left adrenal gland	Therapy response assessment
11	F	NHL	Cervical and mediastinal lymphadenopathy	Therapy response assessment
5	F	Immature teratoma	Left adnexa	Staging
4	F	Retinoblastoma	Right eye	Therapy response assessment
9	M	HL	Mediastinal and axillary lymphadenopathy	Therapy response assessment
14	F	Malign mesenchymal tumor	Anterior projection of the right sacroiliac joint	Therapy response assessment
14	M	NHL	Cervical lymphadenopathy	Therapy response assessment
16	M	NHL	Cervical lymphadenopathy	Therapy response assessment
17	M	HL	Mediastinal and axillary lymphadenopathy	Staging
17	M	Ewing's sarcoma	Left femur	Therapy response assessment
9	M	Rhabdomyosarcoma	Left inguinal mass	Therapy response assessment
15	M	Neuroblastoma	Right adrenal gland	Therapy response assessment
15	M	Ewing's sarcoma	Left tibia	Therapy response assessment
2	F	NHL	Mediastinal, axillar, abdominal lymphadenopathy	Therapy response assessment
14	M	HL	Cervical and mediastinal lymphadenopathy	Therapy response assessment
17	F	HL	Cervical lymphadenopathy	Therapy response assessment
5	F	Germ cell tumor	Left adnexal mass	Therapy response assessment
13	F	Malignant melanoma	Back skin	Therapy response assessment
9	F	Neuroblastoma	Abdominal mass	Therapy response assessment
14	F	Malign mesenchymal tumor	Posterior segment of the S1-2	Therapy response assessment
7	F	Neuroblastoma	Abdominal mass	Therapy response assessment
15	M	Testicular cancer	Right testicle	Therapy response assessment
14	F	Malignant mesenchymal tumor	Posterior segment of the sacrum	Therapy response assessment
14	M	Ewing's sarcoma	Right tibia	Therapy response assessment
17	F	Ewing's sarcoma	Sol femur	Staging
4	M	Neuroblastoma	Abdominal mass	Therapy response assessment
13	F	Rhabdomyosarcoma	Left inguinal mass	Therapy response assessment
17	M	Testicular cancer	Left testicle	Therapy response assessment and restaging
5	M	Neuroblastoma	Abdominal mass	Therapy response assessment
13	M	HL	Mediastinal, axillar, abdominal lymphadenopathy	Therapy response assessment

Table 1. Continued

Age	Gender	Diagnosis	Site of primary tumor	PET indication
14	F	NHL (Burkitt's lymphoma)	Cervical lymphadenopathy	Therapy response assessment
11	M	Peripheral primitive neuroectodermal tumor	Left posterior mediastinum	Therapy response assessment
8	F	Ewing's sarcoma	Right femur	Therapy response assessment
15	M	NHL (Burkitt's lymphoma)	Mediastinal, abdominal, and pelvic lymphadenopathy	Staging and therapy response assessment
15	M	NHL	Abdominal lymphadenopathy	Staging and therapy response assessment
14	M	NHL	Abdominal lymphadenopathy	Staging and therapy response assessment
14	M	NHL	Abdominal and pelvic lymphadenopathy	Staging and therapy response assessment
16	M	HL	Cervical lymphadenopathy	Staging and therapy response assessment
15	M	HL	Cervical and mediastinal lymphadenopathy	Staging and therapy response assessment
13	F	NHL	Abdominal lymphadenopathy	Staging and therapy response assessment
11	F	NHL	Abdominal and pelvic lymphadenopathy	Restaging
16	M	HL	Cervical lymphadenopathy	Restaging
15	M	HL	Cervical lymphadenopathy	Therapy response assessment
12	M	NHL	Mediastinal, axillar, abdominal lymphadenopathy	Staging and therapy response assessment
11	M	NHL	Abdominal lymphadenopathy	Staging and therapy response assessment

M: Male, F: Female, HL: Hodgkin's lymphoma, NHL: Non-Hodgkin's lymphoma, PET: Positron emission tomography

in the skeletal system and bone marrow increased the stage in these patients (Figure 1).

Patients with Ewing's sarcoma (ES), rhabdomyosarcoma, neuroblastoma, malignant melanoma, malignant mesenchymal tumor, retinoblastoma, nasopharynx carcinoma, and germ cell tumors did not undergo ^{18}F-FDG PET/CT study before treatment, and ^{18}F-FDG PET/CT was performed after treatment to evaluate the response to treatment. Metastatic disease was detected by ^{18}F-FDG PET/CT in the bone, liver, brain, and abdominal and mediastinal lymph nodes of the patients with neuroblastoma (n=7) during follow-up.

Seven patients with ES and one with peripheric primitive neuroendocrine tumor were evaluated with ^{18}F-FDG PET/CT for local and systemic involvement after chemotherapy. Three local recurrences and five abdominal/inguinal metastatic lymph nodes were detected with the ^{18}F-FDG PET/CT. In patients with rhabdomyosarcoma, ^{18}F-FDG PET/CT detected three recurrent diseases and one metastatic disease on follow-up after adjuvant therapy (one had Li-Fraumeni syndrome).

^{18}F-FDG PET/CT was performed for evaluation of treatment response in 2 patients with testicular carcinoma. In the other patient, ^{18}F-FDG PET/CT was performed for restaging, and a lung metastasis was detected (Figure 2).

No recurrence or metastasis was identified in ^{18}F-FDG PET/CT of 13 patients. Thirty patients died on follow-up; 7 patients had NHL, and the other 23 patients had ES (n=8), neuroblastoma (n=7), rhabdomyosarcoma (n=1), malignant mesenchymal tumor (n=1), germ cell tumor (n=1), immature teratoma (n=1), and retinoblastoma (n=1) (Table 2).

Discussion

Our findings indicate that ^{18}F-FDG PET/CT is an essential imaging modality and provided important information for diagnosis, staging, restaging, evaluation of the response to treatment, and detection of metastatic disease. However,

this study is limited in early diagnosis of childhood malignancies.

Although childhood malignancies are relatively rare as compared to adults, still they are a significant cause of mortality and constitute the second most frequent cause of death after trauma in children (21). Leukemia accounts for more than half of all childhood solid tumors, and the other frequent childhood cancers are brain tumors, lymphomas, neuroblastoma, soft tissue sarcomas, Wilms' tumor, and bone tumors (8,21).

Childhood cancers differ from adults in terms of epidemiology, histological patterns, clinical behavior,

Table 2. Cancer types, numbers, and follow-up results of all patients

Diagnosis	PET/CT results			Ex (n=30)
	Normal	Recurrence	Metastasis	
Non-Hodgkin's lymphoma (n=14)	5	9	0	7
Hodgkin's lymphoma (n=9)	5	4	0	0
Ewing's sarcoma (n=8)	0	3	5	8
Rhabdomyosarcoma (n=4)	0	3	1	4
Neuroblastoma (n=7)	0	0	7	7
Malignant mesenchymal tumor (n=3)	1	0	2	1
Testicular cancer (n=2)	1	0	1	0
Retinoblastoma (n=1)	0	1	0	1
Immature teratoma (n=1)	0	0	1	1
Malignant melanoma (n=1)	0	0	1	0
Nasopharyngeal tumor (n=1)	1	0	0	0
Germ cell tumor (n=1)	0	0	1	1

PET: Positron emission tomography, CT: Computed tomography

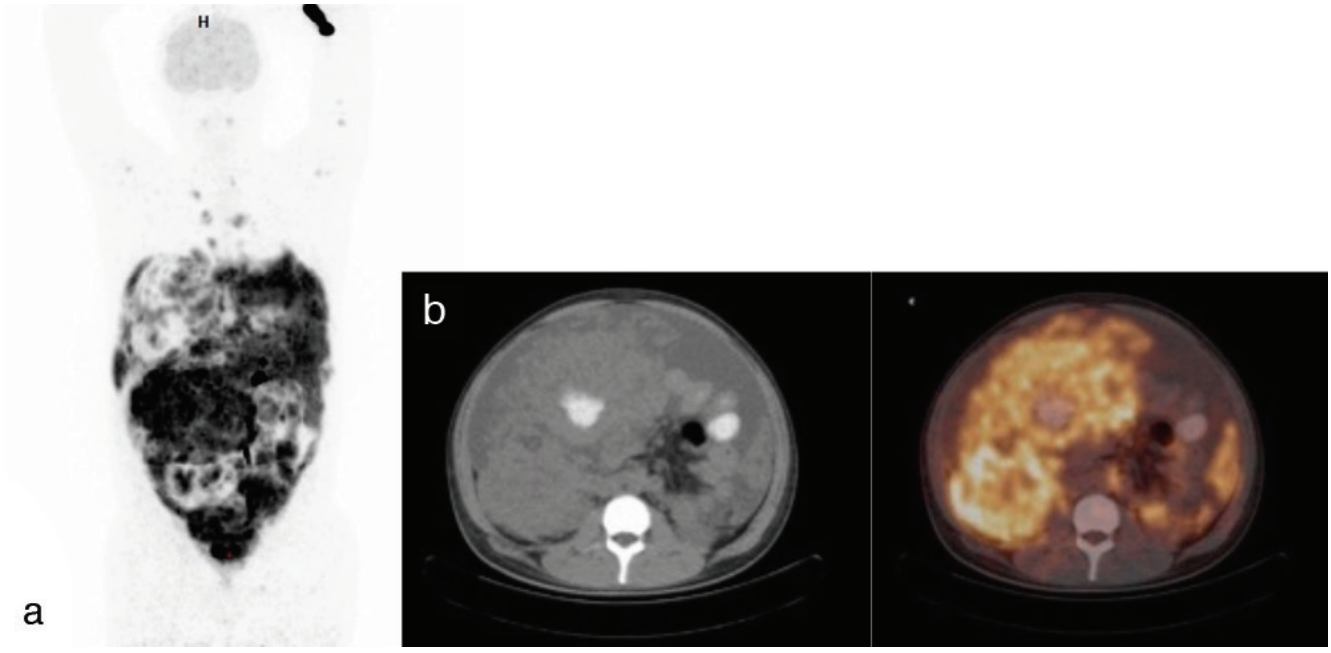

Figure 1. MIP (a), transaxial CT (b), and fusion ^{18}F-FDG PET/CT images of a 15-year-old male patient. Abdominal lymph node biopsy revealed a high-grade malign B-cell lymphoma (Burkitt's lymphoma). Multiple hypermetabolic mediastinal, abdominal, pelvic lymph nodes, massive abdominal fluid, and bone marrow involvement were seen on ^{18}F-FDG PET/CT imaging

^{18}F-FDG: ^{18}Fluorine-fluorodeoxyglucose, PET: Positron emission tomography, CT: Computed tomography, MIP: Maximum intensity projection

treatment response, and prognosis. Appropriate treatment reduces the mortality rate. Early and correct diagnosis is essential. Improved oncological results lead to an increased incidence of late complications of childhood cancers. ^{18}F-FDG PET/CT as an imaging technique is well studied in adults. ^{18}F-FDG PET/CT is increasingly used for staging, prognosis, determination of biopsy location, evaluation of treatment response, radiotherapy planning, and follow-up in many types of childhood cancers (5,22,23,24,25,26,27,28). The role of ^{18}F-FDG PET/CT is, however, limited for the early diagnosis of childhood cancers but has a significant role for staging, treatment response, and detection of metastatic disease. Thus, ^{18}F-FDG PET/CT has been used increasingly in children with malignancy for these features.

^{18}F-FDG is the most commonly used radiopharmaceutical in PET for oncological purposes. ^{18}F-FDG is a cyclotron radiopharmaceutical with a half-life of 110 minutes. ^{18}F-FDG is a glucose analog and is transported into the cell by glucose transporters and often participates in the first stage of the physiological glycolytic pathway. Therefore, the degree of ^{18}F-FDG uptake indicates the metabolic activity of the cells (29). Evaluation after treatment with therapeutic agents does not affect tumor size immediately but inhibits tumor metabolism and proliferation. So, accumulation of ^{18}F-FDG in metabolically active tumor cells has revolutionized oncological imaging. Although this discovery was made several decades ago, the ability of ^{18}F-FDG PET imaging for differentiation of active/stable disease and to provide more clinical information than the simple anatomical localization of the disease has been appreciated recently.

New generation PET devices are faster and have higher resolution. ^{18}F-FDG PET reflects both the metabolic status and the proliferative potential of the disease in patients receiving either conventional or experimental therapy. ^{18}F-FDG PET can be used in the majority of childhood cancers as convenient as CT and magnetic resonance imaging (MRI) (30,31,32,33). Metabolic changes induced by chemotherapy occur before morphological changes. Since the ^{18}F-FDG intake provides direct measurement of tumor glucose metabolism, the tumor's response to treatment can be evaluated earlier before the tumor shrinks. The response to treatment may also be predicted more accurately than conventional techniques (34,35,36,37). In our study, we also used ^{18}F-FDG as imaging radiopharmaceutical in all pediatric patients. We adjusted the radiopharmaceutical doses in children in line with the 2016 North American Consensus Guidelines renewed in 2010 and later (38,39).

Lymphomas are the third most common type of tumor in the childhood group that account for 14% of all cancer cases. While NHL is more commonly found in young children, HL is more common in the adolescent group. ^{18}F-FDG PET/CT is used for staging, evaluation of treatment response, and relapse of disease, before bone marrow or stem cell

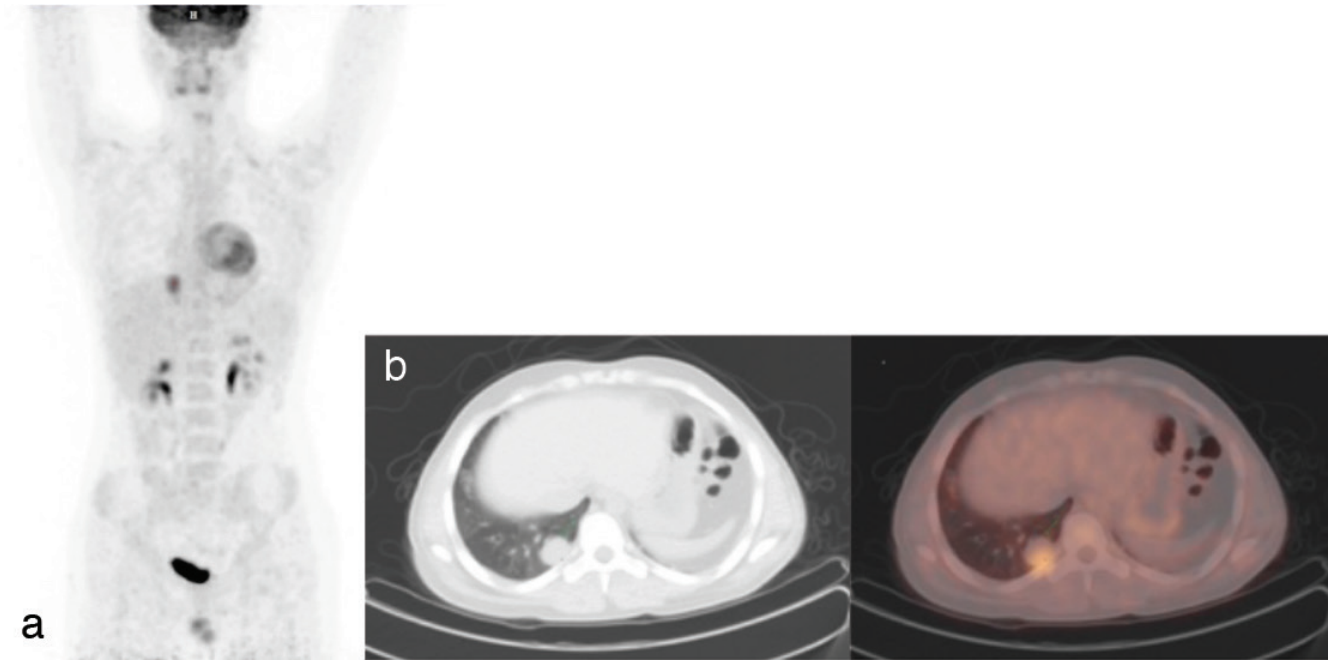

Figure 2. MIP (a), transaxial CT (b), and fusion ^{18}F-FDG PET/CT images of a 16-year-old male patient. Histopathologically, diagnosis was rhabdomyosarcoma. Hypermetabolic metastatic nodule was seen in the right lung posterobasal segment on ^{18}F-FDG PET/CT imaging

^{18}F-FDG: ^{18}Fluorine-fluorodeoxyglucose, PET: Positron emission tomography, CT: Computed tomography, MIP: Maximum intensity projection

transplantation for diagnostic and prognostic information in children (40). London et al. (41) in their study compared conventional imaging methods (CT, ultrasonography, MRI, and bone scintigraphy) with ^{18}F-FDG PET/CT in pediatric patients diagnosed with HL and NHL to differentiate malignant lesion and to predict poor response to treatment. The sensitivity, specificity, and accuracy (95.9%, 99.7%, and 99.6%, respectively) of ^{18}F-FDG PET/CT were found to be higher than other conventional imaging methods (70.1%, 99.0%, and 98.3%, respectively) for lymphoma in children. In a study by Cheng et al. (6), ^{18}F-FDG PET/CT detected lesions that could not be detected by CT in 50% of children with HL and 42.9% of children with NHL. In our study ^{18}F-FDG PET/CT detected more nodal lesions than CT in 10 patients (50% of children with HL and 50% of children with NHL). The stage of malignancy was also increased because of additional lesions in the skeletal system and bone marrow in these patients.

Tumors of sympathetic nervous system constitute about 7% of all childhood tumors, and neuroblastoma is the most common tumor in this group (42). Approximately 10% of neuroblastomas do not uptake metaiodobenzylguanidine (MIBG), and ^{18}F-FDG PET/CT can be used in the evaluation of MIBG-negative patients (42,43,44). Another study reported that MIBG scintigraphy and ^{18}F-FDG PET/CT were equally effective for patients with distant disease in demonstrating bone metastases after primary tumor resection and chemotherapy (45). Choi et al. (46) showed that ^{18}F-FDG PET/CT is more sensitive than CT for evaluation of distant lymph node metastases and can detect recurrent lymph node metastases. Similarly, bone, liver, brain, and widespread lymph node metastases in the abdomen and mediastinum were detected by ^{18}F-FDG PET/CT in our patients with neuroblastoma after the adjuvant therapy. Other alternative diagnostic imaging technique in neuroblastoma without MIBG uptake has been investigated including radiolabeled somatostatin analogs such as octreotide and DOTA-conjugated peptides [e.g., ^{68}Ga DOTATATE (DOTA0-Try3) octreotate], ^{68}Ga DOTATOC (DOTA0-Try3) octreotide, and ^{68}Ga DATANOC (DOTA0-1NaI3) octreotide. These analogs can bind selectively to somatostatin receptors 2 (47). DOTA-peptides can also be labeled with beta-emitting isotopes, for example, ^{177}Lu or ^{90}Y, to provide peptide receptor radionuclide therapy for neuroendocrine tumors in adults (48,49,50,51,52,53,54) and have been used in small studies with relapsed neuroblastoma in children (55,56,57,58).

ES is a heterogenous tumor including ES of the bone, extraosseous ES, and peripheral primitive neuroectodermal tumor. It is the second most common bone malignancy in the pediatric age group, and its incidence among all childhood cancers is approximately 3% (59). Like many other malignant tumors, ES has an increased glycolysis rate, and as a result, it shows increased ^{18}F-FDG accumulation. ^{18}F-FDG PET/CT is particularly useful in detecting, staging, and restaging of the bone metastases in musculoskeletal tumors and often provides important additional information that may alter the treatment plan (60). Seven patients with ES and one patient with peripheral primitive neuroectodermal tumor were evaluated with ^{18}F-FDG PET/CT for local and systemic disease after chemotherapy in our study. Three local recurrences and five abdominal/inguinal metastatic lymph nodes were detected with the ^{18}F-FDG PET/CT.

Rhabdomyosarcoma is responsible for 4%-8% of malignant diseases in children under 15 years of age (2). Although most of the cases are sporadic, some related congenital and genetic diseases are reported (61). One of our four rhabdomyosarcoma patients had Li-Fraumeni syndrome. ^{18}F-FDG PET/CT detected three recurrent and one metastatic disease on follow-up after treatment of rhabdomyosarcoma. There are few studies in the literature on the role of ^{18}F-FDG PET/CT in treatment response evaluation in childhood rhabdomyosarcoma. Eugene et al. (62) reported that ^{18}F-FDG PET/CT predicted the treatment response better than conventional imaging methods in a study group of 23 patients after 3 cycles of treatment. They also had demonstrated 69% complete radiological response with ^{18}F-FDG PET/CT while it was reported as 8% in conventional methods. This finding supports that the metabolic response of the treatment occurred earlier than the response in tumor size. ^{18}F-FDG PET/CT was also performed in our clinic for evaluating response to treatment in patients with malignant mesenchymal tumor, testicular tumors, retinoblastoma, immature teratoma, nasopharyngeal cancers, and germ cell tumors. ^{18}F-FDG PET/CT guided the treatment in these patients by evaluating the local recurrence and metastatic disease.

^{18}F-FDG PET/CT detected more nodal lesions than CT in 10 staged patients in our study. ^{18}F-FDG PET/CT also increased the stage in these patients by detecting multiple lesions in the skeletal system and bone marrow. So, it has been confirmed that ^{18}F-FDG PET/CT has addictive effects on the outcomes and the prognosis of patients.

Despite the above-mentioned beneficial roles of ^{18}F-FDG PET/CT in malignancy, it has some limitations. Level of radiation dose is a severe problem in children. Lack of simultaneous data acquisition causes image artifacts because of patient movement. Another drawback is

that CT provides only limited soft tissue contrast. These problems could be overcome by integrating the PET detectors into MR scanner. Dose reductions of up to 73% have been reported when performing PET/MRI instead of ^{18}F-FDG PET/CT because of lack of the CT component, and decreasing the amount of PET tracer administered (because of longer imaging times in PET/MRI) could further reduce the radiation dose (63). Other advantage of PET/MRI is improved soft tissue contrast. Improved soft tissue contrast of MRI leads to improved localization of PET tracer uptake (64). Although ^{18}F-FDG PET/CT remains the mainstay for functional imaging of oncologic and neurologic processes in children, early experience shows that PET/MRI has great potential in diagnostic algorithms of several pediatric diseases.

The acquisition parameters for the CT portion of the scan should be tailored to the patient's size. CT parameters were obtained with ultra-low dose (80 kVp, 5 mAs, and 1.5:1 pitch) in our study. Decreasing the absorbed radiation dose without compromising the image quality can be provided by reducing milliamperes proportionately. This modification results in lower exposed radiation dose in ^{18}F-FDG PET/CT than the diagnostic CT. Combination of ^{18}F-FDG PET/CT and diagnostic CT has been reported to be used in the literature to prevent doubled radiation exposure to the patient (65). The follow-up of the patients can be performed reliably with ^{18}F-FDG PET/CT in order to further reduce the radiation exposure.

Conclusion

To conclude, ^{18}F-FDG PET/CT provides important information for the staging, restaging, response to treatment, and detection of metastatic disease, but it has limited contribution to early diagnosis in childhood tumors particularly in lymphoma, primary bone, and soft tissue tumors. It is a non-invasive imaging method that reflects both the metabolic features and the structural status of the tumors. As the preparation and image interpretation of the pediatric patients differ from adults, these procedures should be performed with specific information and experience on this age group. It should also be noted that indications of ^{18}F-FDG PET/CT must be considered appropriately since the exposure to radiation in children has more severe consequences than the adults.

Ethics

Ethics Committee Approval: The study was approved by the University of Health Sciences Turkey, Samsun Training and Research Hospital of Local Ethics Committee (protocol number: GOKA/2020/10/6).

Informed Consent: Consent form was filled out by all participants.

Peer-review: Externally peer-reviewed.

Authorship Contributions

Surgical and Medical Practices: N.B., M.E., Concept: N.B., Design: N.B., M.E., Data Collection or Processing: N.B., M.E., Analysis or Interpretation: N.B., Literature Search: N.B., Writing: N.B.

Conflict of Interest: No conflict of interest was declared by the authors.

Financial Disclosure: The authors declared that this study has received no financial support.

References

1. Voss SD. Pediatric oncology and the future of oncological imaging. Pediatr Radiol 2011;41:172-185.
2. Freebody J, Wegner EA, Rossleigh MA. 2-deoxy-2-((18)F) fluoro-D-glucose positron emission tomography/computed tomography imaging in paediatric oncology. World J Radiol 2014;6:741-755.
3. Costantini DL, Vali R, Chan J, McQuattie S, Charron M. Dual-time-point FDG PET/CT for the evaluation of pediatric tumors. AJR Am J Roentgenol 2013;200:408-413.
4. Shulkin BL. PET imaging in pediatric oncology. Pediatr Radiol 2004;34:199-204.
5. Uslu L, Donig J, Link M, Rosenberg J, Quon A, Daldrup-Link HE. Value of 18F-FDG PET and PET/CT for evaluation of pediatric malignancies. J Nucl Med 2015;56:274-286.
6. Cheng G, Servaes S, Zhuang H. Value of (18)F-fluoro-2-deoxy-D-glucose positron emission tomography/computed tomography scan versus diagnostic contrast computed tomography in initial staging of pediatric patients with lymphoma. Leuk Lymphoma 2013;54:737-742.
7. Miller E, Metser U, Avrahami G, Dvir R, Valdman D, Sira LB, Sayar D, Burstein Y, Toren A, Yaniv I, Even-Sapir E. Role of 18F-FDG PET/CT in staging and follow-up of lymphoma in pediatric and young adult patients. J Comput Assist Tomogr 2006;30:689-694.
8. Steliarova-Foucher E, Stiller C, Lacour B, Kaatsch P. International Classification of Childhood Cancer, third edition. Cancer 2005;103:1457-1467.
9. Percy CL, Smith MA, Linet M. Et al. Lymphomas and reticuloendothelial neoplasms.In: Ries LAG, Smith MA, Gurney, et al., eds. Cancer incidance and Survival Among children and adolescents: United States SEER Program 1975-1995. Bethesda MD: National Cancer İnstitude;1999. NIH publication 99-4649.
10. Amankwah EK, Conley AP, Reed DR. Epidemiology and therapies for metastatic sarcoma. Clin Epidemiol 2013;5:147-162.
11. Ducimetière F, Lurkin A, Ranchère-Vince D, Decouvelaere AV, Péoc'h M, Istier L, Chalabreysse P, Muller C, Alberti L, Bringuier PP, Scoazec JY, Schott AM, Bergeron C, Cellier D, Blay JY, Ray-Coquard I. Incidence of sarcoma histotypes and molecular subtypes in a prospective epidemiological study with central pathology review and molecular testing. PLoS One 2011;6:20294.
12. Arndt CA, Crist WM. Common musculoskeletal tumors of childhood and adolescence. N Engl J Med 1999;341:342-352.
13. Burns DK, Kumar V. The musculoskeletal system. In: Kumar V, Cotran RS, Robbins SL, eds. Robbins Basic Pathology. 7th ed. Philadelphia, Pennsylvania: Saunders; 2003:769-770.
14. Bhojwani D, McCarville MB, Choi JK, Sawyer J, Metzger ML, Inaba H, Davidoff AM, Gold R, Shulkin BL, Sandlund JT. The role of FDG-PET/CT in

the evaluation of residual disease in paediatric non-Hodgkin lymphoma. Br J Haematol 2015;168:845-853.
15. Uslu-Beşli L, Atay Kapucu LÖ, Karadeniz C, Akdemir ÜÖ, Pinarli FG, Aydos U, Okur A, Kaya Z, Samanci C, Karabacak NI. Comparison of FDG PET/MRI and FDG PET/CT in Pediatric Oncology in Terms of Anatomic Correlation of FDG-positive Lesions. J Pediatr Hematol Oncol 2019;41:542-550.
16. American Academy of Pediatrics Committee on Drugs: Guidelines for monitoring and management of pediatric patients during and after sedation for diagnostic and therapeutic procedures. Pediatrics 1992;89:1110-1115.
17. American Society of Anesthesiologists Task Force on Sedation and Analgesia by Non-Anesthesiologists. Practice guidelines for sedation and analgesia by non-anesthesiologists. Anesthesiology 2002;96:1004-1017.
18. Cohade C, Mourtzikos KA, Wahl RL. "USA-Fat": prevalence is related to ambient outdoor temperature-evaluation with 18F-FDG PET/CT. J Nucl Med 2003;44:1267-1270.
19. Cohade C, Osman M, Pannu HK, Wahl RL. Uptake in supraclavicular area fat ("USA-Fat"): description on 18F-FDG PET/CT. J Nucl Med 2003;44:170-176.
20. Yeung HW, Grewal RK, Gonen M, Schöder H, Larson SM. Patterns of (18)F-FDG uptake in adipose tissue and muscle: a potential source of false-positives for PET. J Nucl Med 2003;44:1789-1796.
21. Steliarova-Foucher E, Colombet M, Ries LAG, Moreno F, Dolya A, Bray F, Hesseling P, Shin HY, Stiller CA; IICC-3 contributors. International incidence of childhood cancer, 2001-10: a population-based registry study. Lancet Oncol 2017;18:719-731.
22. Nihayah S, Shammas A, Vali R, Parra D, Alexander S, Amaral J, Connolly B. Correlation of PET/CT and Image-Guided Biopsies of Pediatric Malignancies. AJR Am J Roentgenol 2017;208:656-662.
23. Dong Y, Zhang X, Wang S, Chen S, Ma C. 18F-FDG PET/CT is useful in initial staging, restaging for pediatric rhabdomyosarcoma. Q J Nucl Med Mol Imaging 2017;61:438-446.
24. Hurley C, McCarville MB, Shulkin BL, Mao S, Wu J, Navid F, Daw NC, Pappo AS, Bishop MW. Comparison of (18) F-FDG-PET-CT and Bone Scintigraphy for Evaluation of Osseous Metastases in Newly Diagnosed and Recurrent Osteosarcoma. Pediatr Blood Cancer 2016;63:1381-1386.
25. Treglia G, Taralli S, Bertagna F, Salsano M, Muoio B, Novellis P, Vita ML, Maggi F, Giordano A. Usefulness of whole-body fluorine-18-fluorodeoxyglucose positron emission tomography in patients with neurofibromatosis type 1: a systematic review. Radiol Res Pract 2012;2012:431029.
26. London K, Cross S, Onikul E, Dalla-Pozza L, Howman-Giles R. 18F-FDG PET/CT in paediatric lymphoma: comparison with conventional imaging. Eur J Nucl Med Mol Imaging 2011;38:274-284.
27. Kluge R, Kurch L, Georgi T, Metzger M. Current Role of FDG-PET in Pediatric Hodgkin's Lymphoma. Semin Nucl Med 2017;47:242-257.
28. Flerlage JE, Kelly KM, Beishuizen A, Cho S, De Alarcon PA, Dieckmann U, Drachtman RA, Hoppe BS, Howard SC, Kaste SC, Kluge R, Kurch L, Landman-Parker J, Lewis J, Link MP, McCarten K, Punnett A, Stoevesandt D, Voss SD, Wallace WH, Mauz-Körholz C, Metzger ML. Staging Evaluation and Response Criteria Harmonization (SEARCH) for Childhood, Adolescent and Young Adult Hodgkin Lymphoma (CAYAHL): Methodology statement. Pediatr Blood Cancer 2017;64.
29. Gatenby RA, Gillies RJ. Why do cancers have high aerobic glycolysis? Nat Rev Cancer 2004;4:891-899.
30. Portwine C, Marriott C, Barr RD. PET imaging for pediatric oncology: an assessment of the evidence. Pediatr Blood Cancer 2010;55:1048-1061.
31. McCarville MB. PET-CT imaging in pediatric oncology. Cancer Imaging 2009;9:35-43.
32. Franzius C. FDG-PET/CT in pediatric solid tumors. Q J Nucl Med Mol Imaging 2010;54:401-410.
33. Kleis M, Daldrup-Link H, Matthay K, Goldsby R, Lu Y, Schuster T, Schreck C, Chu PW, Hawkins RA, Franc BL. Diagnostic value of PET/CT for the staging and restaging of pediatric tumors. Eur J Nucl Med Mol Imaging 2009;36:23-36.
34. Furth C, Steffen IG, Amthauer H, Ruf J, Misch D, Schönberger S, Kobe C, Denecke T, Stöver B, Hautzel H, Henze G, Hundsdoerfer P. Early and late therapy response assessment with [18F] fluorodeoxyglucose positron emission tomography in pediatric Hodgkin's lymphoma: analysis of a prospective multicenter trial. J Clin Oncol 2009;27:4385-4391.
35. Gallamini A, Hutchings M, Avigdor A, Polliack A. Early interim PET scan in Hodgkin lymphoma: where do we stand? Leuk Lymphoma 2008;49:659-662.
36. Hawkins DS, Conrad EU 3rd, Butrynski JE, Schuetze SM, Eary JF. [F-18]-fluorodeoxy-D-glucose-positron emission tomography response is associated with outcome for extremity osteosarcoma in children and young adults. Cancer 2009;115:3519-3525.
37. Hawkins DS, Schuetze SM, Butrynski JE, Rajendran JG, Vernon CB, Conrad EU 3rd, Eary JF. [18F]Fluorodeoxyglucose positron emission tomography predicts outcome for Ewing sarcoma family of tumors. J Clin Oncol 2005;23:8828-8834.
38. Gelfand MJ, Parisi MT, Treves ST; Pediatric Nuclear Medicine Dose Reduction Workgroup. Pediatric radiopharmaceutical administered doses: 2010 North American consensus guidelines. J Nucl Med 2011;52:318-322.
39. Treves ST, Gelfand MJ, Fahey FH, Parisi MT. 2016 Update of the North American Consensus Guidelines for Pediatric Administered Radiopharmaceutical Activities. J Nucl Med 2016;57:15-18.
40. Qiu L, Chen Y, Wu J. The role of 18F-FDG PET and 18F-FDG PET/CT in the evaluation of pediatric Hodgkin's lymphoma and non-Hodgkin's lymphoma. Hell J Nucl Med 2013;16:230-236.
41. London K, Cross S, Onikul E, Dalla-Pozza L, Howman-Giles R. 18F-FDG PET/CT in paediatric lymphoma: comparison with conventional imaging. Eur J Nucl Med Mol Imaging 2011;38:274-284.
42. Sharp SE, Gelfand MJ, Shulkin BL. Pediatrics: diagnosis of neuroblastoma. Semin Nucl Med 2011;41:345-353.
43. Piccardo A, Lopci E, Conte M, Foppiani L, Garaventa A, Cabria M, Villavecchia G, Fanti S, Cistaro A. PET/CT imaging in neuroblastoma. Q J Nucl Med Mol Imaging 2013;57:29-39.
44. Mueller WP, Coppenrath E, Pfluger T. Nuclear medicine and multimodality imaging of pediatric neuroblastoma. Pediatr Radiol 2013;43:418-427.
45. Kushner BH, Yeung HW, Larson SM, Kramer K, Cheung NK. Extending positron emission tomography scan utility to high-risk neuroblastoma: fluorine-18 fluorodeoxyglucose positron emission tomography as sole imaging modality in follow-up of patients. J Clin Oncol 2001;19:3397-3405.
46. Choi YJ, Hwang HS, Kim HJ, Jeong YH, Cho A, Lee JH, Yun M, Lee JD, Kang WJ. (18)F-FDG PET as a single imaging modality in pediatric neuroblastoma: comparison with abdomen CT and bone scintigraphy. Ann Nucl Med 2014;28:304-313.
47. Alexander N, Vali R, Ahmadzadehfar H, Shammas A, Baruchel S. Review: The Role of Radiolabeled DOTA-Conjugated Peptides for Imaging and Treatment of Childhood Neuroblastoma. Curr Radiopharm 2018;11:14-21.
48. Bodei L, Cremonesi M, Grana CM, Fazio N, Iodice S, Baio SM, Bartolomei M, Lombardo D, Ferrari ME, Sansovini M, Chinol M, Paganelli G. Peptide receptor radionuclide therapy with ^{177}Lu-DOTATATE: the IEO phase I-II study. Eur J Nucl Med Mol Imaging 2011;38:2125-2135.
49. Bodei L, Mueller-Brand J, Baum RP, Pavel ME, Hörsch D, O'Dorisio MS, O'Dorisio TM, Howe JR, Cremonesi M, Kwekkeboom DJ, Zaknun JJ. The joint IAEA, EANM, and SNMMI practical guidance on peptide receptor radionuclide therapy (PRRNT) in neuroendocrine tumours. Eur J Nucl Med Mol Imaging 2013;40:800-816.

50. Brans B, Mottaghy FM, Kessels A. 90Y/177Lu-DOTATATE therapy: survival of the fittest? Eur J Nucl Med Mol Imaging 2011;38:1785-1787.
51. Delpassand ES, Samarghandi A, Zamanian S, Wolin EM, Hamiditabar M, Espenan GD, Erion JL, O'Dorisio TM, Kvols LK, Simon J, Wolfangel R, Camp A, Krenning EP, Mojtahedi A. Peptide receptor radionuclide therapy with 177Lu-DOTATATE for patients with somatostatin receptor-expressing neuroendocrine tumors: the first US phase 2 experience. Pancreas 2014;43:518-525.
52. Kunikowska J, Królicki L, Hubalewska-Dydejczyk A, Mikołajczak R, Sowa-Staszczak A, Pawlak D. Clinical results of radionuclide therapy of neuroendocrine tumours with 90Y-DOTATATE and tandem 90Y/177Lu-DOTATATE: which is a better therapy option? Eur J Nucl Med Mol Imaging 2011;38:1788-1797.
53. Maecke HR, Reubi JC. Somatostatin receptors as targets for nuclear medicine imaging and radionuclide treatment. J Nucl Med 2011;52:841-844.
54. Waldherr C, Pless M, Maecke HR, Haldemann A, Mueller-Brand J. The clinical value of [90Y-DOTA]-D-Phe1-Tyr3-octreotide (90Y-DOTATOC) in the treatment of neuroendocrine tumours: a clinical phase II study. Ann Oncol 2001;12:941-945.
55. Kong G, Hofman MS, Murray WK, Wilson S, Wood P, Downie P, Super L, Hogg A, Eu P, Hicks RJ. Initial Experience With Gallium-68 DOTA-Octreotate PET/CT and Peptide Receptor Radionuclide Therapy for Pediatric Patients With Refractory Metastatic Neuroblastoma. J Pediatr Hematol Oncol 2016;38:87-96.
56. Gains JE, Bomanji JB, Fersht NL, Sullivan T, D'Souza D, Sullivan KP, Aldridge M, Waddington W, Gaze MN. 177Lu-DOTATATE molecular radiotherapy for childhood neuroblastoma. J Nucl Med 2011;52:1041-1047.
57. Menda Y, O'Dorisio MS, Kao S, Khanna G, Michael S, Connolly M, Babich J, O'Dorisio T, Bushnell D, Madsen M. Phase I trial of 90Y-DOTATOC therapy in children and young adults with refractory solid tumors that express somatostatin receptors. J Nucl Med 2010;51:1524-1531.
58. Sadowski SM, Neychev V, Millo C, Shih J, Nilubol N, Herscovitch P, Pacak K, Marx SJ, Kebebew E. Prospective Study of 68Ga-DOTATATE Positron Emission Tomography/Computed Tomography for Detecting Gastro-Entero-Pancreatic Neuroendocrine Tumors and Unknown Primary Sites. J Clin Oncol 2016;34:588-596.
59. Ludwig JA. Ewing sarcoma: historical perspectives, current state-of-the-art, and opportunities for targeted therapy in the future. Curr Opin Oncol 2008;20:412-418.
60. Bestic JM, Peterson JJ, Bancroft LW. Pediatric FDG PET/CT: Physiologic uptake, normal variants, and benign conditions [corrected]. Radiographics 2009;29:1487-1500.
61. Hartley AL, Birch JM, Blair V, Kelsey AM, Harris M, Jones PH. Patterns of cancer in the families of children with soft tissue sarcoma. Cancer 1993;72:923-930.
62. Eugene T, Corradini N, Carlier T, Dupas B, Leux C, Bodet-Milin C. ^{18}F-FDG-PET/CT in initial staging and assessment of early response to chemotherapy of pediatric rhabdomyosarcomas. Nucl Med Commun 2012;33:1089-1095.
63. Schäfer JF, Gatidis S, Schmidt H, Gückel B, Bezrukov I, Pfannenberg CA, Reimold M, Ebinger M, Fuchs J, Claussen CD, Schwenzer NF. Simultaneous whole-body PET/MR imaging in comparison to PET/CT in pediatric oncology: initial results. Radiology 2014;273:220-231.
64. Rausch I, Quick HH, Cal-Gonzalez J, Sattler B, Boellaard R, Beyer T. Technical and instrumentational foundations of PET/MRI. Eur J Radiol 2017;94:3-13.
65. Qi Z, Gates EL, O'Brien MM, Trout AT. Radiation dose reduction through combining positron emission tomography/computed tomography (PET/CT) and diagnostic CT in children and young adults with lymphoma. Pediatr Radiol 2018;48:196-203.

Original Article
Mol Imaging Radionucl Ther 2021;30:28-33 DOI:10.4274/mirt.galenos.2020.31932

Correlation Between Perfusion Abnormalities Extent in Ventilation/Perfusion SPECT/CT with Hemodynamic Parameters in Patients with Chronic Thromboembolic Pulmonary Hypertension

Kronik Tromboembolik Pulmoner Hipertansiyonlu Hastalarda Ventilasyon/Perfüzyon SPECT/BT'de Saptanan Perfüzyon Defekti Yaygınlığı ile Hemodinamik Parametreler Arasındaki İlişki

Salih Özgüven[1], Selin Kesim[1], Kevser Öksüzoğlu[1], Mehmed Yanartaş[2], Serpil Taş[2], Feyza Şen[1], Tunç Öneş[1], Sabahat İnanır[1], Halil Turgut Turoğlu[1], Bülent Mutlu[3], Tanju Yusuf Erdil[1], Bedrettin Yıldızeli[4]

[1]*Marmara University Pendik Training and Research Hospital, Clinic of Nuclear Medicine, İstanbul, Turkey*
[2]*University of Health Sciences Turkey, Kartal Koşuyolu Training and Research Hospital, Clinic of Cardiovascular Surgery, İstanbul, Turkey*
[3]*Marmara University Pendik Training and Research Hospital, Clinic of Cardiology, İstanbul, Turkey*
[4]*Marmara University Pendik Training and Research Hospital, Clinic of Thoracic Surgery, İstanbul, Turkey*

Abstract

Objectives: Chronic thromboembolic pulmonary hypertension (CTEPH) is a type of pulmonary hypertension with persistent pulmonary vascular obstruction and exercise intolerance, which may benefit from pulmonary endarterectomy (PEA). Ventilation/perfusion (V/Q) scan is the preferred screening test of CTEPH, which can be used to assess the anatomical extent of the disease. This study aimed to analyze the correlation between the extent of mismatched Q defects in V/Q single photon emission computed tomography/computed tomography (SPECT/CT) with preoperative clinical and hemodynamic parameters in patients with CTEPH.

Methods: A total of 102 patients with CTEPH prior to PEA having V/Q SPECT/CT scans were retrospectively reviewed. Age, gender, New York Heart Association classification, intraoperative right-sided heart catheterization (mPAP and PVR), and 6-minute walk test (6MWT) findings were obtained from clinical records of patients.

Results: Linear regression analysis showed a significant but weak correlation between the preoperative mPAP and PVR with the extent of mismatched Q defects in V/Q SPECT/CT (rs=0.09474 with p=0.0016 and rs=0.045 with p=0.045, respectively). No significant correlation was found between 6MWT and extent of mismatched Q defects in V/Q SPECT/CT (p>0.05).

Conclusion: A quantitative assessment of Q defects on V/Q SPECT/CT might provide information about hemodynamic parameters in patients with CTEPH.

Keywords: Chronic thromboembolic pulmonary hypertension, ventilation/perfusion scintigraphy, mean pulmonary arterial pressure, pulmonary vascular resistance, 6-minute walk distance

Öz

Amaç: Kronik tromboembolik pulmoner hipertansiyon (KTEPH), kalıcı pulmoner vasküler obstrüksiyon ve egzersiz intoleransı ile karakterize bir pulmoner hipertansiyon grubudur ve pulmoner endarterektomiden (PEA) fayda görebilir. Ventilasyon/perfüzyon (V/Q) sintigrafisi, hastalığın

Address for Correspondence: Salih Özgüven MD, Marmara University Pendik Training and Research Hospital, Clinic of Nuclear Medicine, İstanbul, Turkey
Phone: +90 532 251 17 69 **E-mail:** drsozg@gmail.com ORCID ID: orcid.org/0000-0002-2790-7206
Received: 26.11.2020 **Accepted:** 15.12.2020

anatomik yaygınlığını değerlendirmek için kullanılabilen KTEPH'nin tercih edilen tarama testidir. Bu çalışmanın amacı, KTEPH tanılı hastalarda ameliyat öncesi klinik ve hemodinamik parametreler ile V/Q tek foton emisyon tomografisi/bilgisayarlı tomografideki (SPECT/BT) Q defektlerinin yaygınlığı arasındaki korelasyonu araştırmaktır.

Yöntem: PEA ile tanısı doğrulanmış 102 KTEPH hastasının PEA öncesi V/Q SPECT/BT görüntüleri retrospektif olarak incelendi. PEA öncesi yaş, cinsiyet, New York Kalp Derneği sınıfı, intraoperatif sağ kalp kateterizasyonu sonuçları [ortalama pulmoner arter basıncı (OPAB), pulmoner vasküler rezistans (PVR)] ve 6 dakikalık yürüme testi (6DYT) gibi klinik parametreleri hastaların klinik kayıtlarından elde edildi.

Bulgular: Doğrusal regresyon analizi, preoperative OPAB ve PVR ile V/Q SPECT/BT'deki eşleşmeyen Q defektlerinin yaygınlığı ile anlamlı ancak zayıf bir korelasyon gösterdi (rs=0,09474, p=0,0016; rs=0,045, p=0,045). 6DYT mesafesi ile eşleşmeyen Q defektlerinin yaygınlığı arasında ise anlamlı bir ilişki bulunmadı (p>0,05).

Sonuç: V/Q SPECT/BT'de saptanan Q defektlerinin kantitatif değerlendirilmesi, KTEPH tanılı hastalarda hemodinamik parametreler hakkında fikir sağlayabilir.

Anahtar kelimeler: Kronik tromboembolik pulmoner hipertansiyon, ventilasyon/perfüzyon sintigrafisi, ortalama pulmoner arter basıncı, pulmoner vasküler direnç, 6 dakikalık yürüme testi

Introduction

Chronic thromboembolic pulmonary hypertension (CTEPH) is a progressive pre-capillary pulmonary hypertension, which results from incomplete resolution of a pulmonary embolus, leading to elevated pulmonary vascular resistance (PVR), mean pulmonary artery pressure (mPAP), and right-sided heart failure (1,2). Acute embolism can vary from a total resolution to persistent perfusion (Q) defects after an adequate anticoagulation therapy. Approximately, 30% of patients have permanent defects after 6 months of anticoagulation; however, only 10% of defects consequently developed CTEPH (3).

CTEPH should be questioned in patients with abnormal ventilation (V)/Q scintigraphy including at least one mismatched segmental Q defect and imaging findings of organized thrombi in pulmonary arteries following >3 months of therapeutic anticoagulation (3). Invasive pulmonary angiography historically remains as the objective reference standard for diagnosis and evaluation for chronic emboli extent, whereas V/Q scan is the preferred first-line screening test for CTEPH (4,5). V/Q scintigraphy is used to diagnose and assess the anatomical extension of mold, and estimate therapy response in patients with CTEPH (6).

The only curative treatment option for CTEPH is the pulmonary endarterectomy (PEA) in appropriate patients (7). This technique is associated with improved survival, functional capacity, and quality of life (1,8). PEA may be related with high mortality rates regarding to the extent of the disease (9,10).

Factors that need to be assessed before PEA include the anatomical location and distribution of disease and left and right ventricular systolic functions (6). Previous studies showed that hemodynamic parameters play a crucial part in the evaluation of prognosis, disease severity, and operability (11,12). This study aimed to assess the association of the extent of mismatched Q abnormalities in V/Q single photon emission computed tomography/computed tomography (SPECT/CT) with preoperative hemodynamic and clinical parameters in patients with CTEPH.

Materials and Methods

Study Subjects

Over a period of nine years (January 2011 to May 2020), a total of 677 patients with a diagnosis of CTEPH at the preoperative evaluation underwent PEA. Of which, 102 patients with CTEPH whose V/Q SPECT/CT images obtained in our clinic prior to PEA were retrospectively reviewed.

Study exclusion incudes patients with isolated pulmonary artery vasculitis (n=8), hydatid cyst (n=8), pulmonary artery sarcomas (n=9), no mismatched V/Q defects in scintigraphy (n=7), and whose preoperative V/Q scans not acquired in our institution or lacking in our database (n=543).

Age, gender, New York Heart Association (NYHA) classification, intraoperative right-sided heart catheterization (RHC) (mPAP and PVR), and 6-minute walk test (6MWT) findings were obtained from clinical records of patients.

An informed consent was taken from all patients before the examination. Marmara University Faculty of Medicine Clinical Studies Ethics Committee approval was also obtained (date: September 2020, no: 09.2020.852).

V/Q SPECT/CT Protocol

V/Q scans were performed with a one-day protocol (13). The V SPECT images were obtained before the Q scan. A 12-15 millicurie (444-555 megabecquerel) technetium-99m (Tc-99m)-Technegas generated by the "TechnegasPlus" generator device (Cyclomedica Australia Pty Ltd., Australia) was used for the V phase. SPECT images of patients using a 180° dual head detector on SPECT/CT (Siemens Symbia TruePoint, Siemens Medical Solutions, USA) were

acquired. Afterward, a Q SPECT with low dose CT scans was immediately obtained on the same table. After a slow (within 20-30 s) injection of 4-5 millicurie (148-185 megabecquerel). Tc-99m-macro aggregated albumin, (TechneScan LyoMAA; Mallinckrodt Medical) containing 100,000-200,000 particles, SPECT/CT was taken on the same device using similar SPECT parameters as those used for the V phase (low-energy high-resolution collimator, 128x128 matrix, 64 projections of 10 s, 1.00 zoom factor, and 140±10% keV energy window) and 13-25 mAs, 130 kV, and slice width of 5 mm for CT. Raw data of SPECT images processed with the "Tomo Reconstruction v.8.2.26.4" (Syngo-Siemens AG) application and reconstruction was conducted with ordered subset expectation maximization method.

Image Analysis

V/Q SPECT/CT images were evaluated by two nuclear medicine physicians without knowledge of the preoperative hemodynamic parameters and 6MWT records of patients. To figure out CTEPH severity, V/Q images were analyzed together for each pulmonary segment (14). Two physicians discussed each case to reach a final consensus.

Clinical Data Analysis

RHC protocol and 6MWT protocol was carried out in accordance with previously described standard procedures (15,16,17). Data of the RHC (mPAP and PVR) and 6MWT were obtained from the clinical records of patients.

Statistical Analysis

For continuous variables a mean value ± standard deviation and for categorical variables number and percentage were calculated. Per-segment basis analysis for each patient was used to estimate disease severity. Linear regression analysis was conducted to examine the concordance of mismatched Q defects severity on V/Q SPECT/CT with RHC and 6MWT results. Data analysis and graphs were plotted using GraphPad Prism version 8.0 for macOS, GraphPad Software, La Jolla California USA. P values of 0.05 or less were regarded as significant.

Results

A statistical analysis of 102 patients with a diagnosis of CTEPH is presented, wherein 46 patients (45.1%) were women and 56 patients (54.9%) were men. The mean age of patients was 51.66 years (range of 19-77 years and standard deviation of 15.95). A total of 11 patients (10.8%) were NYHA class II, 74 patients (72.5%) were NYHA class III, and 17 patients (16.6%) were NYHA class IV. The mean preoperative mPAP and mean preoperative PVR were 43.73±14.77 mmHg and 681.62±411.75 dyn•s•cm^{-5}, respectively. The mean 6MWT distance was 334.40±113.62 meters. The average number of abnormally perfused segments was 12.84±5.30.

The linear regression analysis showed a significant but weak correlation between the preoperative mPAP and PVR with the extent of mismatched Q defects in V/Q SPECT/CT (rs=0.09474 with p=0.0016 and rs=0.045 with p=0.045, respectively) (Figure 1, 2).

No significant correlation was found between 6MWT distance and extent of the mismatched Q defects in V/Q SPECT/CT (p>0.05) (Figure 3).

Discussion

The correlation of the degree of persistent thromboembolic disease (mismatched Q defects in V/Q SPECT/CT) with preoperative clinical and hemodynamic parameters was examined in the present research with the greatest number of patients with CTEPH proven by post-PEA surgical histopathological examinations. Results showed a statistically significant correlation between the number of mismatched Q defects in V/Q SPECT/CT and preoperative mPAP and PVR, but not with 6MWT. PVR and mPAP are the essential hemodynamic parameters in patients with CTEPH. Increased PVR is mainly caused by endothelial dysfunction, vasoconstriction, vascular remodeling, and obstruction of small pulmonary arteries. Interleukin-1 (IL-1), IL-6, and tumor necrosis factor-a are

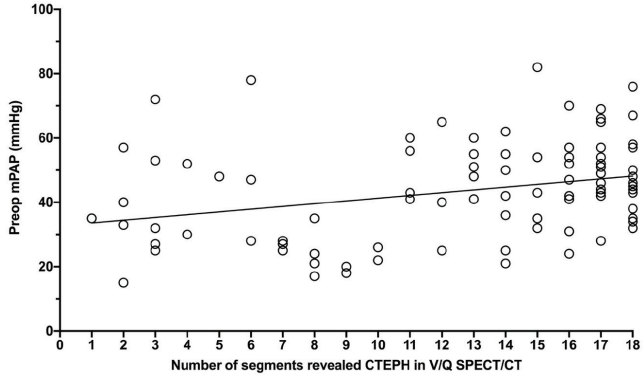

Figure 1. Correlation between preoperative mean pulmonary arterial pressure (mPAP) levels and number of segments revealed in chronic thromboembolic pulmonary hypertension ventilation/perfusion single photon emission computed tomography/computed tomography (V/Q SPECT/CT). Application of linear regression analysis revealed a significant but weak correlation between the preoperative mPAP and extent of mismatched perfusion defects in V/Q SPECT/CT (rs=0.09474 and p=0.0016)

CTEPH: Chronic thromboembolic pulmonary hypertension, mPAP: Mean pulmonary arterial pressure, V/Q: Ventilation/perfusion, SPECT/CT: Single photon emission computed tomography/computed tomography

pro-inflammatory cytokines that are relevant to the pathogenesis (18). Dartevelle et al. (19) reported higher mortality rates for patients with PVR >900 dyn • s • cm^{-5} than those with PVR <900 dyn • s • cm^{-5}. Furthermore, no patients with PVR <300 dyn • s • cm^{-5} pre-operatively died after PEA in a study performed by Yıldızeli et al. (17). In addition, increased mPAP, which induces right ventricular dysfunction, is found to be associated with higher mortality (20). In a study by Saouti et al. (21), the risk of mortality is higher in patients with mPAP >40 mmHg than those with an mPAP <40 mmHg. The association between the extent of the disease and hemodynamic parameters has been described in literature (22). Fukuchi et al. (23) found a correlation between planar Q index with mPAP and right ventricular ejection fraction using planar pulmonary Q scintigraphy. Recently, Derlin and colleagues, who investigated the correlation between V/Q SPECT/CT imaging findings and RHC, showed a statistically significant association between Q defect score, perfused lung volume, Q index with mPAP, and PVR (24). In line with other studies, a statistically significant difference between mismatched Q defects in V/Q SPECT/CT and preoperative mPAP (rs=0.095 and p=0.0016) and PVR (rs=0.045 and p=0.035) values was observed.

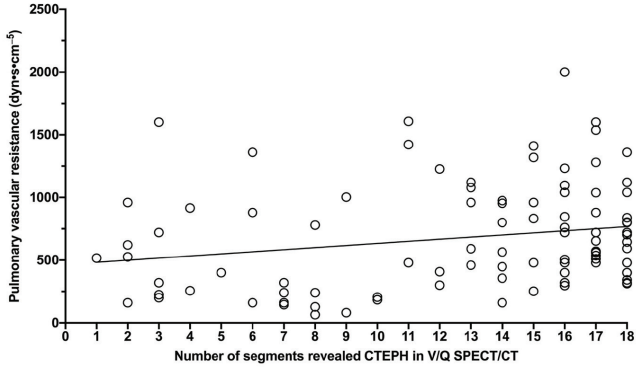

Figure 2. Correlation between preoperative pulmonary vascular resistance (PVR) and number of segments revealed in chronic thromboembolic pulmonary hypertension ventilation/perfusion (V/Q) single photon emission computed tomography/computed tomography (SPECT/CT). Linear regression analysis showed a significant but weak correlation between the preoperative PVR and extent of mismatched perfusion defects in V/Q SPECT/CT (rs=0.045 and p=0.045)

CTEPH: Chronic thromboembolic pulmonary hypertension, V/Q: Ventilation/perfusion, SPECT/CT: Single photon emission computed tomography/computed tomography

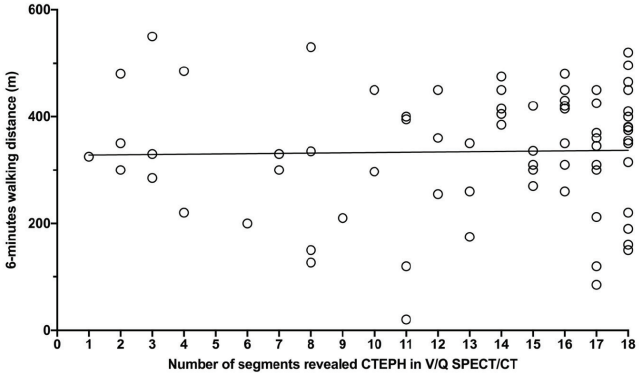

Figure 3. Correlation between 6-minutes walking distance and number of segments revealed in chronic thromboembolic pulmonary hypertension ventilation/perfusion (V/Q) single photon emission computed tomography/computed tomography (SPECT/CT). No significant correlation was found between 6-minute walk distance and extent of mismatched perfusion defects in V/Q SPECT/CT (p>0.05)

CTEPH: Chronic thromboembolic pulmonary hypertension, V/Q: Ventilation/perfusion, SPECT/CT: Single photon emission computed tomography/computed tomography

Patients with CTEPH generally display a decreased exercise capacity that is most commonly assessed with 6MWT. The prognostic value of the 6MWT has been reported in several studies (15,21). In a study by Reesink et al. (25), 6MWT had significantly increased one year after PEA, reflecting clinical and hemodynamic improvement (25). However, the correlation of the 6MWT distances with the extent of disease in CTEPH has not been widely studied. In fact, the 6MWT distances did not correlate with the number of mismatched Q abnormalities in our study. Variance in walking distance can be explained by the individual's determinants such as age, sex, height, and weight on 6MWT.

Study Limitations

Following are the limitations of this study. First, this study was designed as a retrospective, single-center study. Nevertheless, our study has the largest number of patients whose diagnoses were proven by histopathology. Second, it is not rare to find matched V/Q abnormalities in patients with CTEPH that are seen late in the course of the disease. Hence, this problem might lead us to underestimate the extent of disease-related defects.

Conclusion

In conclusion, our study suggests that the extent of chronic thromboembolic disease revealed on V/Q SPECT/CT correlates with the preoperative hemodynamic parameters, thus predicting the severity and prognosis of the disease. Conversely, 6MWT was not found as a reliable indicator for the extent of the disease. Further studies are required in extended patient series to better represent the association between V/Q SPECT/CT Q defects with hemodynamic parameters and 6MWT in patients with CTEPH.

Acknowledgement

Authors would like to thank Asst. Prof. Dr. Tolga Sütlü for his help in the statistical analyses.

Ethics

Ethics Committee Approval: Marmara University Faculty of Medicine Clinical Studies Ethics Committee approval was also obtained (date: September 2020, no: 09.2020.852).

Informed Consent: Informed consents were obtained from the patients for conducting V/Q SPECT/CT examinations.

Peer-review: Externally and internally peer-reviewed.

Authorship Contributions

Surgical and Medical Practices: S.Ö., S.K., K.Ö., M.Y., S.T., F.Ş., T.Ö., S.İ., H.T.T., B.M., T.Y.E., B.Y., Concept: S.Ö., S.K., T.Ö., B.Y., Design: S.Ö., S.K., T.Ö., B.Y., Data Collection or Processing: S.Ö., S.K., Analysis or Interpretation: S.Ö., S.K., Literature Search: S.Ö., S.K., Writing: S.Ö., S.K.

Conflict of Interest: No conflict of interest was declared by the authors.

Financial Disclosure: The authors declared that this study has received no financial support.

References

1. Jenkins D, Madani M, Fadel E, D'Armini AM, Mayer E. Pulmonary endarterectomy in the management of chronic thromboembolic pulmonary hypertension. Eur Respir Rev 2017;26:160111.
2. Pengo V, Lensing AW, Prins MH, Marchiori A, Davidson BL, Tiozzo F, Albanese P, Biasiolo A, Pegoraro C, Iliceto S, Prandoni P; Thromboembolic Pulmonary Hypertension Study Group. Incidence of chronic thromboembolic pulmonary hypertension after pulmonary embolism. N Engl J Med 2004;350:2257-2264.
3. Fernandes T, Planquette B, Sanchez O, Morris T. From Acute to Chronic Thromboembolic Disease. Ann Am Thorac Soc 2016;13:207-214.
4. O'Connell C, Montani D, Savale L, Sitbon O, Parent F, Seferian A, Bulifon S, Fadel E, Mercier O, Mussot S, Fabre D, Dartevelle P, Humbert M, Simonneau G, Jaïs X. Chronic thromboembolic pulmonary hypertension. Presse Med 2015;44:409-416.
5. Galiè N, Humbert M, Vachiery JL, Gibbs S, Lang I, Torbicki A, Simonneau G, Peacock A, Vonk Noordegraaf A, Beghetti M, Ghofrani A, Gomez Sanchez MA, Hansmann G, Klepetko W, Lancellotti P, Matucci M, McDonagh T, Pierard LA, Trindade PT, Zompatori M, Hoeper M; ESC Scientific Document Group. 2015 ESC/ERS Guidelines for the diagnosis and treatment of pulmonary hypertension: The Joint Task Force for the Diagnosis and Treatment of Pulmonary Hypertension of the European Society of Cardiology (ESC) and the European Respiratory Society (ERS): Endorsed by: Association for European Paediatric and Congenital Cardiology (AEPC), International Society for Heart and Lung Transplantation (ISHLT). Eur Heart J 2016;37:67-119.
6. Renapurkar RD, Bolen MA, Shrikanthan S, Bullen J, Karim W, Primak A, Heresi GA. Comparative assessment of qualitative and quantitative perfusion with dual-energy CT and planar and SPECT-CT V/Q scanning in patients with chronic thromboembolic pulmonary hypertension. Cardiovasc Diagn Ther 2018;8:414-422.
7. Lang IM, Madani M. Update on chronic thromboembolic pulmonary hypertension. Circulation 2014;130:508-518.
8. Inami T, Kataoka M, Ando M, Fukuda K, Yoshino H, Satoh T. A new era of therapeutic strategies for chronic thromboembolic pulmonary hypertension by two different interventional therapies; pulmonary endarterectomy and percutaneous transluminal pulmonary angioplasty. PLoS One 2014;9:e94587.
9. Thistlethwaite PA, Kaneko K, Madani MM, Jamieson SW. Technique and outcomes of pulmonary endarterectomy surgery. Ann Thorac Cardiovasc Surg 2008;14:274-282.
10. Thistlethwaite PA, Kemp A, Du L, Madani MM, Jamieson SW. Outcomes of pulmonary endarterectomy for treatment of extreme thromboembolic pulmonary hypertension. J Thorac Cardiovasc Surg 2006;131:307-313.
11. Yanartas M, Kalkan ME, Arslan A, Tas SG, Koksal C, Bekiroglu N, Yildizeli B. Neutrophil/Lymphocyte Ratio Can Predict Postoperative Mortality in Patients with Chronic Thromboembolic Pulmonary Hypertension. Ann Thorac Cardiovasc Surg 2015;21:229-235.
12. Sunbul M, Kivrak T, Durmus E, Yildizeli B, Mutlu B. Evaluation of right and left heart mechanics in patients with chronic thromboembolic pulmonary hypertension before and after pulmonary thromboendarterectomy. Int J Cardiovasc Imaging. 2015;31:1159-1167.
13. Bajc M, Schümichen C, Grüning T, Lindqvist A, Le Roux PY, Alatri A, Bauer RW, Dilic M, Neilly B, Verberne HJ, Delgado Bolton RC, Jonson B. EANM guideline for ventilation/perfusion single-photon emission computed tomography (SPECT) for diagnosis of pulmonary embolism and beyond. Eur J Nucl Med Mol Imaging 2019;46:2429-2451.
14. Boyden EA. Segmental Anatomy of the Lungs. Blakiston Division. McGraw-Hill Co. New York, 1955.
15. Boxer R, Kleppinger A, Ahmad A, Annis K, Hager D, Kenny A. The 6-minute walk is associated with frailty and predicts mortality in older adults with heart failure. Congest Heart Fail 2010;16:208-213.
16. ATS Committee on Proficiency Standards for Clinical Pulmonary Function Laboratories. ATS statement: guidelines for the six-minute walk test. Am J Respir Crit Care Med 2002;166:111-117.
17. Yıldızeli B, Taş S, Yanartaş M, Kaymaz C, Mutlu B, Karakurt S, Altınay E, Eldem B, Ermerak NO, Batırel HF, Koçak T, Bekiroğlu N, Yüksel M, Sunar H. Pulmonary endarterectomy for chronic thrombo-embolic pulmonary hypertension: an institutional experience. Eur J Cardiothorac Surg 2013;44:219-227.
18. Humbert M, Monti G, Brenot F, Sitbon O, Portier A, Grangeot-Keros L, Duroux P, Galanaud P, Simonneau G, Emilie D. Increased interleukin-1 and interleukin-6 serum concentrations in severe primary pulmonary hypertension. Am J Respir Crit Care Med 1995;151:1628-1631.
19. Dartevelle P, Fadel E, Mussot S, Chapelier A, Hervé P, de Perrot M, Cerrina J, Ladurie FL, Lehouerou D, Humbert M, Sitbon O, Simonneau G. Chronic thromboembolic pulmonary hypertension. Eur Respir J 2004;23:637-648.
20. Sandoval J, Bauerle O, Palomar A, Gómez A, Martínez-Guerra ML, Beltrán M, Guerrero ML. Survival in primary pulmonary hypertension. Validation of a prognostic equation. Circulation 1994;89:1733-1744.
21. Saouti N, de Man F, Westerhof N, Boonstra A, Twisk J, Postmus PE, Vonk Noordegraaf A. Predictors of mortality in inoperable chronic thromboembolic pulmonary hypertension. Respir Med 2009;103:1013-1019.
22. Leone MB, Giannotta M, Palazzini M, Cefarelli M, Martìn Suàrez S, Gotti E, Bacchi Reggiani ML, Zompatori M, Galiè N. A new CT-score as index of hemodynamic changes in patients with chronic thromboembolic pulmonary hypertension. Radiol Med 2017;122:495-504.
23. Fukuchi K, Hayashida K, Nakanishi N, Inubushi M, Kyotani S, Nagaya N, Ishida Y. Quantitative analysis of lung perfusion in patients with primary pulmonary hypertension. J Nucl Med 2002;43:757-761.

24. Derlin T, Kelting C, Hueper K, Weiberg D, Meyer K, Olsson KM, Thackeray JT, Welte T, Bengel FM, Hoeper MM. Quantitation of Perfused Lung Volume Using Hybrid SPECT/CT Allows Refining the Assessment of Lung Perfusion and Estimating Disease Extent in Chronic Thromboembolic Pulmonary Hypertension. Clin Nucl Med 2018;43:170-177.

25. Reesink HJ, van der Plas MN, Verhey NE, van Steenwijk RP, Kloek JJ, Bresser P. Six-minute walk distance as parameter of functional outcome after pulmonary endarterectomy for chronic thromboembolic pulmonary hypertension. J Thorac Cardiovasc Surg 2007;133:510-516.

Original Article
Mol Imaging Radionucl Ther 2021;30:34-38 DOI:10.4274/mirt.galenos.2020.58569

Comparison of Radiochemical and Chemical Impurities in Liquid Wastes of Two Different ^{68}Ge/^{68}Ga Generators used in Nuclear Medicine PET Chemistry

Nükleer Tıp PET Kimyasında Kullanılan İki Farklı ^{68}Ge/^{68}Ga Jeneratörünün Sıvı Atıklarındaki Radyokimyasal ve Kimyasal Kirliliklerinin Karşılaştırılması

Ayşe Uğur[1], Olga Yaylalı[2], Doğangün Yüksel[2]

[1]*Pamukkale University Training and Research Hospital, Clinic of Nuclear Medicine, Denizli, Turkey*
[2]*Pamukkale University Faculty of Medicine, Department of Nuclear Medicine, Denizli, Turkey*

Abstract

Objectives: Germanium-68/gallium-68 (^{68}Ge/^{68}Ga) generator eluate contains a number of metal cations that can compete with $^{68}GaCl_3$, reducing specific radioactivity. The first step in peptide labeling with $^{68}GaCl_3$ is to remove ^{68}Ge and several other metals with a long half-life. In this purification step, the elution residue that is passed through the cartridge is collected in glass waste bottles. Waste management is included in good production practices, and in particular, the activity of long half-life ^{68}Ge (270.95 days) and other toxic metal levels need to be examined. Our objective in this study is to determine the ^{68}Ge activity in liquid waste produced by the generation of ^{68}Ga and heavy metal concentrations from the generator column materials and to assess whether it can be disposed of as normal waste.

Methods: Liquid wastes produced by passing the ^{68}Ge/^{68}Ga generator eluate of 2 different identities via PSH$^+$ cartridge have been analyzed with the inductively coupled plasma mass spectrometry device in the advanced technology application and research center of our university.

Results: The average of the ^{68}Ge radioactive pollution was estimated to be 0.142 ppm (μg.mL^{-1}) in the liquid waste analysis after passing through the PSH$^+$ cartridge in the pre-elution in the GalluGEN brand generator. While there was no tin (Sn) impurity, it was determined that the average zinc (Zn) was 1.95 ppm (μg.mL^{-1}) and the average aluminum (Al) impurity was 10.95 ppm (μg.mL^{-1}). While no ^{68}Ge radioactive pollution was determined in the iThemba LABS brand generator, the average Sn was 0.098 ppm (μg.mL^{-1}), average Zn 48.6 ppm (μg.mL^{-1}), and average Al impurity 4.135 ppm (μg.mL^{-1}).

Conclusion: All ^{68}Ge/^{68}Ga generators produced have their own certificates. Metallic contamination in the postmarking waste of ^{68}Ge/^{68}Ga generators can be different. It would be a safe method to keep these wastes in place until they are dumped into the sewage systems, given their half-lives in terms of long half-life radioactive metallic contamination.

Keywords: Gallium-68, ^{68}Ge/^{68}Ga generator, chemical impurity, GMP

Öz

Amaç: Germanyum-68/galyum-68 (^{68}Ge/^{68}Ga) jeneratör sağım eluatında $^{68}GaCl_3$ ile rekabet edebilen, spesifik radyoaktiviteyi azaltan bir dizi metal katyon bulunmaktadır. ^{68}Ge/^{68}Ga jeneratörlerinde, elüat bileşimindeki metal kontaminasyonu, kolon matrislerine ve sağım yapılan çözücüye bağlı olarak değişir. $^{68}GaCl_3$ ile peptid işaretlemede ilk basamak uzun yarı ömürlü ^{68}Ge ve birçok metalin uzaklaştırılmasıdır. Bu saflaştırma basamağında kartuştan geçirilen elüsyon artığı cam atık şişelerinde biriktirilmektedir. Atık yönetimi iyi üretim uygulamalarına dahildir ve özellikle atığın uzun yarı ömre sahip ^{68}Ge (270,95 gün) aktivitesinin ve diğer toksik metal içeriğin incelenmesi gerekmektedir. Bu çalışmada amacımız ^{68}Ga elde edilmesinde

Address for Correspondence: Ayşe Uğur MD, Pamukkale University Training and Research Hospital, Clinic of Nuclear Medicine, Denizli, Turkey
Phone: +90 554 646 22 28 **E-mail:** ayseugur@pau.edu.tr ORCID ID: orcid.org/0000-0003-0913-6943
Received: 10.09.2020 **Accepted:** 06.12.2020

oluşan sıvı atıkta ^{68}Ge aktivitesini ve jeneratör kolon malzemelerinden kaynaklanan ağır metal konsantrasyonlarını belirlemek ve normal atık olarak atılıp atılamayacağını değerlendirmektir.

Yöntem: Merkezimizde iki farklı kimlikteki ^{68}Ge/^{68}Ga jeneratör eluatlarının PSH$^+$ kartuşundan geçirilmesi ile açığa çıkan sıvı atıklar, üniversitemiz ileri teknoloji uygulama ve araştırma merkezinde bulunan indüktif eşleşmiş plazma-kütle spektrometres cihazıyla analiz ettirilmiştir.

Bulgular: GalluGEN marka jeneratörde ön elüsyonda PSH$^+$ kartuşundan geçtikten sonra sıvı atık analizinde ortalama ^{68}Ge radyoaktif kirlilik 0,142 ppm (µg.mL-1), olarak tespit edildi. Kalay (Sn) safsızlığı yokken, ortalama çinkonun (Zn) 1.95 ppm (µg.mL^{-1}) ve ortalama alüminyum (Al) safsızlığının 10,95 ppm (µg.mL^{-1}), olduğu belirlendi. İThemba LABS marka jeneratör atıklarında ^{68}Ge radyoaktif kirliliği tespit edilmezken, ortalama Sn 0,098 ppm (µg.mL^{-1}), ortalama Zn 48,6 ppm (µg.mL^{-1}) ve ortalama Al safsızlık 4,135 ppm (µg.mL^{-1}) tespit edildi.

Sonuç: Üretilen tüm ^{68}Ge/^{68}Ga jeneratörlerinin kendine ait sertifikası bulunmaktadır. ^{68}Ge/^{68}Ga jeneratörlerin işaretleme sonrası atıklarındaki metalik kontaminasyonlar farklı olabilir. Bu atıkların kanalizasyon sistemlerine verilmeden önce içeriklerindeki uzun yarı ömürlü radyoaktif metalik kontaminasyonlar açısında yarı ömürleri dikkate alınarak bekletilmeleri güvenli bir yöntem olacaktır.

Anahtar kelimeler: Galyum-68, ^{68}Ge/^{68}Ga jeneratör, kimyasal safsızlık, GMP

Introduction

Gallium-68 (^{68}Ga) is a significant radionuclide due to its successful clinical application. Currently, ^{68}Ga is manufactured and supplied in preclinical and clinical settings using germanium-68 (^{68}Ge)/^{68}Ga generator systems (1). The interest in ^{68}Ga has grown tremendously in recent years as it has become a routinely used radioisotope in clinical positron emission tomography (PET) imaging facilities around the world. The ^{68}Ge has a half-life of 270.95 days (2) and can be used as the main nuclide in radionuclide generator system (3). In this radionuclide generator, the ^{68}Ge solid binds to an insoluble, inert carrier and forms a secular radioactive balance with ^{68}Ga ($T_{1/2}$=68 minute). ^{68}Ga can be eluted from the generator using a suitable solvent.

The limit value of ^{68}Ge fraction in a ^{68}Ga solution used in the labeling of radiopharmaceuticals is set as 0.001% in the European Pharmacopoeia monograph (4). With the increase in the age of the generator and increase in the number of elutions performed, the ^{68}Ge value may increase in addition to the regular activity. Furthermore, metal impurity from the generator may not be just radionuclides. Toxic metals from the column material are also among the impurities that can compete with ^{68}Ga in the complexation reaction. Moreover, zinc (Zn) formation occurs with the decay of ^{68}Ga. The presence of non-radioactive metals such as tin (Sn), arsenic, nickel, manganese, and aluminum (Al) that are considered metallic impurities in the ^{68}Ge/^{68}Ga generator eluate are known (5).

Prior to labeling with ^{68}Ga in radiopharmaceuticals, the ^{68}Ge/^{68}Ga generator eluate is subjected to pre-concentration and pre-purification. The various methods used for these processes are based on anion exchange chromatography, cation exchange chromatography, or combination thereof (5,6,7,8). The PSH$^+$ cartridge (from cation exchange cartridges) holds pure ^{68}Ga; other metals are collected in the waste bottle (Figure 1). We contrasted the two different generator eluates used in our department by separating them from the PSH$^+$ cartridge and analyzing the metallic contamination in liquid wastes with inductively coupled plasma-mass spectrometry (ICP-MS).

Materials and Methods

Sampling

These 2 generators, which are available at the nuclear medicine department of our university, have different column matrices. The identities of these generators are shown below:

- iThemba LABS (South Africa) ^{68}Ge/^{68}Ga generator
- PARS Isotope-GalluGEN (Iran) ^{68}Ge/^{68}Ga generator

$GaCl_3$ eluates were obtained from iThemba and PARS Isotope-GalluGEN commercial ^{68}Ga/^{68}Ge generators with

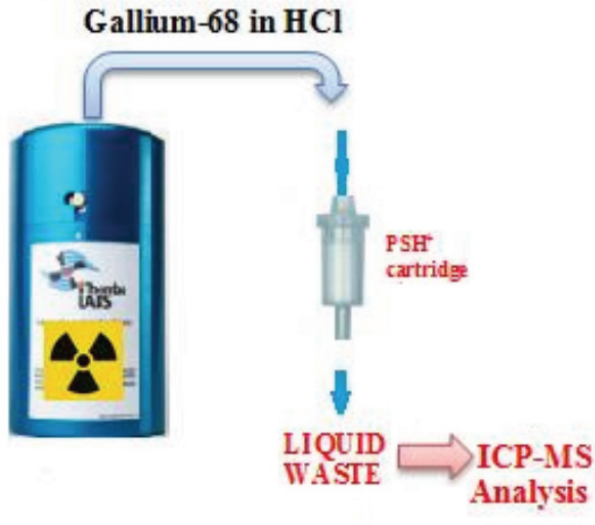

Figure 1. Schematic representation of liquid waste eluting from ^{68}Ge/^{68}Ga generator

^{68}Ge: Germanium-68, ^{68}Ga: Gallium-68, ICP: Inductively coupled plasma, MS: Mass spectrometry

HCl solution in the Scintomics GmbH GRP module 4V synthesis module. In addition, hydrochloric acids (0.6 M ultra-pure HCl, 0.1 M ultra-pure HCl) was obtained from ABX D-01454 Radeberg (Germany). Cation exchange cartridge (PSH^+, non-preconditioned) (ABX D-01454 Radeberg, Germany) was used to remove metals in $GaCl_3$ solution eluated from the ^{68}Ge/^{68}Ga generator. $GaCl_3$ was eluated from the PSH^+ cartridge with 5.0 M NaCl (ABX D-01454 Radeberg, Germany). Then, 7 mL (n=3) of waste solution was taken to the glass vial for analysis.

Measurements

The eluate from generators and leftover after ion exchange prior to radiolabeling is acidic and contains a certain amount of ^{68}Ge activity (7). Before the analysis, the eluates waited ten half-lives in the vials in compliance with the TAEA transport regulation.

Further, qualitative and quantitative analyses of metal contents in liquid waste were measured at the ppm level using the ICP-MS device located in the advanced technology application and research center of our university.

ICP-MS standard solutions were obtained from PerkinElmer (UK). Moreover, certified levels of standard solutions are as follows: Zn, 998 $\mu g.mL^{-1}$±5 µg/mL; Sn, 1.002 $\mu g.mL^{-1}$±5 µg mL; Al, 1.002 $\mu g.mL^{-1}$±5 µg mL; and Ge, 999 $\mu g.mL^{-1}$±5 µg/mL. Zn, Sn, Al, and Ge were used as internal standards for ICP-MS analysis. Further, no statistical method was used in the results, and the average of the sample analysis repeats was taken.

Results

As specified in the generator usage protocols, the generators were regularly eluted every day to avoid high ^{68}Ge excretion in the eluate. In both generators, the elutions, generated at one-day intervals, were passed through the PSH^+ cartridge, and samples (n=3) of the liquids discharged to waste were collected. Each sample (total of six samples) was analyzed three times with ICP-MS, and the averages are shown in Table 1. The average of ^{68}Ge radioactive pollution was estimated to be 0.142±0.05 ppm ($\mu g.mL^{-1}$) in the liquid waste analysis after passing through the PSH^+ cartridge in the pre-elution in the GalluGEN brand generator. While there was no Sn impurity, it was determined that the average Zn was 1.95±0.05 ppm ($\mu g.mL^{-1}$) and the average Al impurity was 10.95±0.05 ppm ($\mu g.mL^{-1}$) ppm. In the iThemba LABS brand generator waste, no ^{68}Ge radioactive pollution was calculated; on the other hand, the average Sn was 0.098±0.05 ppm ($\mu g.mL^{-1}$), average Zn 48.6±0.05 ppm ($\mu g.mL^{-1}$), and average Al impurity 4.135±0.05 ppm ($\mu g.mL^{-1}$).

Discussion

In nuclear medicine PET chemistry, liquid waste is the result of the production of radiopharmaceuticals and is able to contain heavy metals, chemicals, and radioactive compounds (8). Wastes from generator elution used in the production of radiopharmaceuticals with ^{68}Ga chemistry in many production centers are left to the sewer. Studies are performed on the reduction of ^{68}Ge activity in liquid waste and disposal of radioactively contaminated waste in nuclear medicine ^{68}Ga PET chemistry using a recirculation system with a sorbent (9,10). The ^{68}Ga radionuclide used in PET chemistry is typically obtained using commercial SnO_2- or TiO_2-based ^{68}Ge/^{68}Ga generators. It has been reported that the cleaning level of ^{68}Ge activity in wastes cannot exceed 10 Bq/g in the European Directive 96/29/EURATOM (11). The amount of ^{68}Ge in the elution specified in the generator manufacturer's certificates is ^{68}Ge <0.001% of nominal activity. The exemption concentrations and

Table 1. Comparison of the metal contents in the elution after passing the 2 different ^{68}Ge/^{68}Ga generator elutions through the PSH^+ cartridge (n=6). Elution conditions

					Metal impurity detected by ICP-MS (µg/mL) (n=3) SD (±0.05 µg.mL-1, ppm)			
Generator	**The age of the generator**	**Column material**	**Eluate solution (HCl)**	**Elution volume**	**^{68}Ge**	**Sn**	**Zn**	**Al**
PARS Isotope-GalluGEN	10 months	SnO_2,TiO_2	0.6 N	7 mL	0.142	ND	1.95	10.95
					0.158	ND	1.84	11.22
					0.126	ND	2.06	10.68
iThemba LABS	10 months	SnO_2	0.1 N	7 mL	ND	0.084	52.24	4.002
					ND	0.098	48.6	4.135
					ND	0.112	44.96	4.268

After the elutions were passed through the PSH^+ cartridge, the cartridge was washed with NaCl, ND: Not detected, ICP: Inductively coupled plasma, MS: Mass spectrometry, ^{68}Ge: Germanium-68, ^{68}Ga: Gallium-68, Sn: Tin, Zn: Zinc, Al: Aluminum

exemption activities of radionuclides in IAEA Safety Standards are shown in Table 2. The exemption limit for ^{68}Ge is 1x10^{1} (Bq/g) (12). Column materials are specially filled and approved for each of the ^{68}Ge/^{68}Ga generators used in clinical pet chemistry. Radioisotopes with a half-life of more than 100 days are not covered by the TAEA regulation; it is understood that they must be delivered to the National Storage Centers when they have exhausted their useful lives. The recycling or subsequent use of this radioisotope outside the specified landfill or reintroduction into the economic cycle should be strictly excluded. After passing through the PSH^{+} cartridge of the PARS Isotope-GalluGEN brand (10-month) generator from 2 different generators that we used in our study, we determined the ^{68}Ge radioactive pollution in the liquid waste above the value of 0.000036% specified in the certificate.

At the same time, the toxic metal threshold concentrations in liquid wastes were determined by the Hazardous Waste Control Regulation. ^{68}Ga decays with a half-life of 68 minutes to stable ^{68}Zn. After the iThemba brand generator elution, the Zn impurity in the waste is estimated to be 48.6 ppm, well above the 10 ppm value specified in the certificate. Waste resulting from the production and preparation of pharmaceutical products included in the "hazardous waste category according to their natural character or the activity that creates them" of the Hazardous Waste Control Regulation are evaluated in compliance with Annex 5 of the same regulation (13). According to the regulation, a highly toxic substance has a total concentration ≥0.1%, toxic substance at total concentration ≥3%, and harmful substance at total concentration ≥25%. In our study, Zn, Al, and Sn determined at the ppm level are below the 0.1% level defined in the regulation and toxic metal class. Zn pollution in waste is above the 10 ppm limit value specified in the certificate of the generator; it is also below the maximum toxic metal limit for the recycling of waste.

Table 2. The operating conditions of the ICP-MS device

The operating conditions	
Rf powers	1300 W
Gas flow rate	1.5 mL/min
Plasma gas flow	15 mL/min
Auxiliary gas flow	0.2 mL/min
Nebulizer gas flow	0.65 mL/min
Sample flow rate	1.5 mL/min
Flush time	20 sec
Read time	3 s

ICP: Inductively coupled plasma, MS: Mass spectrometry, Rf: Radio frequency, min: Minute

Conclusion

In our study, the toxic metal contents determined at the ppm level for both generators are below the levels to be specified in international regulations. In addition, increased metallic impurities associated with the increasing age of generators are an expected result. For aged ^{68}Ge/^{68}Ga generators, it is recommended that the generators pass the milking products through the PSH^{+} cartridge and hold for long half-life radioactive metals (especially for ^{68}Ge) before they are released into the sewer.

Disclosure Statement

The author has no personal interest in the commercial suppliers of ^{68}Ge/^{68}Ga generators or ^{68}Ga-labeled imaging pharmaceuticals.

Ethics

Ethics Committee Approval: This work does not contain any studies with human participants or animals performed by any of the authors.

Informed Consent: Not applicable.

Peer-review: Externally and internally peer-reviewed.

Authorship Contributions

Concept: O.Y., D.Y., Design: O.Y., D.Y., Analysis or Interpretation: A.U., Writing: A.U.

Conflict of Interest: No conflict of interest was declared by the authors.

Financial Disclosure: The authors declared that this study has received no financial support.

References

1. Kumar K. The Current Status of the Production and Supply of Gallium-68. Cancer Biother Radiopharm 2020;35:163-166.
2. Meinkin GE, Kurczak S, Mausner LF, Kolsky KL, Srivastava SC. Production of high specific activity 68Ge at Brookhaven National Laboratory. J Radioanal Nucl Chem 2005;263:553-557.
3. International Atomic Energy Agency (2010), Productıon of long lıved parent radıonuclıdes for generators: 68Ge, 82Sr, 90Sr and 188W, Radioisotopes and radiopharmaceuticals Series No.2, IAEA, Vienna.
4. European Pharmacopoeia 8.0, http://193.164.228.37/en/european-pharmacopoeia-8th-edition-1563.html
5. Velikyan I. 68Ga-Based radiopharmaceuticals: production and application relationship. Molecules 2015;20:12913-12943.
6. Rösch F. Past, present and future of 68Ge/68Ga generators. Appl Radiat Isot 2013;76:24-30.
7. Fitzsimmons JM, Mausner L. Production scale purification of Ge-68 and Zn-65 from irradiated gallium metal. Appl Radiat Isot 2015;101:60-64.
8. Breeman WA, de Jong M, de Blois E, Bernard BF, Konijnenberg M, Krenning EP. Radiolabelling DOTA-peptides with 68Ga. Eur J Nucl Med Mol Imaging 2005;32:478-485.

9. Vis R, Lavalaye J, van de Garde EM. GMP-compliant (68)Ga radiolabelling in a conventional small-scale radiopharmacy: a feasible approach for routine clinical use. EJNMMI Res 2015;5:27.
10. de Blois E, Chan HS, Roy K, Krenning EP, Breeman WA. Reduction of 68Ge activity containing liquid waste from 68Ga PET chemistry in nuclear medicine and radiopharmacy by solidification. J Radioanal Nucl Chem 2011;288:303-306.
11. The councıl of the european unıon, Council Directive 96/29/Euratom of 13 May 1996 laying down basic safety standards for the protection of the health of workers and the general public against the dangers arising from ionizing radiation, Official Journal of the European communities, L 159 39, Office for Official Publications of the European Communities, Luxembourg (1996).
12. Boal TJ, Pinak M. Dose limits to the lens of the eye: International Basic Safety Standards and related guidance. Ann ICRP 2015;44:112-117.
13. Tehlikeli Atıkların Kontrolü Yönetmeliği, tehlikeli kabul edilen atıkların özellikleri, Ek.5/2.madde, https://www.resmigazete.gov.tr/eskiler/2005/03/20050314-1.html

Original Article
Mol Imaging Radionucl Ther 2021;30:39-46 DOI:10.4274/mirt.galenos.2021.37268

Physiological Biodistribution of ^{68}Ga-DOTA-TATE in Normal Subjects

Normal Olgularda ^{68}Ga-DOTA-TATE'nin Fizyolojik Biyolojik Dağılımı

Salih Özgüven, Nuh Filizoğlu, Selin Kesim, Kevser Öksüzoğlu, Feyza Şen, Tunç Öneş, Sabahat İnanır, Halil Turgut Turoğlu, Tanju Yusuf Erdil

Marmara University Pendik Training and Research Hospital, Clinic of Nuclear Medicine, İstanbul, Turkey

Abstract

Objectives: Somatostatin is an endocrine peptide hormone that regulates neurotransmission and cell proliferation by interacting with G protein-coupled somatostatin receptors (SSTRs). SSTRs are specific molecular targets of several radiotracers for neuroendocrine tumor (NET) imaging. Gallium-68 (^{68}Ga)-DOTA-TATE is widely used for positron emission tomography/computed tomography (PET/CT) imaging of SSTRs and has shown a higher affinity for SSTR2, the most common SSTR subtype found in NETs. We aimed to analyze the distribution pattern of ^{68}Ga-DOTA-TATE in normal subjects.

Methods: A total of 617 consecutive ^{68}Ga-DOTA-TATE PET/CT whole-body scans performed in our department from May 2015 through April 2020 with known or suspected neuroendocrine malignancies, mostly to evaluate adrenal adenomas, were retrospectively analyzed by 2 nuclear medicine physicians. One hundred eighteen subjects without a diagnosis of NET, with no tracer avid lesion of NET on ^{68}Ga-DOTA-TATE PET/CT, and followed up for at least 6 months (average 2-3 years) without any biochemical, clinical, or imaging findings suggestive of NET were included in this study.

Results: The highest uptake of ^{68}Ga-DOTA-TATE was noted in the spleen followed by the kidneys, adrenal glands, liver, stomach, small intestine, prostate gland, pancreas head, pancreas body, thyroid gland, and uterus, in descending order. Minimal to mild uptake was detected in the submandibular glands, parotid glands, thymus, muscles, bones, breast, lungs, and mediastinum.

Conclusion: Our study shows the biodistribution pattern of ^{68}Ga-DOTA-TATE in normal subjects and the ranges of the maximum standard uptake value (SUV_{max}) and SUV_{mean} values of ^{68}Ga-DOTA-TATE obtained in several tissues for reliably identifying malignancy in ^{68}Ga-DOTA-TATE PET/CT studies.

Keywords: ^{68}Ga-DOTA-TATE, neuroendocrine tumors, PET/CT, somatostatin receptors, normal subjects

Öz

Amaç: Somatostatin, G proteinine bağlı somatostatin reseptörleri (SSTR) ile etkileşerek endokrin sistemi, nörotransmisyonu ve hücre proliferasyonunu düzenleyen bir peptid hormonudur. SSTR'ler, nöroendokrin tümör (NET) görüntüleme için çeşitli radyoaktif madde işaretli spesifik moleküllerin hedefidir. Galyum-68 (^{68}Ga)-DOTA-TATE, SSTR'lerin pozitron emisyon tomografisi/bilgisayarlı tomografi (PET/BT) görüntülemesinde yaygın olarak kullanılmaktadır ve NET'lerde bulunan en yaygın SSTR alt tipi olan SSTR2 için daha yüksek afinite gösterir.

Yöntem: Mayıs 2015'ten Nisan 2020'ye kadar, çoğu adrenal adenomların değerlendirilmesi amacı ile olmak üzere, nöroendokrin malignitesi şüphesi olan veya NET tanılı olgulara bölümümüzde yapılan 617 ^{68}Ga-DOTA-TATE PET/BT tüm vücut taraması, iki nükleer tıp hekimi tarafından geriye dönük olarak incelendi. NET tanısı olmayan, ^{68}Ga-DOTA-TATE PET/BT'de aktivite tutulumu gösteren lezyon saptanmayan ve klinik, biyokimyasal veya görüntülemede NET bulgusu olmaksızın en az 6 ay (ortalama 2-3 yıl) izlenen yüz on sekiz olgu bu çalışmaya dahil edilmiştir.

Address for Correspondence: Salih Özgüven MD, Marmara University Pendik Training and Research Hospital, Clinic of Nuclear Medicine, İstanbul, Turkey
Phone: +90 532 251 17 69 **E-mail:** drsozg@gmail.com ORCID ID: orcid.org/0000-0002-2790-7206
Received: 07.12.2020 **Accepted:** 09.01.2021

Bulgular: En yüksek ^{68}Ga-DOTA-TATE tutulumu dalakta kaydedildi ve bunu sırasıyla böbrekler, adrenal bezler, karaciğer, mide, ince bağırsak, prostat bezi, pankreas başı, pankreas gövdesi, tiroid bezi ve uterus takip etti. Submandibular bezlerde, parotis bezlerinde, timusta, kaslarda, kemiklerde, memede, akciğerlerde ve mediastende minimal veya hafif tutulum tespit edildi.

Sonuç: Bu çalışma, ^{68}Ga-DOTA-TATE PET/BT görüntülemede maligniteyi güvenilir bir şekilde tanımlayabilmek için normal olgularda ^{68}Ga-DOTA-TATE'nin biyolojik dağılım modelini ve çeşitli organlardan elde edilen maksimum standardize uptake değeri (SUV_{maks}) ve $SUV_{ortalama}$ değerlerinin aralıklarını gösterir.

Anahtar kelimeler: ^{68}Ga-DOTA-TATE, nöroendokrin tümörler, PET/BT, somatostatin reseptörleri, normal olgular

Introduction

Somatostatin is a peptide hormone that controls neurotransmission, hormone secretion, and cell proliferation by binding to somatostatin receptors (SSTRs). SSTRs are G protein-coupled membrane receptors presented on the cell surface of neuroendocrine cells. Five such receptor subtypes have been defined in humans (1,2). SSTRs are specific molecular targets of several radiotracers for neuroendocrine tumor (NET) imaging (3,4,5). However, the emergence of new positron emission tomography (PET) tracers has made PET/computed tomography (CT) imaging of SSTRs possible.

The somatostatin analogs Gallium-68 (^{68}Ga)-DOTA-TOC (DOTA-Tyr^3-octreotide), ^{68}Ga-DOTA-NOC (DOTA-Nal^3-octreotide), and ^{68}Ga-DOTA-TATE (DOTA-Tyr^3-octreotate) bind with varying affinity to SSTRs, and ^{68}Ga-DOTA-TATE has shown higher affinity for SSTR subtype 2 (SSTR2) (6). The majority of gastroenteropancreatic NETs overexpress SSTR2, thus ^{68}Ga-DOTA-TATE PET/CT is widely used to localize SSTR-expressing neuroendocrine neoplasms.

SSTRs are not only confined to NETs but are also demonstrated in various organs and hence, represent potential pitfalls. SSTR receptors have been described in the spleen, liver, pituitary gland, adrenal glands, head of the pancreas, thyroid, and urinary tract. It may be difficult to detect lesions in these organs, which show variable ^{68}Ga-DOTA-TATE uptake (7). Therefore, it is crucial to know the biodistribution of ^{68}Ga-DOTA-TATE when interpreting PET/CT imaging.

Recently, the number of studies outlining the role of ^{68}Ga-DOTA-TATE PET/CT in the staging and management of NETs has increased (8,9,10,11); however, there are few studies in the literature that define the physiological uptake patterns of ^{68}Ga-DOTA-TATE (7,12). In addition, there are limited data about the physiological uptake of ^{68}Ga-DOTA-TATE in disease-free patients (13).

The objective of this study is to investigate the normal distribution pattern and physiological variants of ^{68}Ga-DOTA-TATE in normal subjects on PET/CT imaging. This study presents the spectrum of normal standard uptake value (SUV) values in several organs and compares the results with previous reports. The main difference between this study and those previously reported is that our study population was proven to be clinically or pathologically disease-free before the examination and during follow-up.

Materials and Methods

Study Subjects

We retrospectively analyzed 617 consecutive ^{68}Ga-DOTA-TATE PET/CT whole-body scans performed in our department from May 2015 through April 2020 on patients with known or suspected neuroendocrine malignancies, mostly to evaluate adrenal adenomas. One hundred eighteen subjects without a diagnosis of NET, with no tracer avid lesion of NET on ^{68}Ga-DOTA-TATE PET/CT, and followed up for at least 6 months (average: 2-3 years) without any clinical, biochemical, or imaging evidence of NET were included in this study. Patients with a history or diagnosis of malignancy and younger than 18 years were excluded.

This study was performed with Marmara University Faculty of Medicine Research Ethics Committee review approval (date: December 2020, no: 09.2020.1317). All patients included in the study gave written informed consent before the examination.

Preparation of ^{68}Ga-DOTA-TATE

The ^{68}Ga-DOTA-TATE was prepared on a fully automated system using a standardized labeling sequence. Briefly, a commercially available germanium-68 (^{68}Ge)/^{68}Ga generator (iThemba Labs, SA) was eluted with 0.6 M hydrochloric acid. Effluent containing the ^{68}Ga fraction was transmitted to the PS-H+ cartridge to concentrate and purify ^{68}Ga from residual ^{68}Ge. The purified ^{68}Ga was then eluted with 1.7 mL 5 M sodium chloride into the reaction vial. Twenty-five micrograms DOTA-TATE (ABX, Germany) was dissolved using 3 mL of 1.5 M HEPES buffer solution in the reaction vial. The reaction was performed at 100 °C for 8 minutes. A C-18 light cartridge was used to purify the ^{68}Ga-DOTA-TATE. The purified ^{68}Ga-DOTA-TATE was eluted with 1 mL ethanol and 1 mL water solutions and passed

into a sterile vial. Radiochemical purity was over 95% in all cases, based on high-performance liquid chromatography.

^{68}Ga-DOTA-TATE Imaging

All ^{68}Ga-DOTA-TATE PET/CT scans were conducted using a hybrid PET/CT scanner (Discovery- 16 LS; GE Healthcare, Waukesha, Wisconsin, USA) in the Nuclear Medicine Department. Iohexol (Omnipaque; GE Healthcare) was used as the oral contrast agent. ^{68}Ga-DOTA-TATE (2 MBq/kg) was administered intravenously. Whole-body images from skull base to mid-thigh were acquired 60±10 minutes after the injection. A low-dose 16-slice multidetector CT scan (parameters: 80 mA, 140 kV, table speed 27 mm/rotation, and slice width of 5.0 mm) was used to screen the body from mid-thigh to the base of the skull. A standard whole-body PET scan was conducted in 3D mode with an acquisition time of 3 min per bed position (six to eight bed positions) scanning the exact area with the CT scan. PET images were reconstructed with and without correction for attenuation using an iterative algorithm. Next, a workstation (Advantage Windows Workstation 4.6; GE Advantage) was used for processing and interpretation.

Image Analysis

^{68}Ga-DOTA-TATE PET/CT images were analyzed by two nuclear medicine physicians. Maximum SUV (SUV_{max}) and SUV_{mean} values were calculated from a volume of interest (ROI) applied in the transaxial attenuation-corrected PET slice. ROIs obtained on CT images were applied to PET images. SUV_{max} was defined as the SUV_{max} in the ROI. SUV_{mean} was taken as the average SUV concentration in ROI. SUV_{max} and SUV_{mean} were evaluated on axial images in 29 normal anatomical structures for each patient using at least 2cm circular ROIs, avoiding inclusion of any activity from adjacent organs (Figure 1). Lung measurements were performed in the lower lobes away from the hilar vasculature, and kidney measurements were performed by avoiding the inclusion of pelvicalyceal urinary activity. SUV_{max} and SUV_{mean} values for the pituitary gland, parotid glands, submandibular glands, thymus, thyroid gland, mediastinum, lungs, breast, stomach, small intestine, liver, spleen, pancreas head, pancreas body, right adrenal gland, left adrenal gland, right kidney, left kidney, prostate, uterus, trapezius muscle, gluteal muscles, iliac crest, and femora were obtained. The maximum SUV_{max} and SUV_{mean} values are accepted as the representative values for that organ.

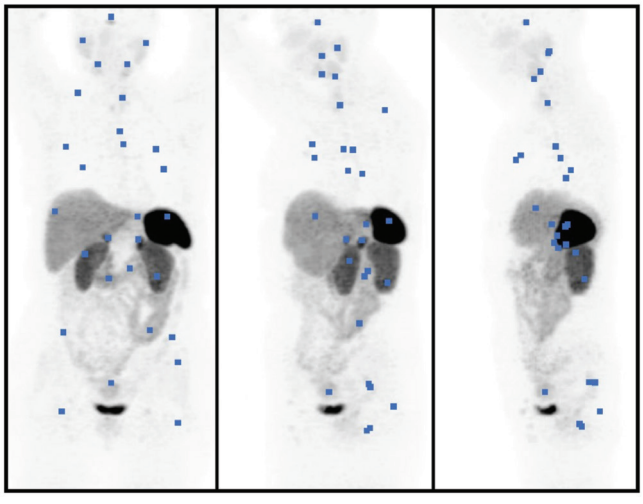

Figure 1. Regions of interest drawn on anterior, oblique, and lateral (from left to right) maximum intensity projection images

Statistical Analysis

Univariate descriptive statistics [mean, median, standard deviation (SD), frequency, and range] were calculated on Microsoft Excel for Mac version 16.37 (Microsoft Corporation).

Results

From our cohort of 118 subjects, 45 patients (38.1%) were men, and 73 patients (61.9%) were women. The average age of the patients was 51.83 years (range 18-85 years; SD 13.99 years). The SUV_{max} values were categorized as high, moderate, mild, and minimal in accordance with the study of Moradi et al. (7).

Maximum physiological uptake was detected in the spleen. In addition to the spleen, high physiological uptake (average SUV_{max} >8.98 g/mL, which is the 50th percentile of hepatic uptake) was also noted in the kidneys, adrenal glands, and liver, in descending order. Moderate uptake (average SUV_{max} >3.92, which demonstrated lower uptake than the liver) was observed in the stomach, small intestine, prostate gland, pancreas head and body, thyroid gland, and uterus. Mild uptake (from minimal uptake to moderate uptake) was revealed in the submandibular and parotid glands. Minimal uptake (average SUV_{max} <2 g/mL) of tracer was observed in the thymus (n=12), gluteal and trapezius muscles, femora, iliac crest, breast tissue, lungs, and mediastinum. No specific uptake (less than mediastinal blood pool activity) was seen in the subcutaneous fat tissue and brain tissue. The average SUV_{max} (± SD), average SUV_{mean} (± SD), and range of uptake on ^{68}Ga-DOTA-TATE PET/CT for all the organs considered are summarized in Table 1. Figure 2, 3 represent the average and the range of physiological uptake of the organs as measured by SUV_{max} and SUV_{mean}, respectively.

Table 1. Average SUV_{max} (± SD), average SUV_{mean} (± SD), and range of uptake of ^{68}Ga DOTA-TATE PET/CT for all organs						
Organ	**SUV_{max} (average)**	**SUV_{max} (± SD)**	**SUV_{max} (range)**	**SUV_{mean} (average)**	**SUV_{mean} (± SD)**	**SUV_{mean} (range)**
Pituitary gland	5.40	2.06	1.51-11.73	3.47	1.40	0.83-9.03
Parotid gland	2.43	1.02	0.38-5.72	1.42	0.63	0.21-3.30
Submandibular gland	2.5	0.72	1.08-4.61	1.44	0.43	0.64-2.79
Thyroid gland	4.33	1.63	1.48-10.97	2.43	0.92	0.81-5.93
Thymus	1.71	0.70	0.84-2.90	0.95	0.39	0.49-1.63
Breast	0.78	0.3	0.27-1.72	0.43	0.16	0.18-0.94
Lungs	0.71	0.27	0.24-1.71	0.39	0.14	0.14-0.93
Mediastinum	0.68	0.32	0.19-2.54	0.4	0.19	0.11-1.49
Stomach	7.78	3.05	1.75-15.96	4.05	1.8	1.00-9.64
Liver	9.13	2.18	3.92-15.72	5.58	1.46	2.77-9.34
Spleen	28.27	5.99	11.08-45.07	19.25	4.36	7.74-30.94
Pancreas head	4.94	2.37	1.59-15.43	2.9	1.24	1.19-8.27
Pancreas body	4.46	1.54	1.71-8.29	2.87	0.88	1.24-5.82
Right adrenal gland	10.89	3.46	2.41-20.51	6.37	1.97	1.42-12.17
Left adrenal gland	11.57	3.36	3.81-21.04	6.77	1.99	2.16-12.35
Right kidney	14.39	4.16	5.53-19.74	8.64	2.36	3.02-16.06
Left kidney	14.2	4.35	4.6-30.03	8.55	2.36	2.41-15.45
Small intestine	5.64	1.81	2.23-12.54	3.17	0.99	1.17-6.72
Prostate	5.46	1.98	2.13-11.13	3.17	1.64	1.20-6.64
Uterus	3.98	1.4	1.77-7.35	2.24	0.28	0.25-1.72
Trapezius muscle	0.88	0.28	0.25-1.72	0.5	0.15	0.15-0.9
Gluteal muscle	1.2	0.41	0.35-2.66	0.65	0.2	0.25-1.37
Iliac crest	1.14	0.37	0.38-3.12	0.65	1.19	0.23-1.68
Femora	1.16	0.41	0.38-3.31	0.62	0.23	0.21-1.70
SUV_{max}: Maximum standard uptake values, SD: Standard deviation, ^{68}Ga: Gallium-68, PET/CT: Positron emission tomography/computed tomography						

Discussion

To the best of our knowledge, this is the first study to investigate the physiological distribution pattern of ^{68}Ga-DOTA-TATE in normal subjects who had not previously been diagnosed with malignancy and who were proven to be clinically or pathologically disease-free during follow-up. This study also shows the ranges of the SUV_{max} and SUV_{mean} values of ^{68}Ga-DOTA-TATE obtained in the different organs of normal subjects. The highest uptake of ^{68}Ga-DOTA-TATE was documented in the spleen followed by the kidneys, adrenal glands, liver, stomach, small intestine, prostate gland, pancreas head, pancreas body, thyroid gland, and uterus, in descending order. Minimal to mild uptake was detected in the submandibular glands, parotid glands, thymus, muscles, bones, breast, lungs, and mediastinum.

In this study, when the distribution of ^{68}Ga-DOTA-TATE was analyzed from the vertex to the mid-thigh, regarding the head region, moderate ^{68}Ga-DOTA-TATE uptake in the pituitary gland was observed. This can be explained easily by the presence of SSTR2 in the anterior lobe cells of the pituitary gland (14). However, no activity uptake was observed in the cranium other than the pituitary gland. Although both SSTR1 and SSTR2 have been described in the cerebral cortex, the limbic system, the paraventricular nuclei of the hypothalamus and basal ganglia, ^{68}Ga-DOTA-TATE cannot pass through the blood-brain barrier (15). Hence, ^{68}Ga-DOTA-TATE uptake was not recorded in the brain parenchyma. The salivary glands, including the parotid and submandibular glands, demonstrated diffuse and homogenous uptake of ^{68}Ga-DOTA-TATE, which is expected as Anzola et al. (16) demonstrated that SSTRs are commonly expressed in the salivary glands.

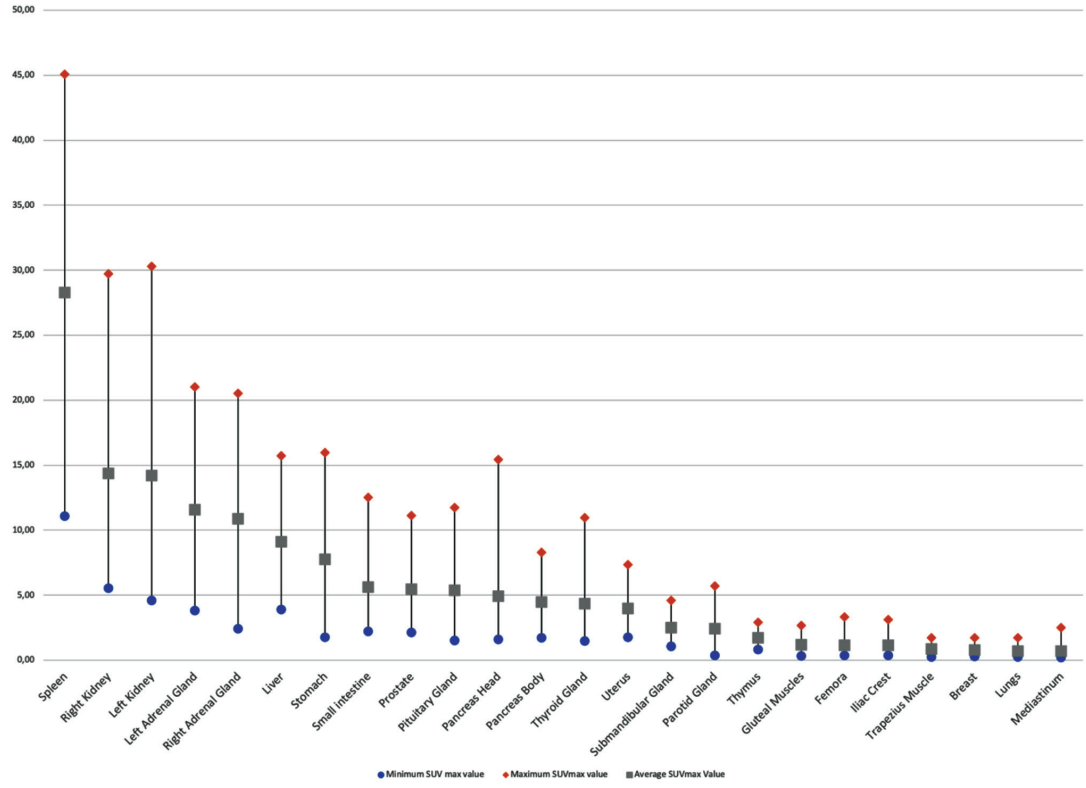

Figure 2. Average and range of maximum SUVs of different organs in normal subjects

SUVs: Standard uptake values

In the neck region, the thyroid gland showed wide variation in the uptake of ^{68}Ga-DOTA-TATE in our study, and the ranges of SUV_{max} and SUV_{mean} were 1.48-10.97 and 0.81-5.93, respectively. SSTR2 expression in both normal and pathological thyroid tissues explain this situation. Thyroid adenomas, Grave's disease, multinodular goiters, and active Hashimoto disease have been reported to increase the uptake of ^{68}Ga-DOTA-TATE (17).

Since the glandular tissue of the breast expresses no significant SSTR2 (18), low levels of SUVs were observed in the breast. Unlike normal breast tissue, breast tumors may express different types of SSTRs (19). The risk of breast cancer should also be considered when focal and increased ^{68}Ga-DOTA-TATE is detected.

In the chest, minimal ^{68}Ga-DOTA-TATE uptake was observed in the lungs. SSTR2 is expressed on various components of lung inflammation, such as epithelial cells, inflammatory cells, and potentially fibroblasts (20). However, normal lung tissue mainly has SSTR4, which does not bind to ^{68}Ga-DOTA-TATE, and in the absence of inflammation, lung tissue shows minimal uptake of ^{68}Ga-DOTA-TATE, as in our study (20). Minimal ^{68}Ga-DOTA-TATE uptake related to the mediastinal blood pool activity was also observed in our study. Adams et al. (21) showed the expression of SSTR1 and SSTR3 on inactivated endothelial cells, while SSTR2 is overexpressed on activated endothelial cells. Besides, granulocytes and red blood cells have no SSTRs (21). Therefore, only minimal uptake of ^{68}Ga-DOTA-TATE in the mediastinum was detected in our normal subject group.

There are two primary components in the spleen, the red pulp and the white pulp. Studies have shown that SSTRs are primarily found in the red pulp of the spleen (22). Reubi et al. (23) also reported that red pulp comprises diffusely disseminated SSTRs. SSTR2 is the most frequent SSTR subtype presented in the spleen (24). As a result of this, the spleen showed intense ^{68}Ga-DOTA-TATE uptake, resulting as expected in the highest SUV values, with average SUV_{max} and SUV_{mean} values of 28.27±5.99 and 19.25±4.36, respectively.

Relatively high ^{68}Ga-DOTA-TATE uptake was also seen in the liver. The liver, which metabolizes peptides, is believed to extract ^{68}Ga-DOTA-TATE from the blood, and this leads

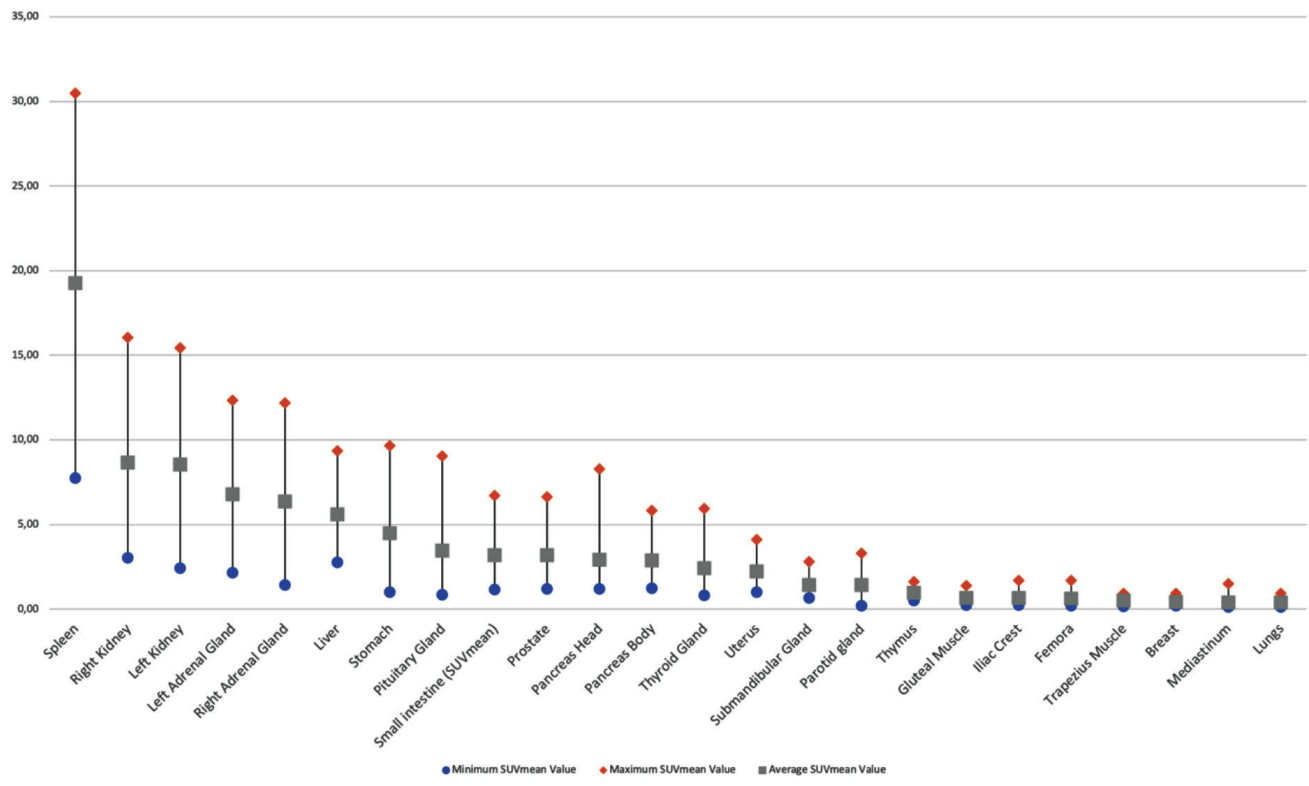

Figure 3. Average and range of mean SUVs of different organs in normal subjects

SUVs: Standard uptake values

to hepatic uptake of ^{68}Ga-DOTA-TATE (25). Furthermore, studies have shown that hepatocytes and hepatic stellate cells of the normal liver parenchyma do not express any of the SSTR subtypes (26). Although SSTR2 and SSTR4 are found in cholangiocytes and endothelial cells, we did not detect any ^{68}Ga-DOTA-TATE activity in the biliary system.

Variable uptake of ^{68}Ga-DOTA-TATE was detected throughout the pancreas. Higher physiological uptake in the uncinate process has been reported in previous studies due to the existence of subtypes 2, 3, and 5 of SSTR on islet cells and the higher density of islet cells in this region (27). However, Ionescu-Tirgoviste et al. (28) proved that the number of islets in the head of the pancreas is alike to that of other parts of the pancreas. In correlation with this, we observed similar SUV values in the head and body of the pancreas in our study (average SUV_{max} and SUV_{mean} were 4.94 and 2.90 for the pancreas head versus 4.46 and 2.87 for the pancreas body). Since islets may be present in clusters in any area of the pancreas, increased 68Ga-DOTA-TATE activity in such a region can be a normal variant for the pancreas.

A high uptake of ^{68}Ga-DOTA-TATE was also found in the adrenal glands. The reason for this relatively high uptake is the presence of the five subtypes of SSTRs, mostly SSTR2, in the adrenal gland, which has been shown by Epelbaum et al. (29). SSTR2 expression in gastric cells has been demonstrated in previous *in vitro* immunohistochemistry studies (30). In correlation with these studies, we recorded high ^{68}Ga-DOTA-TATE uptake in the stomach wall.

In our study, irregular and variable ^{68}Ga-DOTA-TATE uptake was also observed in the intestine. It should be noted that this irregular and variable uptake may be the result of bowel motility and movement artifacts, as well as the expression of SSTR2 at different rates in the entire gastrointestinal (GI) tract. Previous studies have identified the SSTRs in the lymphoid tissue associated with the gut, myenteric, and submucosal plexus (30,31). Finally, the vessels in the inflammatory regions of the GI tract have been found to overexpress SSTR2, which can be another cause of focal uptake in the intestine (23).

In the evaluation of the urogenital system, the highest activity uptake was noted in the kidneys. DOTA peptide

can be filtered through glomeruli but is also partially reabsorbed in the proximal tubule, which leads to increased activity besides the absorbed activity in the renal cortex (32). In the kidney, somatostatin lowers the glomerular filtration rate and reduces renal blood flow directly by renal vasoconstriction. It exerts an anti-diuretic effect by suppressing free water clearance at the cellular level and inhibiting vasopressin-induced water permeability in the distal tubules (33). Reubi et al. (34) demonstrated that vasa recta in the human kidney expresses high-density SSTR2. This could be the major reason for the high SUV values in the kidneys. SSTR2 receptors have also been shown in the tubular cells of the renal cortex, albeit at a lower density (34).

SSTRs have been found particularly in the stromal component of the prostate tissue. SSTR2 is preferably expressed in the normal prostate, while SSTR1 and SSTR5 are expressed in prostate cancer (35). SSTR2 deficiency in prostate cancer may explain the treatment ineffectiveness of some selective somatostatin analogs.

Green et al. (36) demonstrated SSTR2 expression in the endometrium during all stages of the menstrual cycle. Moreover, Schulz et al. (37) showed high SSTR1, SSTR2, and SSTR3 immunoreactivity in endometrial cancers. In line with these studies, a mild heterogeneous ^{68}Ga-DOTA-TATE uptake in the uterus was seen in normal subjects.

A very low level of ^{68}Ga-DOTA-TATE uptake in skeletal muscle and bones was observed. The reason for this minimal uptake is the expression of low levels of SSTRs in both osteoblasts and myoblasts. Therefore, a high level of ^{68}Ga-DOTA-TATE uptake is not seen in the musculoskeletal system unless there is an inflammatory condition or malignancy (12).

Study Limitations

This study had some limitations. For example, it included only subjects of Turkish nationality, so the results may not be generalized to populations of different ethnic origins. Another limitation is that our sample size was relatively small (n=12) to infer the range of normal SUV values of physiological thymic ^{68}Ga-DOTA-TATE uptake.

Conclusion

This study shows the biodistribution pattern of ^{68}Ga-DOTA-TATE in normal subjects. The ranges of the SUV_{max} and SUV_{mean} values of ^{68}Ga-DOTA-TATE obtained in the various organs is important for reliably identifying malignancy in ^{68}Ga-DOTA-TATE PET/CT studies.

Ethics

Ethics Committee Approval: This study was performed with Marmara University Faculty of Medicine Research Ethics Committee review approval (date: December 2020, no: 09.2020.1317).

Informed Consent: Informed consents were obtained from the patients for conducting V/Q 68Ga-DOTA-TATE PET/CT examinations.

Peer-review: Externally peer-reviewed.

Authorship Contributions

Surgical and Medical Practices: S.Ö., N.F., S.K., K.Ö., F.Ş., T.Ö., S.İ., H.T.T., T.Y.E., Concept: S.Ö., N.F., S.K., Design: S.Ö., N.F., S.K., Data Collection or Processing: S.Ö., N.F., S.K., Analysis or Interpretation: S.K., N.F., S.K., Literature Search: S.Ö., N.F., S.K., Writing: S.Ö., N.F., S.K.

Conflict of Interest: No conflict of interest was declared by the authors.

Financial Disclosure: The authors declared that this study has received no financial support.

References

1. Bhanat E, Koch CA, Parmar R, Garla V, Vijayakumar V. Somatostatin receptor expression in non-classical locations - clinical relevance? Rev Endocr Metab Disord 2018;19:123-132.
2. Reubi JC, Waser B, Schaer JC, Laissue JA. Somatostatin receptor sst1-sst5 expression in normal and neoplastic human tissues using receptor autoradiography with subtype-selective ligands. Eur J Nucl Med 2001;28:836-846.
3. Olsen JO, Pozderac RV, Hinkle G, Hill T, O'Dorisio TM, Schirmer WJ, Ellison EC, O'Dorisio MS. Somatostatin receptor imaging of neuroendocrine tumors with indium-111 pentetreotide (Octreoscan). Semin Nucl Med 1995;25:251-261.
4. van den Anker-Lugtenburg PJ, Krenning EP, Oei HY, Van Hagen MP, Gerrits CJ, Reubi JC, Lamberts SW, Löwenberg B. Somatostatin receptor scintigraphy in the initial staging of Hodgkin's disease. Br J Haematol 1996;93:96-103.
5. Kwekkeboom DJ, Krenning EP. Somatostatin receptor imaging. Semin Nucl Med 2002;32:84-91.
6. Virgolini I, Ambrosini V, Bomanji JB, Baum RP, Fanti S, Gabriel M, Papathanasiou ND, Pepe G, Oyen W, De Cristoforo C, Chiti A. Procedure guidelines for PET/CT tumour imaging with 68Ga-DOTA-conjugated peptides: 68Ga-DOTA-TOC, 68Ga-DOTA-NOC, 68Ga-DOTA-TATE. Eur J Nucl Med Mol Imaging 2010;37:2004-2010.
7. Moradi F, Jamali M, Barkhodari A, Schneider B, Chin F, Quon A, Mittra ES, Iagaru A. Spectrum of 68Ga-DOTA TATE Uptake in Patients With Neuroendocrine Tumors. Clin Nucl Med 2016;41:281-287.
8. Ilhan H, Fendler WP, Cyran CC, Spitzweg C, Auernhammer CJ, Gildehaus FJ, Bartenstein P, Angele MK, Haug AR. Impact of (68) Ga-DOTATATE PET/CT on the surgical management of primary neuroendocrine tumors of the pancreas or ileum. Ann Surg Oncol 2015;22:164-171.
9. Mojtahedi A, Thamake S, Tworowska I, Ranganathan D, Delpassand ES. The value of (68)Ga-DOTATATE PET/CT in diagnosis and management of neuroendocrine tumors compared to current FDA approved

imaging modalities: a review of literature. Am J Nucl Med Mol Imaging 2014;4:426-434.

10. Gabriel M, Decristoforo C, Kendler D, Dobrozemsky G, Heute D, Uprimny C, Kovacs P, Von Guggenberg E, Bale R, Virgolini IJ. 68Ga-DOTA-Tyr3-octreotide PET in neuroendocrine tumors: comparison with somatostatin receptor scintigraphy and CT. J Nucl Med 2007;48:508-518.
11. Al-Nahhas A, Win Z, Szyszko T, Singh A, Nanni C, Fanti S, Rubello D. Gallium-68 PET: a new frontier in receptor cancer imaging. Anticancer Res 2007;27:4087-4094.
12. Kuyumcu S, Özkan ZG, Sanli Y, Yilmaz E, Mudun A, Adalet I, Unal S. Physiological and tumoral uptake of (68)Ga-DOTATATE: standardized uptake values and challenges in interpretation. Ann Nucl Med 2013;27:538-545.
13. Shastry M, Kayani I, Wild D, Caplin M, Visvikis D, Gacinovic S, Reubi JC, Bomanji JB. Distribution pattern of 68Ga-DOTATATE in disease-free patients. Nucl Med Commun 2010;31:1025-1032.
14. Shimon I. Somatostatin receptors in pituitary and development of somatostatin receptor subtype-selective analogs. Endocrine 2003;20:265-269.
15. Sharma P, Mukherjee A, Bal C, Malhotra A, Kumar R. Somatostatin receptor-based PET/CT of intracranial tumors: a potential area of application for 68 Ga-DOTA peptides? AJR Am J Roentgenol 2013;201:1340-1347.
16. Anzola LK, Rivera JN, Dierckx RA, Lauri C, Valabrega S, Galli F, Moreno Lopez S, Glaudemans AWJM, Signore A. Value of Somatostatin Receptor Scintigraphy with 99mTc-HYNIC-TOC in Patients with Primary Sjögren Syndrome. J Clin Med 2019;8:763.
17. Druckenthaner M, Schwarzer C, Ensinger C, Gabriel M, Prommegger R, Riccabona G, Decristoforo C. Evidence for Somatostatin receptor 2 in thyroid tissue. Regul Pept 2007;138:32-39.
18. Albérini JL, Meunier B, Denzler B, Devillers A, Tass P, Dazord L, Le Simple T, Laissue J, de Jong R, Le Cloirec J, Reubi JC, Bourguet P. Somatostatin receptor in breast cancer and axillary nodes: study with scintigraphy, histopathology and receptor autoradiography. Breast Cancer Res Treat 2000;61:21-32.
19. Dude I, Zhang Z, Rousseau J, Hundal-Jabal N, Colpo N, Merkens H, Lin KS, Bénard F. Evaluation of agonist and antagonist radioligands for somatostatin receptor imaging of breast cancer using positron emission tomography. EJNMMI Radiopharm Chem 2017;2:4.
20. Gugger M, Waser B, Kappeler A, Schonbrunn A, Reubi JC. Immunohistochemical localization of somatostatin receptor sst2A in human gut and lung tissue: possible implications for physiology and carcinogenesis. Ann N Y Acad Sci 2004;1014:132-136.
21. Adams RL, Adams IP, Lindow SW, Zhong W, Atkin SL. Somatostatin receptors 2 and 5 are preferentially expressed in proliferating endothelium. Br J Cancer 2005;92:1493-1498.
22. Melis M, Kaemmerer D, de Swart J, Kulkarni HR, Lupp A, Sänger J, Groen HC, Konijnenberg MW, de Jong M, Baum RP. Localization of Radiolabeled Somatostatin Analogs in the Spleen. Clin Nucl Med 2016;41:111-114.
23. Reubi JC, Horisberger U, Kappeler A, Laissue JA. Localization of receptors for vasoactive intestinal peptide, somatostatin, and substance P in distinct compartments of human lymphoid organs. Blood 1998;92:191-197.
24. Boy C, Heusner TA, Poeppel TD, Redmann-Bischofs A, Unger N, Jentzen W, Brandau W, Mann K, Antoch G, Bockisch A, Petersenn S. 68Ga-DOTATOC PET/CT and somatostatin receptor (sst1-sst5) expression in normal human tissue: correlation of sst2 mRNA and SUVmax. Eur J Nucl Med Mol Imaging 2011;38:1224-1236.
25. Reynaert H, Rombouts K, Vandermonde A, Urbain D, Kumar U, Bioulac-Sage P, Pinzani M, Rosenbaum J, Geerts A. Expression of somatostatin receptors in normal and cirrhotic human liver and in hepatocellular carcinoma. Gut 2004;1180-1189.
26. Reubi JC, Zimmermann A, Jonas S, Waser B, Neuhaus P, Läderach U, Wiedenmann B. Regulatory peptide receptors in human hepatocellular carcinomas. Gut 1999;45:766-774.
27. Brabander T, Teunissen J, Kwekkeboom D. Physiological Uptake in the Pancreatic Head on Somatostatin Receptor Scintigraphy Using [111In-DTPA]Octreotide: Incidence and Mechanism. Clin Nucl Med 2017;42:15-19.
28. Ionescu-Tirgoviste C, Gagniuc PA, Gubceac E, Mardare L, Popescu I, Dima S, Militaru M. A 3D map of the islet routes throughout the healthy human pancreas. Sci Rep 2015;5:14634.
29. Epelbaum J, Bertherat J, Prevost G, Kordon C, Meyerhof W, Wulfsen I, Richter D, Plouin PF. Molecular and pharmacological characterization of somatostatin receptor subtypes in adrenal, extraadrenal, and malignant pheochromocytomas. J Clin Endocrinol Metab 1995;80:1837-1844.
30. Gugger M, Waser B, Kappeler A, Schonbrunn A, Reubi JC. Cellular detection of sst2A receptors in human gastrointestinal tissue. Gut 2004;53:1431-1436.
31. Reubi JC, Horisberger U, Waser B, Gebbers JO, Laissue J. Preferential location of somatostatin receptors in germinal centers of human gut lymphoid tissue. Gastroenterology 1992;103:1207-1214.
32. Hofman MS, Lau WF, Hicks RJ. Somatostatin receptor imaging with 68Ga DOTATATE PET/CT: clinical utility, normal patterns, pearls, and pitfalls in interpretation. Radiographics 2015;35:500-516.
33. Balster DA, O'Dorisio MS, Summers MA, Turman MA. Segmental expression of somatostatin receptor subtypes sst(1) and sst(2) in tubules and glomeruli of human kidney. Am J Physiol Renal Physiol 2001;280:457-465.
34. Reubi JC, Horisberger U, Studer UE, Waser B, Laissue JA. Human kidney as target for somatostatin: high affinity receptors in tubules and vasa recta. J Clin Endocrinol Metab 1993;77:1323-1328.
35. Reubi JC, Waser B, Schaer JC, Markwalder R. Somatostatin receptors in human prostate and prostate cancer. J Clin Endocrinol Metab 1995;80:2806-2814.
36. Green VL, Richmond I, Maguiness S, Robinson J, Helboe L, Adams IP, Drummond NS, Atkin SL. Somatostatin receptor 2 expression in the human endometrium through the menstrual cycle. Clin Endocrinol (Oxf) 2002;56:609-614.
37. Schulz S, Schmitt J, Weise W. Frequent expression of immunoreactive somatostatin receptors in cervical and endometrial cancer. Gynecol Oncol 2003;89:385-390.

Interesting Image
Mol Imaging Radionucl Ther 2021;30:47-49 DOI:10.4274/mirt.galenos.2020.65668

^{18}F-FDG PET/CT Imaging of Metastatic Testicular Choriocarcinoma Mimicking Gastric Cancer which Initial Symptom is Melena

Başlangıç Semptomu Melena Olan Mide Kanserini Taklit Eden Metastatik Testis Koryokarsinomunun ^{18}F-FDG PET/BT Görüntülemesi

Sibel Göksel[1], Serkan Akın[2], Remzi Adnan Akdoğan[3], Sema Rakıcı[4], Göksu Yavuz Abdioğlu[5], Muhammet Ali Ayvaz[3]

[1]*Recep Tayyip Erdoğan University Faculty of Medicine, Department of Nuclear Medicine, Rize, Turkey*
[2]*Recep Tayyip Erdoğan University Faculty of Medicine, Department of Medical Oncology, Rize, Turkey*
[3]*Recep Tayyip Erdoğan University Faculty of Medicine, Department of Gastroenterology, Rize, Turkey*
[4]*Recep Tayyip Erdoğan University Faculty of Medicine, Department of Radiation Oncology, Rize, Turkey*
[5]*Recep Tayyip Erdoğan University Faculty of Medicine, Department of Pathology, Rize, Turkey*

Abstract

Gastric metastasis of choriocarcinoma is rarely reported in the literature. This case report presents the case of multiple metastatic testicular choriocarcinoma mimicking gastric cancer, with melena as the initial symptom. In this case, ^{18}fluorine-fluorodeoxyglucose positron emission tomography/computed tomography (PET/CT) showed that the testis was the primary focus. The contribution of PET/CT is significant to primary focus detection in metastatic diseases of unknown primary origin that presented gastrointestinal bleeding. In addition to its use in staging of testicular carcinoma, PET/CT provides significant benefit in evaluating patients with increased levels of tumor markers and in detecting recurrence.

Keywords: Gastric metastasis, melena, testicular choriocarcinoma, ^{18}F-FDG PET/CT

Öz

Koryokarsinomun mide metastazı literatürde oldukça nadir bildirilmiştir. Bu olgu raporu, mide kanserini taklit eden, başlangıç semptomu melena olan multipl metastatik testis koryokarsinomlu bir hastayı sunmaktadır. Bu olguda, ^{18}flor-florodeoksiglukoz pozitron emisyon tomografisi/bilgisayarlı tomografi (PET/BT) testisin primer odak olduğunu gösterdi. PET/BT'nin katkısı, gastrointestinal kanama ile gelen primeri bilinmeyen metastatik hastalıkta primer odak tespitinde önemlidir. Testis kanserinde PET/BT, hastalık evrelendirilmesine sağladığı faydalara ek olarak, özellikle tümör belirteçleri artmış ve nüks hastalık açısından şüpheli olan hastalarda rekürrensi tespit etmede önemli fayda sağlar.

Anahtar kelimeler: Mide metastazı, melena, testiküler koryokarsinom, ^{18}F-FDG PET/BT

Address for Correspondence: Sibel Göksel MD, Recep Tayyip Erdoğan University Faculty of Medicine, Department of Nuclear Medicine, Rize, Turkey
Phone: +90 543 389 77 14 **E-mail:** sibelkandemirgoksel@gmail.com ORCID ID: orcid.org/0000-0003-1425-8347
Received: 08.01.2019 **Accepted:** 13.10.2020

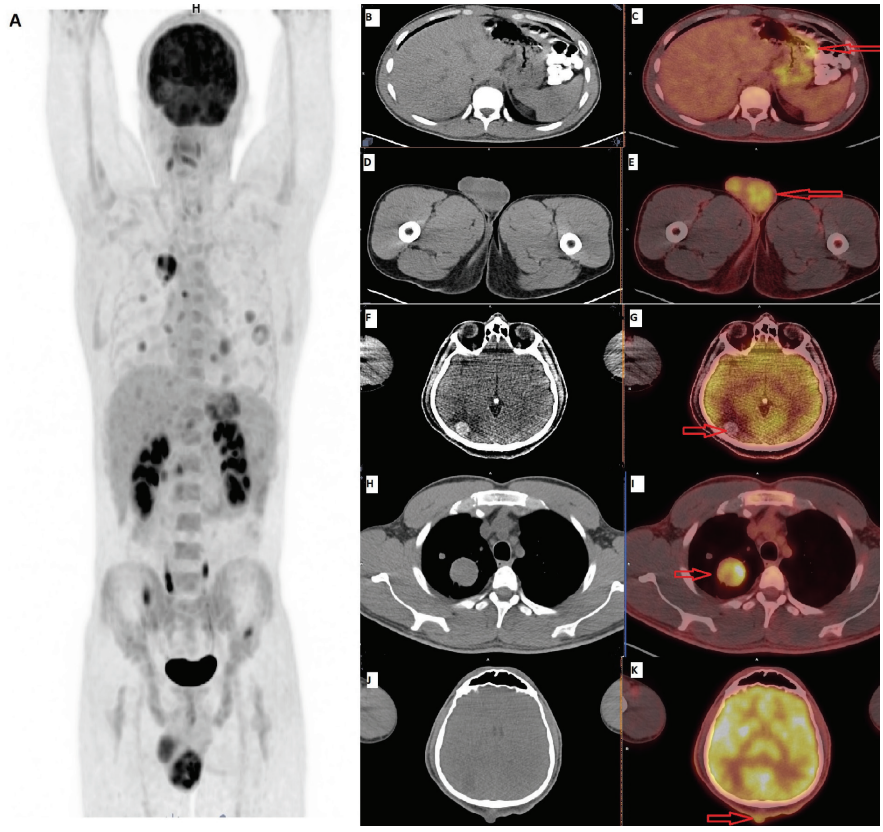

Figure 1. Testicular choriocarcinoma diagnosed with gastric metastases is extremely rare in the literature (1,2,3,4). A 27-year-old male presented with anemia and melena. Polypoid ulcerated lesion on the gastric greater curvature with active bleeding was detected using gastroscopy. The patient underwent ^{18}fluorine-fluorodeoxyglucose (^{18}F-FDG) positron emission tomography/computed tomography (PET/CT) for clinically suspected gastric cancer. Focal ^{18}F-FDG uptake was found on the gastric greater curvature (A, B, C). Metastatic gastrointestinal involvement may be seen in approximately 5% of these cases (5,6). Hypermetabolic focus and asymmetric growth were also found in the left testicle (D, E), and multiple metastatic disease that involves the brain (F, G), lungs (H, I), skin (J, K), liver, lymph node, and bone was detected on PET/CT. Based on PET/CT, all metastases were thought to arise from the testicles. As in this case, in addition to the contribution of PET/CT in diagnosis of testicular cancer, it is very important imaging technique in clinical practice in staging and detection of recurrence (7).

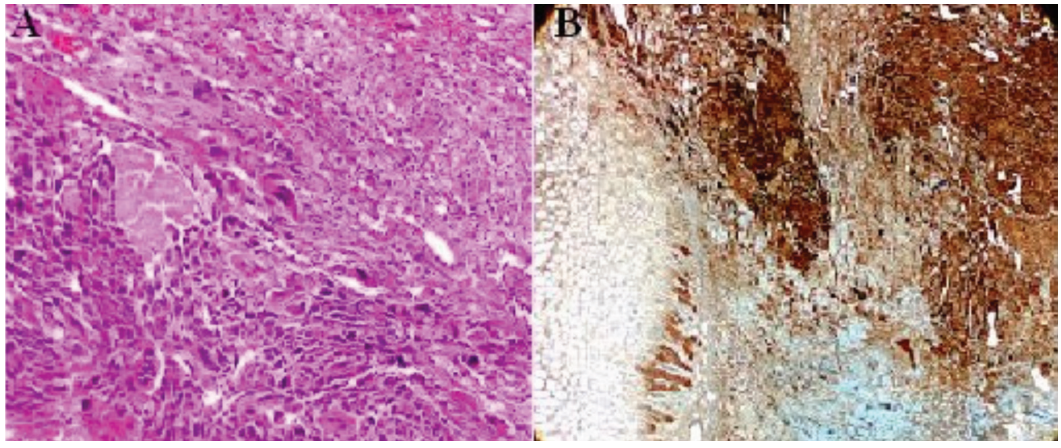

Figure 2. On immunohistochemical examination of the specimen,metastasis of testicular choriocarcinoma was detected in the gastric biopsy specimen. Pathological images of gastric biopsy material. A) Hypercromatic multinuclear and syncytiotrophoblastic cells with large eosinophilic cytoplasm (hematoxylin eosin staining, x400). B) Human chorionic gonadotropin immunohistochemical staining (x400). The germ cell malignancy in young men can present with melena, and malignancy should be suspected in patients presenting with these symptoms.

Ethics

Informed Consent: Consent form was filled out by all participants.

Peer-review: Externally peer-reviewed.

Authorship Contributions

Surgical and Medical Practices: S.G., S.A., R.A.A., S.R., G.Y.A., M.A.A., Concept: S.G., M.A.A., Design: S.G., M.A.A., Data Collection or Processing: S.G., M.A.A., Analysis or Interpretation: S.G, R.A.A., Literature Search: S.G., Writing: S.G.

Conflict of Interest: No conflict of interest was declared by the authors.

Financial Disclosure: The authors declared that this study received no financial support.

References

1. Bosl GJ, Motzer RJ. Testicular germ-cell cancer. N Engl J Med 1997;337:242-253.
2. Harikumar R, Harish K, Aravindan KP, Thomas V. Testicular choriocarcinoma with gastric metastasis presenting as hematemesis. Indian J Gastroenterol 2004;23:223-224.
3. Aydiner A, Olgaç V, Darendeliler E, Oztürk N, Dinçol K, Erseven G, Onat H. Testicular germ cell tumor with gastric metastasis. Acta Oncol 1993;32:459-460.
4. Shariat SF, Duchene D, Kabbani W, Mucher Z, Lotan Y. Gastrointestinal hemorrhage as first manifestation of metastatic testicular tumor. Urology 2005;66:1319.
5. Hsu CC, Chen JJ, Changchien CS. Endoscopic features of metastatic tumors in the upper gastrointestinal tract. Endoscopy 1996;28:249-253.
6. Cook GJ, Sohaib A, Huddart RA, Dearnaley DP, Horwich A, Chua S. The role of 18F-FDG PET/CT in the management of testicular cancers. Nucl Med Commun 2015;36:702-708.
7. Molina Infante J, Beceiro Pedreño I, Ripoll Noiseux C, Marín Jiménez I, González Asanza C, Menchén Fernández-Pacheco P. Gastrointestinal hemorrhage due to metastatic choriocarcinoma with gastric and colonic involvement. Rev Esp Enferm Dig 2004;96:77-80.

Interesting Image
Mol Imaging Radionucl Ther 2021;30:50-53 DOI:10.4274/mirt.galenos.2019.03164

Somatostatin Receptor Scintigraphy in a Patient with Myocarditis

Miyokarditli Bir Hastada Somatostatin Reseptör Sintigrafisi

Abdullatif Amini[1], Firoozeh Dehdar[2], Esmail Jafari[2], Ali Gholamrezanezhad[3], Majid Assadi[2]

[1]Bushehr Medical Heart Center, Bushehr University of Medical Sciences, Department of Cardiology, Bushehr, Iran
[2]Bushehr University of Medical Sciences, Bushehr Medical University Hospital, The Persian Gulf Nuclear Medicine Research Center, Department of Molecular Imaging and Radionuclide Therapy (MIRT), Bushehr, Iran
[3]University of Southern California, Keck School of Medicine, Department of Diagnostic Radiology, Los Angeles, USA

Abstract

We report a case of myocarditis imaged with technetium-99m octreotide cardiac single-photon emission computed tomography which showed diffuse uptake in the myocardium, indicating inflammatory reaction to myocardial damage. Somatostatin receptor scintigraphy of the heart could be considered in patients with suspected cardiac inflammation. This could facilitate early diagnosis and guide appropriate treatment.
Keywords: Myocarditis, somatostatin receptor scintigraphy, Tc-99m octreotide, myocarditis, SPECT

Öz

Bu çalışmada, miyokardiyal hasara enflamatuvar reaksiyonu gösteren, miyokardda yaygın alım gösteren teknesyum-99m oktreotid kardiyak tek foton emisyonlu bilgisayarlı tomografi ile görüntülenen bir miyokardit olgusunu sunuyoruz. Miyokardiyal enflamasyondan şüphelenilen hastalarda göğüs ağrısı değerlendirilirken kalbin somatostatin reseptör sintigrafisi düşünülebilir. Bu, erken teşhisi kolaylaştırabilir ve uygun tedaviyi sağlayabilir.
Anahtar kelimeler: Miyokardit, somatostatin reseptör sintigrafisi, Tc-99m oktreotid, miyokardit, SPECT

Address for Correspondence: Majid Assadi MD, The Persian Gulf Nuclear Medicine Research Center, Bushehr University of Medical Sciences, Bushehr, Iran
Phone: +0098-771-2580169 **E-mail:** assadipoya@yahoo.com ORCID ID: orcid.org/0000-0002-2166-3765
Received: 21.04.2019 **Accepted:** 05.08.2019

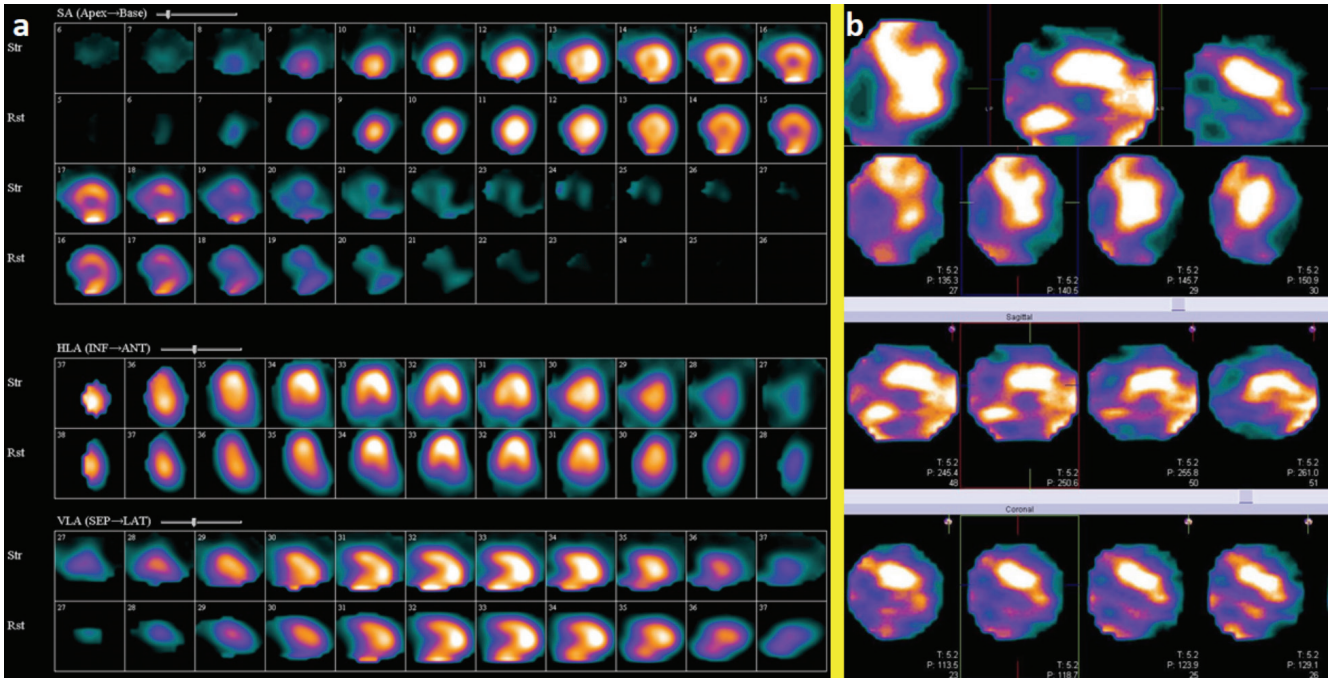

Figure 1. A 21-year-old male patient was admitted in our hospital for mild chest discomfort since 1 month ago and a 2-mm ST-segment elevation in all leads, except in AVR and V1. His workup was performed elsewhere. At that time, he experienced severe acute chest pain accompanied by dyspnea. The patient was afebrile. He had no history of a viral or other infection and drug abuse. On history assessment, he had tachycardia, and his blood pressure was in the normal range. Cardiac laboratory tests, especially troponin and creatine kinase, were markedly elevated, while an echocardiographic examination was unremarkable with an ejection fraction of 55%. The patient has received high-dose antiinflammatory drugs, which was probably associated with acute pericarditis. The aforementioned cardiac biomarkers decreased gradually within a few days of admission, and the patient was discharged that time.

On recent admission, myocardial perfusion imaging using technetium-99m (Tc-99m) methoxyisobutylisonitrile (MIBI) single photon emission computed tomography (SPECT) was carried out, and the results were unremarkable, but revealed ejection fraction of >55%. (a) Due to probable pericarditis/myocarditis, tomographic somatostatin receptor imaging with Tc-99m octerotide was performed, which was suggestive of persistent inflammatory reaction. There was diffuse myocardial Tc-99m-octerotide uptake at the utmost anterior region (b), while the pattern in atherosclerosis usually is focal, depending on the involved artery. On follow-up visits, the symptoms completely improved, and all laboratory tests became normal.

Myocarditis is characterized with myocardial inflammation without ischemia or infarction, and several causes have been identified, with viral infections being the most frequent (1). Currently, endomyocardial biopsy (EMB) is the gold standard for distinguishing myocarditis; nevertheless, it has very low sensitivity of only 20%-30% with a noticeable procedure-related risk (2).

Cardiac magnetic resonance imaging is the standard imaging technique in revealing myocarditis, and it can detect several characteristics of myocarditis; nonetheless, it has some main drawbacks, especially in the detection of chronic myocarditis with accuracies as low as 50%. Furthermore, it cannot show the inflammatory activity, which is highly necessary for monitoring of therapeutic responses (2).

^{18}Fluorine-fluorodeoxyglucose (^{18}F-FDG)-positron emission tomography (PET)/CT can show acute myocardial inflammation suggestive of active myocarditis. In addition, based on the low yield of random EMB, PET-guided myocardial biopsy may be another indication for ^{18}F-FDG-PET/CT in myocarditis. Currently, the research on hybrid PET/magnetic resonance imaging for diagnosing myocarditis is an active area of research (3).

Moreover, due to the low specificity of ^{18}F-FDG-PET, novel PET tracers such as (11C)-methionine for imaging of myocarditis are being explored (4). Similarly, targeting of somatostatin receptor 2 has shown promising findings in a clinical pilot investigation (5).

With regard to radionuclide imaging, gallium-67-citrate and 111In-antimyosin scintigraphy have demonstrated some efficacy in the diagnosis of myocardial inflammation and necrosis, respectively, but their application in the evaluation of myocarditis has deceased largely due to limited specificity and availability (1). In addition, very few cases on somatostatin receptor scintigraphy (SRS) in myocarditis are reported in the literature (1).

The most notable explanation underlying these processes could be related to the expression of somatostatin receptor subtype 2 on activated lymphocytes and macrophages, an abundant cell type in the atherosclerotic plaque and myocarditis; with this difference, vulnerable atherosclerotic plaque is usually a focal process, while myocarditis is a diffuse process (6,7).

In the field of nuclear imaging, ^{18}F-FDG-PET/CT and leukocyte scintigraphy are the most commonly applied techniques in these situations. Other innovative modalities such as bacteria-specific imaging agents and C-X-C motif chemokine receptor CXCR4 have shown promising results in trial studies (8).

Briefly, cardiac SRS may be a valuable imaging modality in the assessment of myocarditis, especially when other standard imaging techniques are unavailable or unsuitable.

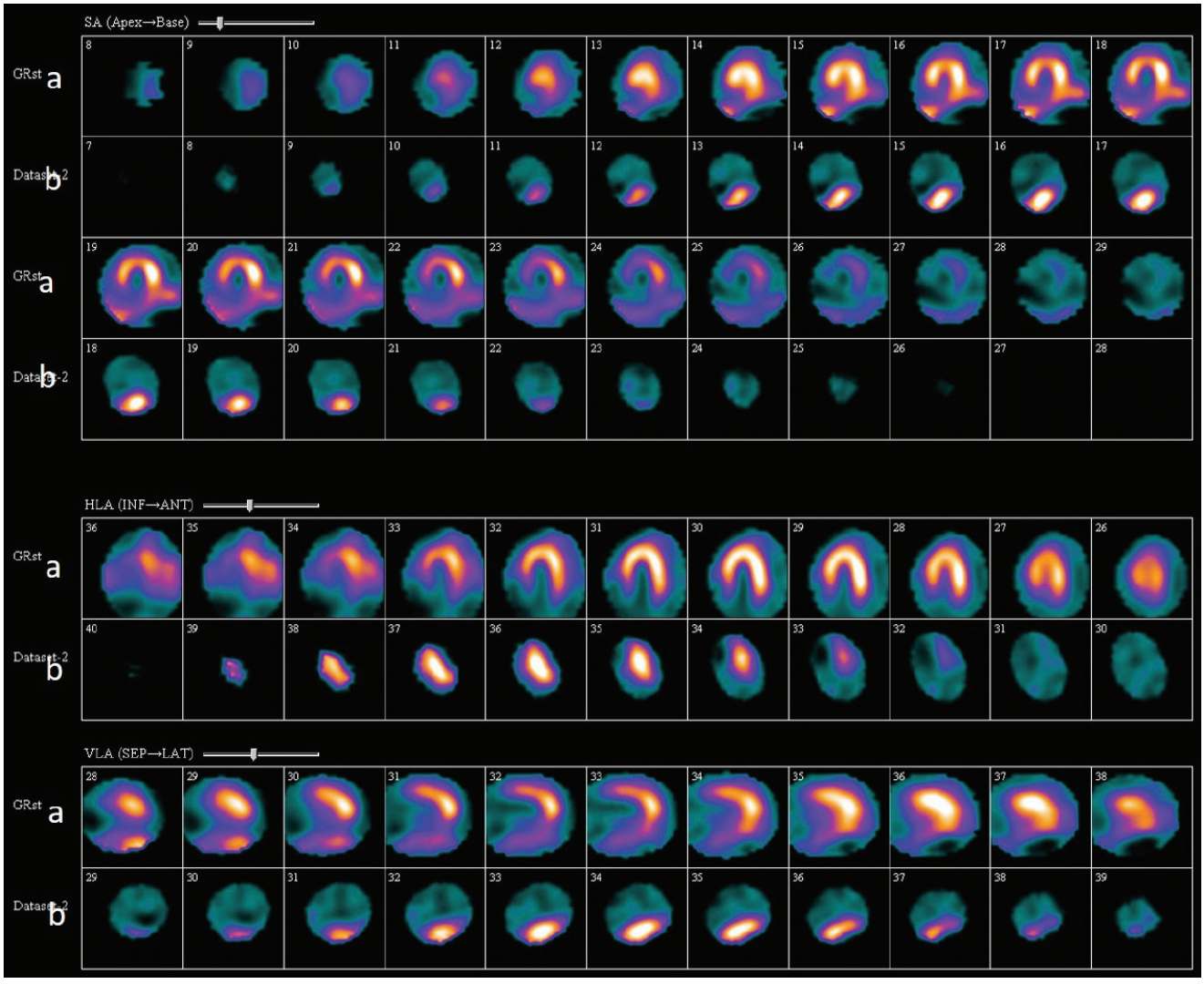

Figure 2. (a) Myocardial perfusion imaging using Tc-99m-MIBI SPECT at rest in a 51-year-old man. Short, vertical, and horizontal slices in the top rows, showing severely decreased uptake in the inferior and inferoseptal walls. (b) Myocardial SSTR imaging with Tc-99m labeled octreotide SPECT in the same patient. Short axis, vertical, and horizontal slices in the lower rows showed uptake in the inferior region suggesting vulnerable plaque.

Ethics

Informed Consent: Written informed consent of the patient was obtained from the patients.

Peer-review: Externally peer-reviewed.

Authorship Contributions

Concept: A.A., A.G., M.A., Design: A.A., A.G., M.A., Data Collection or Processing: F.D., E.J., Literature Search: A.A., M.A., E.J., Writing: M.A., E.J.

Conflict of Interest: No conflict of interest was declared by the authors.

Financial Disclosure: The authors declared that this study received no financial support.

References

1. Moralidis E, Mantziari L, Gerasimou G, Styliadis IH, Gotzamani-Psarrakou A. Somatostatin analogue scintigraphy in a patient with viral myocarditis. Hell J Nucl Med 2012;15:144-146.
2. Lurz P, Eitel I, Adam J, Steiner J, Grothoff M, Desch S, Fuernau G, de Waha S, Sareban M, Luecke C, Klingel K, Kandolf R, Schuler G, Gutberlet M, Thiele H. Diagnostic performance of CMR imaging compared with EMB in patients with suspected myocarditis. JACC Cardiovasc Imaging 2012;5:513-524.
3. Nensa F, Poeppel TD, Krings P, Schlosser T. Multiparametric assessment of myocarditis using simultaneous positron emission tomography/magnetic resonance imaging. Eur Heart J 2014;35:2173.

4. Maya Y, Werner RA, Schütz C, Wakabayashi H, Samnick S, Lapa C, Zechmeister C, Jahns R, Jahns V, Higuchi T. 11C-Methionine PET of Myocardial Inflammation in a Rat Model of Experimental Autoimmune Myocarditis. J Nucl Med 2016;57:1985-1990.
5. Lapa C, Reiter T, Li X, Werner RA, Samnick S, Jahns R, Buck AK, Ertl G, Bauer WR. Imaging of myocardial inflammation with somatostatin receptor based PET/CT - A comparison to cardiac. MRI Int J Cardiol 2015;194:44-49.
6. Malmberg C, Ripa RS, Johnbeck CB, Knigge U, Langer SW, Mortensen J, Oturai P, Loft A, Hag AM, Kjær A. 64Cu-DOTATATE for Noninvasive Assessment of Atherosclerosis in Large Arteries and Its Correlation with Risk Factors: Head-to-Head Comparison with 68Ga-DOTATOC in 60 Patients. J Nucl Med 2015;56:1895-1900.
7. Spiridonidis T, Patsouras N, Papandrianos N, Symeonidis A, Apostolopoulos DJ. Tc-99m Depreotide SPECT/CT depicts myocardial involvement in a case of thrombotic thrombocytopenic purpura. Clin Nucl Med 2008;33:874-875.
8. Kircher M, Lapa C. Novel Noninvasive Nuclear Medicine Imaging Techniques for Cardiac Inflammation. Curr Cardiovasc Imaging Rep 2017;10:6.

Interesting Image
Mol Imaging Radionucl Ther 2021;30:54-56 DOI:10.4274/mirt.galenos.2020.05658

Small-angle Compton Scatter Artifact in Tc-99m-IDA Hepatobiliary Scintigraphy Resulting in the Breast Overlying the Liver in Planar Dynamic Imaging

Tc-99m-IDA Hepatobiliyer Sintigrafi Planar Dinamik Görüntülemede Karaciğer ile Üst Üste Gelen Meme Nedeniyle Oluşan Küçük Açılı Compton Saçılım Artefaktı

Mohsen Qutbi

Shahid Beheshti University of Medical Sciences, Taleghani Educational Hospital, Department of Nuclear Medicine, Tehran, Iran

Abstract

Compton scatter photons are generally considered problematic in nuclear medicine imaging. Therefore, efforts are being made to minimize the involvement of these photons by employing some special strategies in daily practice. Basically, photons scattering at a small angle and traveling in the proper direction stand a chance of getting recorded and thereby participate in the image formation. These photons may create artifactual hot spots in the vicinity of a region with high concentration of radioactivity. The present study focuses on the negative impact of such photons during routine imaging in clinical setting, through an artifact detected in technetium-99m-IDA hepatobiliary scintigraphy, with the purpose of highlighting this issue to the nuclear medicine practitioners.

Keywords: Small-angle Compton scatter, artifact, liver, breast, hepatobiliary scan

Öz

Compton saçılma fotonları genellikle nükleer tıp görüntülemesinde sorunlu olarak kabul edilir. Bu nedenle, günlük pratikte bazı özel stratejiler uygulayarak bu fotonların tutulumunu en aza indirmek için çaba gösterilmektedir. Temel olarak, küçük bir açıyla saçılan ve doğru yönde hareket eden fotonların kaydedilme ve dolayısıyla görüntü oluşumuna katılma şansı vardır. Bu fotonlar, yüksek radyoaktivite konsantrasyonuna sahip bir bölgenin çevresinde yapay sıcak noktalar oluşturabilir. Bu çalışma, bu konuyu nükleer tıp hekimlerine vurgulamak amacıyla, teknesyum-99m-IDA hepatobiliyer sintigrafisinde saptanan bir artefakt yoluyla, bu tür fotonların klinik ortamda rutin görüntüleme sırasında olumsuz etkisine odaklanmaktadır.

Anahtar kelimeler: Küçük açılı Compton scatter, artefakt, karaciğer, meme, hepatobiliyer tarama

Address for Correspondence: Mohsen Qutbi MD, Shahid Beheshti University of Medical Sciences, Taleghani Educational Hospital, Department of Nuclear Medicine, Tehran, Iran
Phone: 00982123031250 **E-mail:** mohsen.qutbi@gmail.com ORCID ID: orcid.org/0000-0002-8347-605X
Received: 16.06.2019 **Accepted:** 12.03.2020

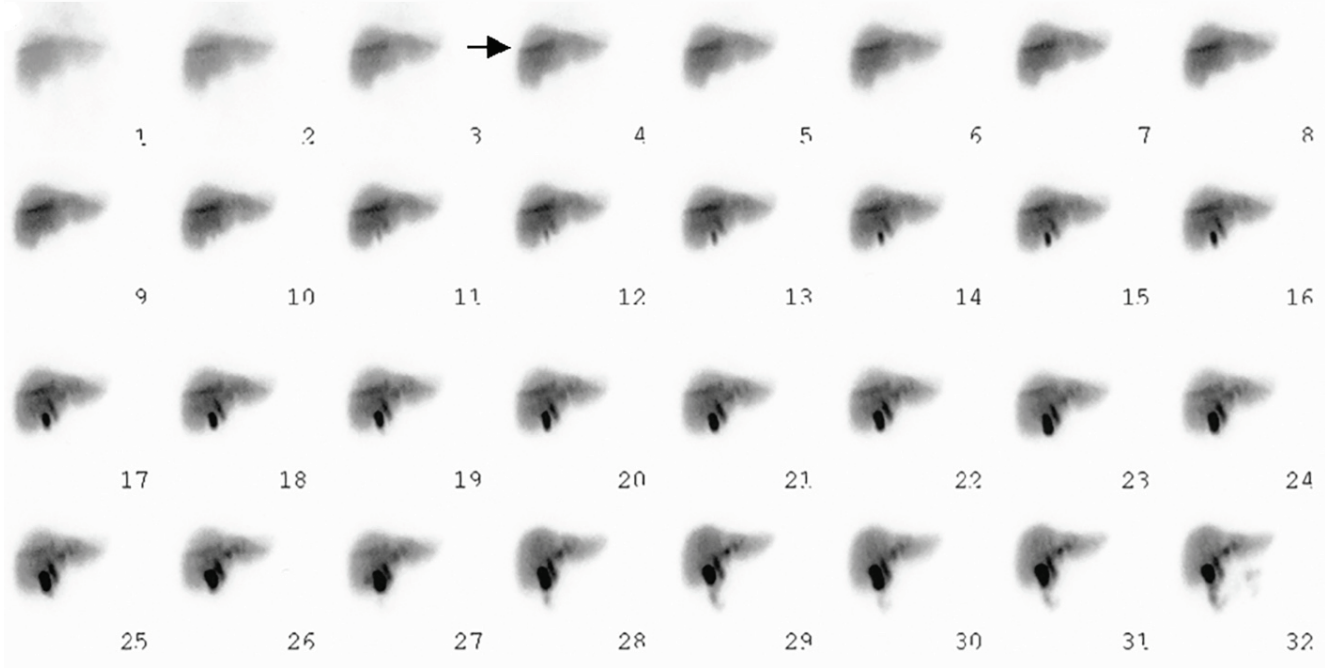

Figure 1. A 45-year-old woman was referred for a technetium-99m (Tc-99m)-mebrofenin hepatobiliary scan, which was performed in dynamic mode for 60 minutes using a single-head Genesys EPIC ADAC γ-camera with a general-purpose collimator and a window width of 20% for 140-Kev Tc-99m photons. The dynamic image showed attenuation of the right breast overlying the liver. Unexpectedly, an artifactual curvilinear zone of intense uptake (shown by arrow) was noted with an intensity higher than that in the unattenuated region of the liver, bordering attenuated and unattenuated regions and presumably coincident with the edge of the breast, from the beginning of the study. The visualization time and uptake pattern was not compatible with radiotracer excretion into the biliary system or any pathology in the liver. Later, in the dynamic phase (at frame 28 on the image), the breast was repositioned, and the curvilinear uptake subsequently disappeared.

In practice, nuclear medicine images are formed mainly by photopeak with varying degrees of contribution of Compton scatter photons. The degree of this contribution depends on certain factors, such as width of the energy window. In Compton scattering, original photons emitted as a result of radioactive decay interact with the surrounding matter and consequently transfer a part of their energy to it. Thus, secondary photon travels in another direction with a lower energy as a function of the angle between the directions of the original and secondary photons (1,2). There are 2 mechanisms that can prevent recording of Compton scatter photons. The first mechanism is through physical collimation (i.e., using a lead collimator) that absorbs photons whose direction is not perpendicular to the collimator face or parallel to the axis of collimator holes. The second mechanism is accomplished by pulse height analyzer using an energy window to discard photons with energies that lie outside the desired range (1,2,3). Despite all these measures, photons that are scattered at a small angle, because of lower energy transfer, might be recorded. Practically, for a window width of 20%, only photons of Tc-99m reaching the camera detector in the range of 126-154 KeV meet the energy criteria to be accepted. Compton photons in proper direction with angle of scattering <53.5° also fulfill the energy criteria and are accepted by the system (1,4,5). In some circumstances, a higher proportion of Compton photons are produced, which was explained in an interesting experiment by Yeh (5). When air intervenes between regions of soft tissues, photons coming from one region scatter at a small angle to higher proportions when hitting the second region, thereby producing a false hot spot (5). One such phenomenon occurs along the lower edge of the breast, especially when it lies geometrically compared with the chest wall, in scans with high concentration of activity in the liver as in the present patient and produces a special artifactual pattern. Counts corresponding to the image in that region originate from the adjacent regions of the patient's body. After repositioning of the breast, and thus change in the geometry of the breast over the chest wall, the false hot spot disappeared. Monte Carlo simulation is a useful technique to validate, although *in silico*, the formation of this artifact based on specific breast configuration and geometry on the chest and its elimination by simulated breast repositioning (6,7,8).

Ethics

Informed Consent: Informed consent was obtained prior to the study.

Peer-review: Externally and internally peer-reviewed.

Financial Disclosure: The author declared that this study received no financial support.

References

1. Cherry SR, Sorenson JA, Phelps ME. Image quality in nuclear medicine. In: Cherry SR, Sorenson JA, Phelps ME (eds). Physics in nuclear medicine, Philadelphia, Elsevier Saunders, 2012, 233-251.
2. Ogawa K. Image distortion and correction in single photon emission CT. Ann Nucl Med 2004;18:171-185.
3. Buvat I, Benali H, Todd-Pokropek A, Di Paola R. Scatter correction in scintigraphy: the state of the art. Eur J Nucl Med 1994;21:675-694.
4. Kojima A, Matsumoto M, Takahashi M. Experimental analysis of scattered photons in Tc-99m imaging with a gamma camera. Ann Nucl Med 1991;5:139-144.
5. Yeh EL. Compton scatter image simulating jugular venous reflux. J Nucl Med 1982;23:58-59.
6. Buvat I, Castiglioni I. Monte Carlo simulations in SPET and PET. Q J Nucl Med 2002;46:48-61.
7. Zaidi H. Relevance of accurate Monte Carlo modeling in nuclear medical imaging. Med Phys 1999;26:574-608.
8. Zaidi H, Koral KF. Scatter modelling and compensation in emission tomography. Eur J Nucl Med Mol Imaging 2004;31:761-782.

Interesting Image
Mol Imaging Radionucl Ther 2021;30:57-59 DOI:10.4274/mirt.galenos.2019.90532

Active Giant Cell Vasculitis Diagnosis with ^{68}Ga PSMA PET/CT Imaging

^{68}Ga PSMA PET/BT Görüntüleme ile Aktif Dev Hücreli Vaskülit Teşhisi

Muhammet Sait Sağer[1], Seçkin Bilgiç[1], Lebriz Uslu[1], Sertaç Asa[1], Güneş Sağer[2], Kerim Sönmezoğlu[1]

[1]*İstanbul University-Cerrahpaşa, Cerrahpaşa Faculty of Medicine, Department of Nuclear Medicine, İstanbul, Turkey*
[2]*Kartal Dr. Lütfi Kırdar City Hospital, Clinic of Pediatry, İstanbul, Turkey*

Abstract

Vasculitis is a multisystem disease characterized by inflammation with infiltration of leukocytes into the blood vessels. Giant cell arteritis (GCA) is the most common form of vasculitis that mostly affects medium- and large-sized arteries. ^{18}Fluorine-fluorodeoxyglucose (^{18}F-FDG) positron emission tomography/computed tomography (PET/CT) is increasingly used to diagnose inflammation of large arteries in GCA. Galium-68 prostate-specific membrane antigen (PSMA) PET/CT has a vital role in the assessment of patients with prostate cancer for recurrence and metastasis of the disease. Various benign and non-prostate malignant conditions may give rise to increased PSMA uptake. Herein, we demonstrate that PSMA uptake can be seen in GCA.

Keywords: Vasculitis, GCA, PSMA PET, ^{18}F-FDG PET

Öz

Vaskülit, lökositlerin kan damarlarına infiltrasyonu sonucunda iltihaplanma ile karakterize multisistemik bir hastalıktır. Dev hücreli arterit (DHA), çoğunlukla orta büyüklükte ve büyük arterleri etkileyen en yaygın vaskülit şeklidir. ^{18}Flor-florodeoksiglukoz (^{18}F-FDG) pozitron emisyon tomografi/bilgisayarlı tomografi (PET/BT), DHA tanısında yaygın olarak kullanılır. Galyum-68 prostat spesifik membran antijeni (PSMA) PET/BT, nüks ve metastatik hastalığı olan prostat kanseri hastalarının değerlendirilmesinde önemli bir role sahiptir. PSMA tutulumuna neden olabilecek çeşitli iyi huylu ve prostat dışı malign durumlar görülebilmektedir. Bu olgu ile büyük damar vaskülitinde PSMA tutulumunu görülebileceğini göstermek istedik.

Anahtar kelimeler: Vaskülit, DHA, PSMA PET, ^{18}F-FDG PET

Address for Correspondence: Muhammet Sait Sağer MD, İstanbul University-Cerrahpaşa, Cerrahpaşa Faculty of Medicine, Department of Nuclear Medicine, İstanbul, Turkey
Phone: +90 212 414 30 00-22984 **E-mail:** saitsager@yahoo.com ORCID ID: orcid.org/000-0003-2013-5845
Received: 13.09.2019 **Accepted:** 17.12.2019

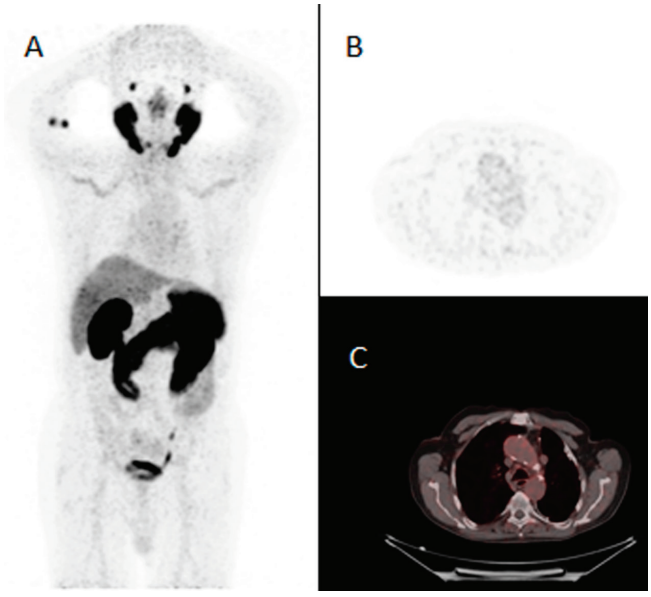

Figure 1. A-56-year-old male patient diagnosed with prostate cancer was referred to nuclear medicine for gallium-68 (^{68}Ga) prostate-specific membrane antigen (PSMA) positron emission tomography/computed tomography (PET/CT) imaging. An intravenous solution of 4 mCi ^{68}Ga PSMA was administered followed by whole-body PET/CT imaging at 1 hour post administration of intravenous solution. No recurrence or metastatic PSMA uptake was observed for prostate cancer. However, increased PSMA uptake was noted bilaterally in the subclavian arteries and common carotid arteries in maximum intensity projection (A), axial PET (B), and axial fusion (C) images. PSMA is a type 2 transmembrane protein with high expression in prostate carcinoma cells (1). ^{68}Ga PSMA PET/CT has an important role in the assessment of patients with prostate cancer and recurrence and metastasis of the disease (2). ^{68}Ga PSMA uptake has been evident in various solid malignant neoplasms such as neuroendocrine tumors, renal cell carcinoma, breast cancer, and differentiated thyroid cancer (3). This form of vessel uptake can be seen with ^{18}fluorine-fluorodeoxyglucose (^{18}F-FDG) PET in vasculitis. This patient was diagnosed with giant cell vasculitis. Recognition of the potential sources of false-positive and false-negative findings is important for accurate interpretation of PSMA-targeted PET imaging studies.

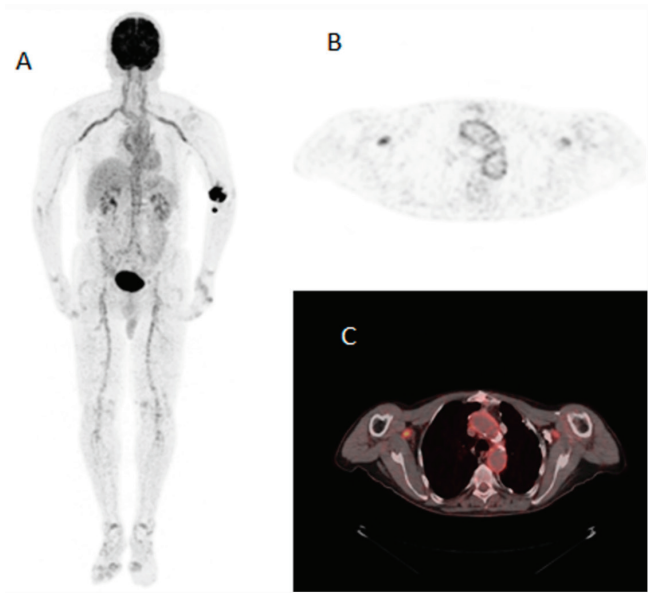

Figure 2. ^{18}F-FDG PET/CT images showed bilateral increased ^{18}F-FDG uptake in the subclavian arteries and common carotid arteries in the maximum intensity projection (A) axial PET (B), and axial fusion (C) images. ^{18}F-FDG uptake was higher than that of PSMA. Giant cell arteritis (GCA), also called temporal arteritis, is a granulomatous inflammation of the aorta and its main branches, most often occurring in patients aged >50 years (4). Vasculitis can be distributed locally in the branches of the internal and external carotid arteries or the aorta. Visual vascular uptake higher than that of liver resulted in the highest diagnostic accuracy for the detection of GCA (5). ^{18}F-FDG PET/CT is routinely used for the diagnosis of vasculitis and evaluation of treatment response.

Ethics

Informed Consent: Was obtained from the patient.

Peer-review: Externally peer-reviewed.

Authorship Contributions

Concept: M.S.S., Design: M.S.S., Data Collection or Processing: K.S., Literature Search: S.B., S.A., Writing: G.S., L.U.

Conflict of Interest: No conflict of interest was declared by the authors.

Financial Disclosure: The authors declared that this study received no financial support.

References

1. Chun AR, Jo HM, Lee SH, Chun HW, Park JM, Kim KJ, Jung CH, Mok JO, Kang SK, Kim CH, Kim BY. Risk of malignancy in thyroid incidentalomas identified by fluorodeoxyglucose-positron emission tomography. EndocrinolMetab (Seoul) 2015;30:71-77.
2. Giovacchini G, Giovannini E, Riondato M, Ciarmiello A. PET/CT With 68Ga-PSMA in Prostate Cancer: Radiopharmaceutical Background and Clinical Implications. Curr Radiopharm 2018;11:4-13.
3. Malik D, Kumar R, Mittal BR, Singh H, Bhattacharya A, Singh SK. 68Ga-Labeled PSMA Uptake in Nonprostatic Malignancies: Has the Time Come to Remove "PS" From PSMA? Clin Nucl Med 2018;43:529-532.
4. Treglia G, Mattoli MV, Leccisotti L, Ferraccioli G, Giordano A. Usefulness of whole-body fluorine-18-fluorodeoxyglucose positron emission tomography in patients with large-vessel vasculitis: a systematic review. Clin Rheumatol 2011;30:1265-1275.
5. Balink H, Bennink RJ, van Eck-Smit BL, Verberne HJ. The role of 18F-FDG PET/CT in large-vessel vasculitis: appropriateness of current classification criteria? Biomed Res Int 2014;2014:687608.

Interesting Image
Mol Imaging Radionucl Ther 2021;30:60-62 DOI:10.4274/mirt.galenos.2020.54366

Unexpected Detection of Abscessualized Lung Carcinoma on Tc-99m-HMPAO-labeled Leukocytes Scintigraphy Misdiagnosed on Chest Computed Tomography

Toraks Bilgisayarlı Tomografisinde Yanlış Teşhis Edilen Apseleşmiş Akciğer Karsinomunun Tc-99m-HMPAO İşaretli Lökosit Sintigrafisi ile Beklenmedik Tespiti

Laura Cosma[1], Viviana Frantellizzi[2], Mariano Pontico[3], Giuseppe De Vincentis[1]

[1]*Sapienza University of Rome, Department of Radiological Sciences, Division of Oncology and Anatomical Pathology, Rome, Italy*
[2]*Sapienza University of Rome, Department of Molecular Medicine, Rome, Italy*
[3]*Sapienza University of Rome, Ph.D. Program in Morphogenesis and Tissue Engineering, Department of Medico-Surgical Sciences and Biotechnologies, Rome, Italy*

Abstract

Technetium-99m (Tc-99m)-hexamethylpropylene amine oxime (HMPAO)-labeled leukocytes scintigraphy is well established for investigating and diagnosing infections in bone and soft tissue, as well as for the detection of occult infection. A 71-year-old female who was recently diagnosed with bronchopulmonary neuroendocrine tumor of the right lung was referred for an intermittent fever of unknown origin associated with chill at night for the last month. Chest computed tomography (CT) scan showed a thrombotic widespread of the superior vena cava and a solid pathological tissue in the superior segment of the inferior lobe of the right lung with consensual atelectasis. Being a carrier of port-a-cath, an infection of this device was suspected. Therefore, Tc-99m-HMPAO-labeled leukocytes single-photon emission computed tomography (SPECT) was performed, and matching pairs of CT scan and Tc-99m-HMPAO-labeled white blood cell SPECT images were fused. Through this means, it was found that the area of the radiotracer increased uptake corresponded with the soft tissue density mass detected by CT scan localized at the inferior lobe of the right lung. The hybrid SPECT/CT fused imaging was crucial for diagnosis of the presence of a lung abscess localized in correspondence with the known lung cancer region.

Keywords: Tc-99m-HMPAO-labeled leukocytes, hybrid imaging, SPECT/CT, FUO, abscess, abscessualized cancer

Öz

Teknesyum-99m (Tc-99m)-heksametilpropilen amin oksim (HMPAO) işaretli lökosit sintigrafisi, kemik ve yumuşak dokudaki enfeksiyonları araştırmak ve teşhis etmek ve ayrıca gizli enfeksiyonu saptamak için iyi bir şekilde tasarlanmıştır. Yakın zamanda sağ akciğerde bronkopulmoner nöroendokrin tümörü teşhisi konan 71 yaşındaki bir kadın, son bir ay içinde geceleri üşüme ile ilişkili bilinmeyen kaynaklı aralıklı ateş nedeniyle sevk edildi. Toraks bilgisayarlı tomografisi (BT) taraması, üst vena kavanın trombotik yayılımını ve sağ akciğerin alt lobunun üst segmentinde karşılıklı atelektazisi olan katı patolojik dokuyu gösterdi. Bir kateter portu taşıyıcısı olduğundan, bu cihazın bir enfeksiyonundan şüpheleniliyordu. Bu nedenle, Tc-99m-HMPAO işaretli lökosit tek foton emisyonlu bilgisayarlı tomografi (SPECT) gerçekleştirildi ve eşleşen BT taraması ve Tc-99m-HMPAO işaretli beyaz kan hücresi SPECT görüntü çiftleri birleştirildi. Bu yolla, artmış radyofarmasötik tutulumun, sağ akciğerin alt lobunda lokalize BT taraması ile tespit edilen yumuşak doku yoğunluğu kütlesine karşılık geldiği bulundu. Hibrid SPECT/BT füzyon görüntüleme, bilinen akciğer kanseri bölgesi ile uyumlu olarak lokalize edilmiş bir akciğer apsesinin varlığının teşhisi için çok önemliydi.

Anahtar kelimeler: Tc-99m-HMPAO işaretli lökositler, hibrit görüntüleme, SPECT/BT, FUO, apse, apseli kanser

Address for Correspondence: Mariano Pontico MD, Sapienza University of Rome, Ph.D. Program in Morphogenesis and Tissue Engineering, Department of Medico-Surgical Sciences and Biotechnologies, Rome, Italy
Phone: 0649978590 **E-mail:** mariano.pontico@uniroma1.it ORCID ID: orcid.org/0000-0001-6143-4775
Received: 27.10.2019 **Accepted:** 12.03.2020

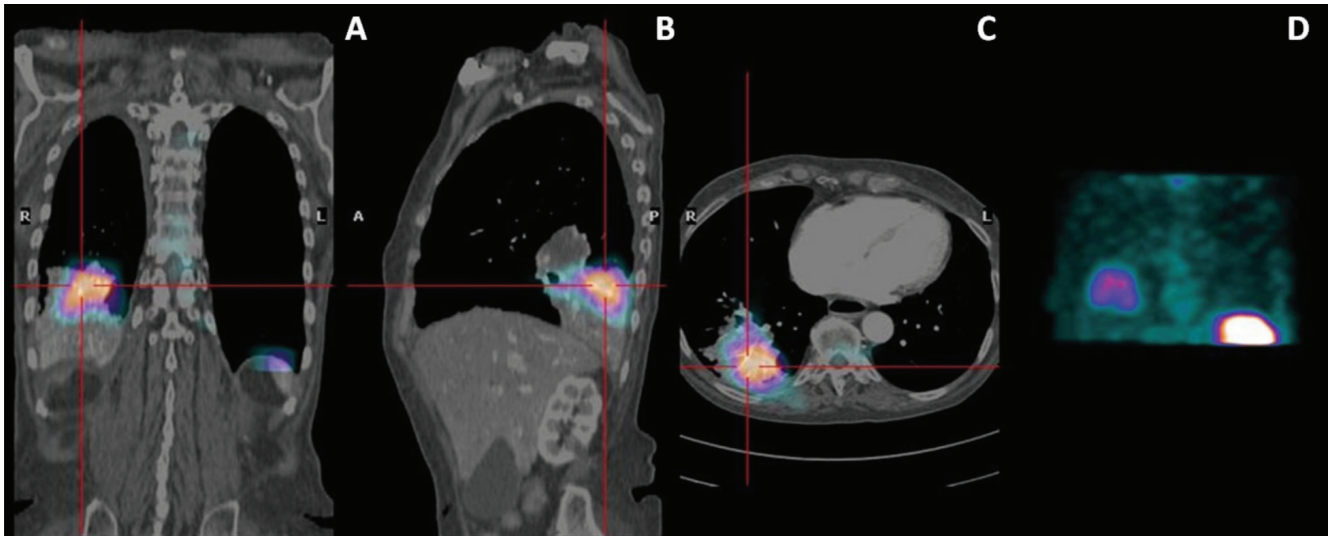

Figure 1. Fused technetium-99m (Tc-99m)-hexamethylpropylene amine oxime (HMPAO)-labeled leukocytes single-photon emission computed tomography/CT (SPECT/CT) hybrid images on coronal (A), sagittal (B), and transaxial (C) planes with Tc-99m-HMPAO-labeled leukocytes chest SPECT coronal maximum intensity projection (D).

Principal clinical indications for Tc-99m-HMPAO-labeled leukocytes scintigraphy include inflammatory bowel disease, osteomyelitis, soft tissue sepsis, and occult fever (1,2). Autologous leukocytes are characterized by high specificity because they only accumulate into the inflamed tissues due to active migration and because very infrequent fixation occurs in neoplastic tissues (1,3).

A 71-year-old Caucasian female was admitted to our department for an intermittent fever of unknown origin associated with chill at night for the last month. She was recently diagnosed with bronchopulmonary neuroendocrine tumor at the right lung superior segment of the inferior lobe. A phlebitic process of intravenous catheter was also depicted.

Chest CT scan showed a thrombotic widespread of the superior vena cava (SVC) and another one near the infusion catheter localized in the proximal tract of the brachiocefalic artery. Moreover, in the superior segment of the inferior lobe of the right lung, a conglobated solid pathological tissue (50x41 mm^2) causing thickening and infiltration of the scissural pleura and incorporating the segmental bronchial vessels, particularly the bronchial branches of the postero-basal segment, almost completely obliterated with consensual atelectasis of the segment was reported.

Being a carrier of a port-a-cath with the catheter guided into the SVC, an infection of this device or the thrombus described above was suspected.

Transthoracic and transesophageal echocardiogram were negative for the infectious source on the SVC catheter and tested blood cultures of all microorganisms.

Tc-99m-HMPAO-labeled leukocytes scintigraphy was performed in order to identify the source of infection responsible for her clinical course. Whole body planar and SPECT images of the chest region were acquired. Matching pairs of CT scan and Tc-99m-HMPAO-labeled white blood cell SPECT images were fused using dedicated Xeleris software (GE Healthcare) to generate hybrid images of overlying transmission and emission data.

The three-plane triangulation showed the clear match between the densitometric alteration found on CT scan and the markedly pathologic Tc-99m-HMPAO-labeled leukocytes uptake in the inferior lobe of the right lung, thus unveiling the presence of an active infectious disease.

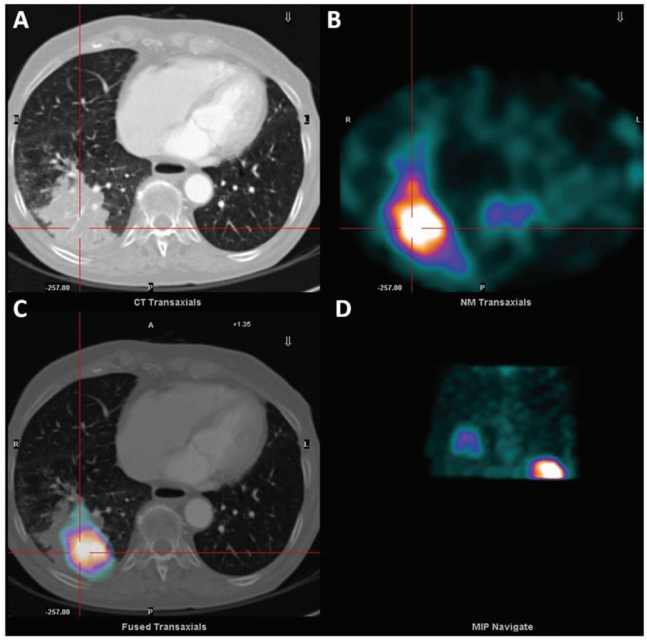

Figure 2. CT scan (A), Tc-99m-HMPAO-labeled leukocytes chest SPECT (B), fused Tc-99m-HMPAO-labeled leukocytes SPECT/CT hybrid image (C), and chest SPECT maximum intensity projection (D) on transaxial planes.

SPECT images showed an area of clearly increased tracer uptake on the right inferior region of the chest, which was more evident in the delayed 24 h images. Fused Tc-99m-HMPAO-labeled leukocytes SPECT and CT scan of the chest demonstrated that the area of increased uptake corresponded with the soft tissue density mass (detected by CT scan) localized at the inferior lobe of the lung (Figure 1, 2). The hybrid SPECT/CT fused images were crucial in order to achieve the right interpretation of this case (4), thus enabling the taken of an informed decision regarding the diagnosis of the presence of a lung abscess localized exactly in correspondence with the known lung cancer region. Therefore, the presence of SCV catheter infection was safely excluded. A proper match between the CT densitometric alteration and the pathologic Tc-99m-HMPAO-labeled leukocytes uptake in the inferior lobe of the right lung was clearly evident.

Based on the findings obtained, antibiotic therapy was administered (amoxicilline and clarithromicine for ten days), and the patient's clinical conditions improved during treatment. Also, a concomitant Erythrocyte Sedimentation Rate and Polymerase Chain Reaction values decline was observed, followed by complete normalization after two weeks from onset of the treatment.

Ethics

Informed Consent: Informed consent was obtained by patient.

Peer-review: Externally peer-reviewed.

Authorship Contributions

Surgical and Medical Practices: L.C., M.P., Concept: G.D.V., V.F., Design: G.D.V., V.F., M.P., Data Collection or Processing: L.C., M.P., Analysis or Interpretation: G.D.V., V.F., Literature Search: L.C., M.P., Writing: L.C., M.P.

Conflict of Interest: No conflict of interest was declared by the authors.

Financial Disclosure: The authors declared that this study received no financial support.

References

1. Signore A, Jamar F, Israel O, Buscombe J, Martin-Comin J, Lazzeri E. Clinical indications, image acquisition and data interpretation for white blood cells and anti-granulocyte monoclonal antibody scintigraphy: an EANM procedural guideline. Eur J Nucl Med Mol Imaging 2018;45:1816-1831.
2. Liberatore M, Gentile G, Follacchio GA, Frantellizzi V, De Vincentis G, Monteleone F, Anagnostou C, Drudi FM, Calvisi V. 99mTc-labeled White Blood Cell Scan as a Guide to Open Biopsy in the Management of Hip and Knee Prosthesis Infection: Preliminary Results. Curr Radiopharm 2017;1029-1034.
3. Lauri C, Tamminga M, Glaudemans AWJM, Juárez Orozco LE, Erba PA, Jutte PC, Lipsky BA, IJzerman MJ, Signore A, Slart RHJA. Detection of Osteomyelitis in the Diabetic Foot by Imaging Techniques: A Systematic Review and Meta-analysis Comparing MRI, White Blood Cell Scintigraphy, and FDG-PET. Diabetes Care 2017;40:1111-1120.
4. Frantellizzi V, Pontico M, Letizia C, De Vincentis G. Bladder wall paraganglioma located using 123I-mIBG SPECT and CT imaging. Rev Esp Med Nucl Imagen Mol 2018;37:253-254.

Interesting Image
Mol Imaging Radionucl Ther 2021;30:63-66 DOI:10.4274/mirt.galenos.2020.86729

^{68}Ga PSMA Uptake at Roux-en-Y Eso-jejunostomy Junction Mimicking the Recurrence of Gastric Carcinoma in PET/CT

^{68}Ga PSMA PET/BT Görüntülemede Roux-en-Y Oeso-jejunostomi Anastomoz Hattında Gastrik Karsinomun Nüksünü Taklit Eden PSMA Tutulumu

Esra Arslan[1], Tamer Aksoy[1], Merve Cin[2], Coşkun Çakır[3], Fadime Didem Can Trabulus[3], Tevfik Fikret Çermik[1]

[1]*University of Health and Sciences Turkey, İstanbul Training and Research Hospital, Clinic of Nuclear Medicine, İstanbul, Turkey*
[2]*University of Health and Sciences Turkey, İstanbul Training and Research Hospital, Department of Pathology, İstanbul, Turkey*
[3]*University of Health and Sciences Turkey, İstanbul Training and Research Hospital, Clinic of Surgery, Istanbul, Turkey*

Abstract

A 67-year-old male patient had undergone total gastrectomy and Roux-en-Y eso-jejunostomy 3 years ago for the treatment of tubular adenocarcinoma located at the corpus of the stomach. The patient was diagnosed with Gleason score 8 (4+4) metastatic prostate cancer during the follow-up period and received hormone therapy. Owing to his elevated prostate-specific antigen levels (77 ng/mL), his clinician referred him gallium-68 (^{68}Ga) prostate-specific membrane antigen 11 (PSMA) positron emission tomography/computed tomography (PET/CT) for restaging. PET/CT showed multiple ^{68}Ga PSMA receptor-positive skeletal lesions and linear PSMA activity at the eso-jejunostomy junction. He was then referred to undergo ^{18}fluorine-fluorodeoxyglucose (^{18}F-FDG) PET/CT to screen for gastric carcinoma recurrence. PET/CT images demonstrated no ^{18}F-FDG avid lesion. However, endoscopy and biopsy performed with samples from the eso-jejunostomy junction revealed superficial benign squamous epithelial fragments.

Keywords: ^{68}Ga-PSMA, ^{18}F-FDG, PET/CT, gastric carcinoma, prostate carcinoma

Öz

Altmış yedi yaşında erkek hastaya mide korpusunda tespit edilen tubular adenokarsinom nedeniyle 3 yıl önce total gastrektomi ve Roux-en-Y oeso-jejunostomi yapılmıştır. Takip süresince hasta Gleason skoru 8 (4+4) metastatik prostat kanseri tanısı da alarak hormonoterapi uygulandı. Prostat spesifik antijen düzeylerinde (77 ng/mL) yükselme saptanması nedeniyle yeniden evreleme amaçlı galyum-68 prostat spesifik membran antijeni 11 (PSMA) pozitron emisyon tomografi/bilgisayarlı tomografi (PET/BT) görüntüleme için hasta kliniğimize refere edildi. ^{68}Ga PSMA PET/BT görüntülemesinde oeso-jejunostomi kavşağında lineer PSMA aktivitesi ve multipl PSMA reseptör pozitif iskelet lezyonları saptandı. Gastrik karsinomun nüksü şüphesi nedeni ile hasta ^{18}F-FDG PET/BT incelemesi açısından yeniden kliniğimize sevk edildi. ^{18}F-FDG PET/BT görüntülerinde FDG pozitif malign prosesi düşündürebilecek lezyon görülmedi. Oeso-jejunostomi anastomoz hattından yapılan endoskopi ve biyopsi incelemesinde yüzeyel benign skuamöz epitelyal fragmanlar saptandı.

Anahtar kelimeler: ^{68}Ga-PSMA, ^{18}F-FDG, PET/BT, mide kanseri, prostat kanseri

Address for Correspondence: Esra Arslan MD, University of Health and Sciences Turkey, İstanbul Training and Research Hospital, Clinic of Nuclear Medicine, İstanbul, Turkey
Phone: +90 212 459 64 55 **E-mail:** dresraarslan@gmail.com ORCID ID: orcid.org/0000-0002-9222-8883
Received: 10.11.2019 **Accepted:** 02.04.2020

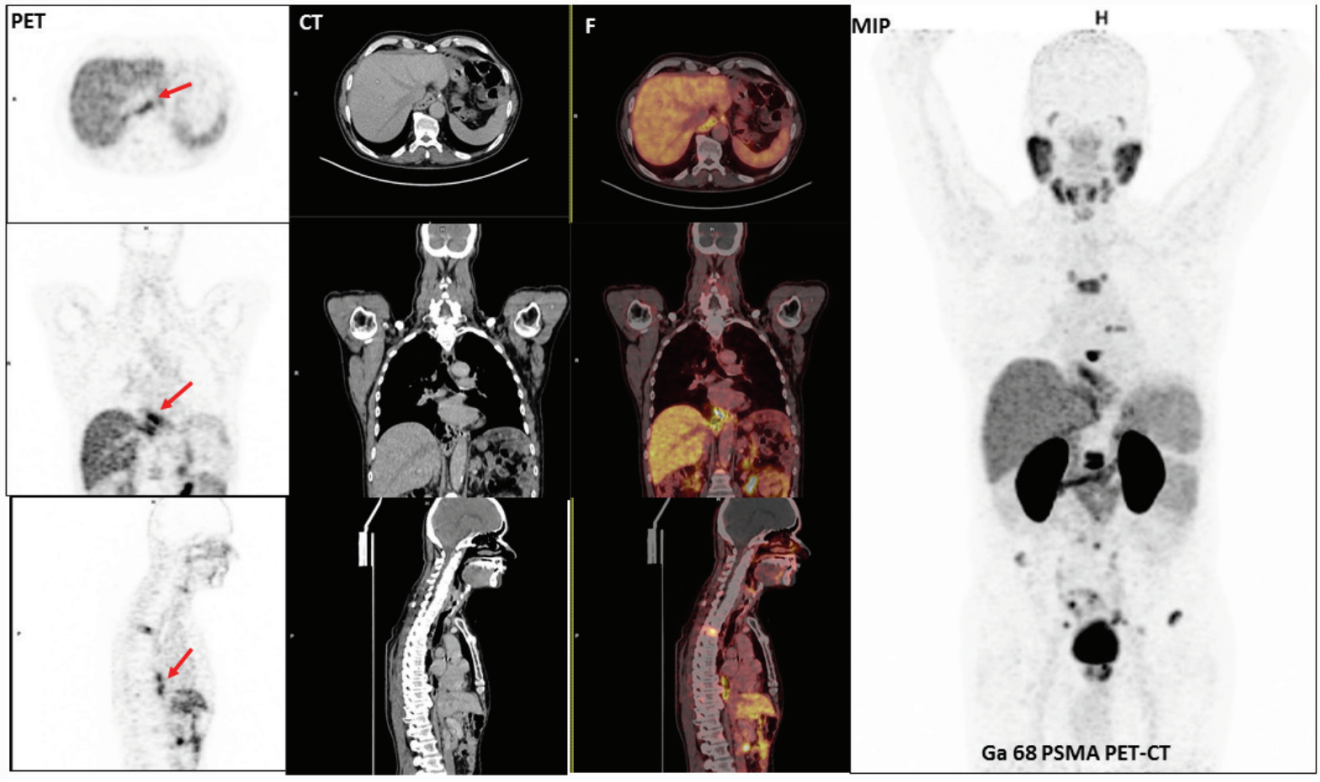

Figure 1. Gallium-68 (^{68}Ga) prostate-specific membrane antigen 11 (PSMA) positron emission tomography/computed tomography (PET/CT) shows increased uptake at multiple metastatic skeletal lesions in the vertebral column and pelvic bones as well as linear PSMA accumulation at the eso-jejunostomy line (red arrows). PSMA is a type 2 transmembrane protein that acts as a glutamate carboxypeptidase enzyme (1,2). Owing to its high expression in prostate cancer cells, PSMA is often used conveniently as a target for diagnostic and therapeutic purposes in nuclear medicine. Normal ^{68}Ga PSMA uptake might be seen in the following structures, with descending avidity: Kidneys (8 times higher than hepatic uptake), submandibular glands, parotid glands (3 times higher than hepatic uptake), descending duodenum, lacrimal glands, spleen, descending colon, Waldeyer ring in the neck, vocal cords, liver, and rectum (3). In case of benign lesions, most ^{68}Ga PSMA uptake is of low intensity or non-focal, with some notable exceptions (e.g., cutaneous, vertebral, and hepatic hemangiomas) exhibiting prominent uptake (4). Prostate cancer commonly spreads to the bones and lymph nodes. Although the spread of prostate cancer to the gastrointestinal tract is very rare, the possibility of metastasizing to the stomach should be kept in mind when a patient presents with gastrointestinal symptoms or hemorrhage (5). A few reports have demonstrated prostate carcinoma metastases in the stomach (5,6,7,8). A study by Shetty et al. (9) reported mild PSMA uptake in the gastric cardia in a case of high-grade invasive gastric adenocarcinoma. In another study, they found PSMA to be expressed by endothelial cells in keloids, granulation tissue from heart valves and pleura, and different phases of the cycling endometrium. It was reported that PSMA was not expressed by endothelium associated with Barrett's mucosa, even in the presence of associated dysplasia (10). It should be kept in mind that patients should be evaluated individually as PSMA uptake might be seen in both benign and malignant lesions.

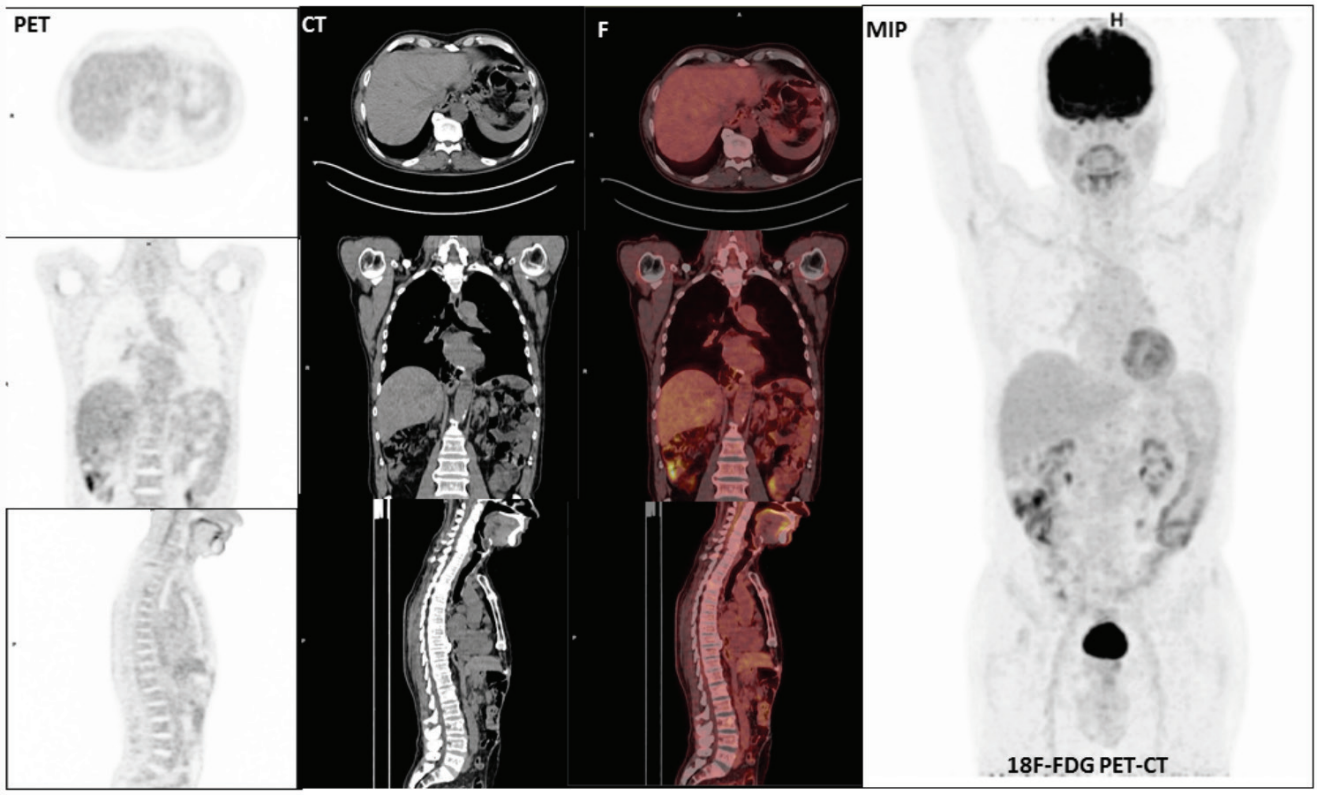

Figure 2. No abnormal ^{18}fluorine-fluorodeoxyglucose (^{18}F-FDG) uptake at the eso-jejunostomy line was detected in ^{18}F-FDG PET/CT computed tomography images.

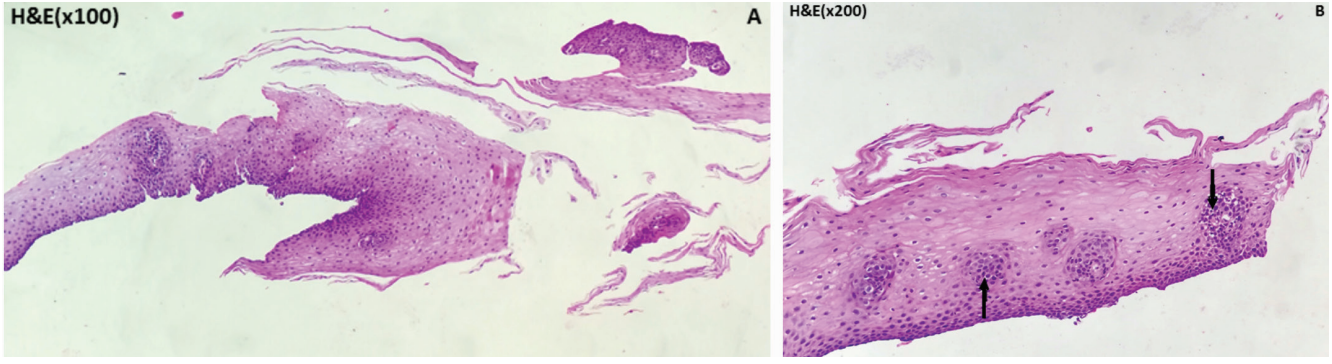

Figure 3. Owing to the suspicious PSMA 11 uptake at the eso-jejunostomy line, endoscopy and biopsy were performed with samples from this line. Benign squamous epithelial fragments stained with hematoxylin and eosin (H and E) with 100 times magnification (A). Black arrow shows benign squamous epithelial fragments stained with H and E with 200 times magnification (B).

Ethics

Informed Consent: The patient was asked for the verbal or written consent for the use of the individual clinical findings for research purposes.

Peer-review: Externally peer-reviewed.

Authorship Contributions

Surgical and Medical Practices: C.Ç., F.D.C.T, M.C., Concept: E.A., T.F.Ç., Design: E.A., T.F.Ç., T.A., Data Collection or Processing: E.A., T.F.Ç., T.A., Analysis or Interpretation: E.A., T.F.Ç., T.A, C.Ç., F.D.C.T, M.C., Literature Search: E.A., T.F.Ç., T.A., Writing: E.A., T.F.Ç., T.A.

Conflict of Interest: No conflict of interest was declared by the authors.

Financial Disclosure: The authors declared that this study received no financial support.

References

1. Afshar-Oromieh A, Malcher A, Eder M, Eisenhut M, Linhart HG, Hadaschik BA, Holland-Letz T, Giesel FL, Kratochwil C, Haufe S, Haberkorn U, Zechmann CM. PET imaging with a [68Ga]gallium-labelled PSMA ligand for the diagnosis of prostate cancer: biodistribution in humans and first evaluation of tumour lesions. Eur J Nucl Med Mol Imaging 2013;40:486-495.
2. Demirci E, Sahin OE, Ocak M, Akovali B, Nematyazar J, Kabasakal L. Normal distribution pattern and physiological variants of 68Ga-PSMA-11 PET/CT imaging. Nucl Med Commun 2016;37:1169-1179.
3. Kirchner J, Schaarschmidt BM, Sawicki LM, Heusch P, Hautzel H, Ermert J, Rabenalt R, Antoch G, Buchbender C. Evaluation of Practical Interpretation Hurdles in 68Ga-PSMA PET/CT in 55 Patients: Physiological Tracer Distribution and Incidental Tracer Uptake. Clin Nucl Med 2017;42:322-327.
4. Hofman MS, Hicks RJ, Maurer T, Eiber M. Prostate-specific Membrane Antigen PET: Clinical Utility in Prostate Cancer, Normal Patterns, Pearls, and Pitfalls. Radiographics 2018;38:200-217.
5. Holderman WH, Jacques JM, Blackstone MO, Brasitus TA. Prostate cancer metastatic to the stomach. Clinical aspects and endoscopic diagnosis. J Clin Gastroenterol 1992;14:251-254.
6. Solis Lara HE, Villarreal Del Bosque N, Sada Treviño MA, Yamamoto Ramos M, Argueta Ruiz RDC. Gastric Metastasis of Prostate Cancer as an Unusual Presentation Using 68Ga-Prostate-Specific Membrane Antigen PET/CT. Clin Nucl Med 2018;43:156-159.
7. Onitilo AA, Engel JM, Resnick JM. Prostate carcinoma metastatic to the stomach: report of two cases and review of the literature. Clin Med Res 2010;8:18-21.
8. Hong KP, Lee SJ, Hong GS, Yoon H, Shim BS. Prostate cancer metastasis to the stomach. Korean J Urol 2010;51:431-433.
9. Shetty D, Patel D, Le K, Bui C, Mansberg R. Pitfalls in Gallium-68 PSMA PET/CT Interpretation-A Pictorial Review. Tomography 2018;4:182-193.
10. Gordon IO, Tretiakova MS, Noffsinger AE, Hart J, Reuter VE, Al-Ahmadie HA. Prostate-specific membrane antigen expression in regeneration and repair. Mod Pathol 2008;21:1421-1427.

Letter to the Editor
Mol Imaging Radionucl Ther 2021;30:67-68 DOI:10.4274/mirt.galenos.2021.58561

Reply to Comment on: Lung Perfusion Imaging with Technetium-99m-macroaggregated Albumin should be Combined with Contrast-enhanced Echocardiography for the Diagnosis of Hepatopulmonary Syndrome

"Hepatopulmoner Sendrom Tanısı için Teknesyum-99m-makroagrege Albümin ile Akciğer Perfüzyon Görüntüleme, Kontrastlı Ekokardiyografi ile Kombine Edilmelidir" Yorumuna Yanıt

Majid Assadi

Bushehr University of Medical Sciences, Bushehr Medical University Hospital, The Persian Gulf Nuclear Medicine Research Center, Department of Molecular Imaging and Radionuclide Therapy (MIRT), Bushehr, Iran

Keywords: Hepatopulmonary syndrome, technetium-99m-macroaggregated albumin, lung perfusion scintigraphy, right-to-left shunt, contrast-enhanced echocardiography
Anahtar kelimeler: Hepatopulmoner sendrom, teknetyum-99m-makrokümelenmiş albümin, akciğer perfüzyon sintigrafisi, sağdan sola şant, kontrastlı ekokardiyografi

Dear Editor,

We appreciate the authors for their interest and knowledgeable comments on our study (1). We completely agree with them on dividing the geometric mean of brain counts by 0.13 since the brain is presumed to receive 13% of the cardiac output (2). We have used this score for shunt calculation.

The relationship between brain uptake and quantitation of the right-to-left (R-L) shunt percentage using technetium-99m (Tc-99m)-macroaggregated albumin (MAA) whole-body imaging has been rarely investigated. Ito et al. (3) studied 53 patients and found that Tc-99-MAA brain uptake could completely distinguish patients with or without an R-L shunt and that it could provide complementary information and appears promising in predicting clinical outcomes.

With our extensive experience in assessing R-L shunting as a routine adjunct protocol in a large number of patients presenting for ventilation/perfusion single photon emission computed tomography scans, in addition to those who are only referred for determining the shunt value, we have observed that semi-quantitative shunt assessment using visual analysis of brain uptake is pragmatic, achievable, and associated with a high success rate. Although the compelling study by Zhao et al. (4) focused only on quantitative analyses, they can test this issue as well.

We agree with Zhao et al. (4) on the important potential role of quantitative parameters derived from Tc-99m-MAA whole-body imaging in computing R-L shunting; however, some aspects need more explanation. This computation of R-L shunting is not free from limitations and might overestimate the true number of patients with shunts primarily because of the interference of unbound

Address for Correspondence: Majid Assadi MD, The Persian Gulf Nuclear Medicine Research Center, Bushehr University of Medical Sciences, Bushehr, Iran
Phone: 0098-771-2580169 **E-mail:** assadipoya@yahoo.com ORCID ID: orcid.org/0000-0002-2166-3765
Received: 22.10.2020 **Accepted:** 07.01.2021

nuclides of free pertechnetate with uptake in the thyroid, salivary glands, and gastric mucosa during whole-body imaging. Such radiopharmaceutical impurities associated with Tc-99m-MAA may cause fluctuations in the R-L shunt percentage. Secondly, there is a logistical limitation because this technique requires longer acquisition times than brain calculation, especially in busy nuclear medicine departments.

Besides, since the majority of the included patients only had mild or moderate hepatopulmonary syndrome (HPS), the findings cannot be generalized in case of patients with severe or very severe HPS. It may bring up a question of making a comparison between 2 scintigraphic methods in terms of underlying diseases and disease severity in different cirrhotic subgroups.

Another point is considering a homogeneous group of participants to ensure an accurate comparison between studies. In this regard, attention should be paid to porto-pulmonary hypertension (PoPH) in addition to HPS, which is not uncommon in patients with chronic liver disease and/or portal hypertension. A major pathogenetic mechanism in HPS is the dilatation of the pulmonary vasculature, which leads to progressive hypoxemia due to intrapulmonary shunting. On the contrary, PoPH may be described as the obstruction of the arterial flow in the pulmonary vascular system in the presence of increased pulmonary vascular resistance, which results from high pulmonary vasoconstriction (5). Presumably, much smaller particles are required to detect R-L shunting in patients with PoPH compared to those with HPS (5).

To our knowledge, no clinical studies have performed long-term follow-up in patients with HPS diagnosed by different protocols to address their clinical outcomes. We believe that the question would be better answered by future clinical research aiming at evaluating outcomes according to shunt severity, based on methods ideally offering a more comprehensive profiling to individualize patient management.

Moreover, we would welcome future research specifically aimed at establishing or validating imaging methods for assessing HPS in patients without cirrhosis who have a better prognosis (6). Another research area is to establish or validate imaging methods to address the treatment efficacy or accurately predict outcomes. Such research would indeed be useful to clinicians when they are considering shunt assessment assuming that brain uptake can facilitate the assessment of surgical outcomes in patients with R-L shunting.

Ethics

Peer-review: Internally peer-reviewed.

Financial Disclosure: The author declared that this study received no financial support.

References

1. Alipour Z, Armin A, Mohamadi S, Tabib SM, Azizmohammadi Z, Gholamrezanezhad A, Assadi M. Hepatopulmonary Syndrome with Right-to-left Shunt in Cirrhotic Patients Using Macro-Aggregated Albumin Lung Perfusion Scan: Comparison with Contrast Echocardiography and Association with Clinical Data. Mol Imaging Radionucl Ther 2020;29:1-6.
2. Meristoudis G, Keramida G, Ilias I. Lung Perfusion Imaging with Technetium-99m Macroaggregated Albumin should be Combined with Contrast-enhanced Echocardiography for the Diagnosis of Hepatopulmonary Syndrome. Mol Imaging Radionucl Ther 2020;29:143-144.
3. Ito K, Kurihara K, Ishibashi A, Morooka M, Mitsumoto T, Minamimoto R, Kubota K. Cut-off value for normal versus abnormal right-to-left shunt percentages using (99m)Tc-macroaggregated albumin. Nucl Med Commun 2011;32:936-940.
4. Zhao H, Tsauo J, Zhang XW, Ma HY, Weng NN, Tang GS, Li X. Technetium-99m-labeled macroaggregated albumin lung perfusion scan for diagnosis of hepatopulmonary syndrome: A prospective study comparing brain uptake and whole-body uptake. World J Gastroenterol 2020;26:1088-1097.
5. Krowka MJ. Hepatopulmonary syndrome versus portopulmonary hypertension: distinctions and dilemmas. Hepatology 1997;25:1282-1284.
6. Teuber G, Teupe C, Dietrich CF, Caspary WF, Buhl R, Zeuzem S. Pulmonary dysfunction in non-cirrhotic patients with chronic viral hepatitis. Eur J Intern Med 2002;13:311-318.